CHALMERS
UNIVERSITY OF TECHNOLOGY

Basis for an Improved Prediction Model and Source Model for Railway Noise in Nord2000

Master's Thesis in Sound and Vibration (M.Sc.)

Vincent Ratay

Department of Architecture and Civil Engineering
Division of Applied Acoustics

CHALMERS UNIVERSITY OF TECHNOLOGY
Gothenburg, Sweden 2024
www.chalmers.se

Master's thesis 2024

Basis for an Improved Prediction Model and Source Model for Railway Noise in Nord2000

Vincent Ratay

CHALMERS
UNIVERSITY OF TECHNOLOGY

Division of Applied Acoustics
Chalmers University of Technology
Gothenburg, Sweden 2024

Basis for an Improved Prediction Model and Source Model for Railway Noise in Nord2000
Vincent Ratay

Supervisors:	Astrid Pieringer	Division of Applied Acoustics
	Magnus Källman	Trafikverket
	Mikael Ögren	Arbets- och Miljömedicin, Göteborgs Universitet
Examiner:	Astrid Pieringer	Division of Applied Acoustics

Master's Thesis 2024
Department of Architecture and Civil Engineering
Division of Applied Acoustics
Chalmers University of Technology
SE-412 96 Gothenburg
Telephone +46 31 772 1000

Typeset in LaTeX
Printed by Chalmers Reproservice
Gothenburg, Sweden 2024

Artificial Intelligence Tools Disclosure

This thesis utilised Artificial Intelligence tools in the following ways:

- Code optimisation
- Plot formatting in Matlab
- Table formatting in LaTeX
- Data structure suggestions

Basis for an Improved Prediction Model and Source Model for Railway Noise in Nord2000
Vincent Ratay
Department of Architecture and Civil Engineering
Division of Applied Acoustics
Chalmers University of Technology

Abstract

The prediction models Nord2000 and CNOSSOS-EU are used to assess railway noise. The source models of these prediction models are simplifications of the complex sound radiation of trains. Therefore, the exposure from these source models close to the train is not accurate. This thesis aims to improve the vertical sound power distribution over equivalent sources, as well as the prediction of the overall sound power radiation from trains in Nord2000, based on the speed and the type of train.

A linear equation system, which describes the propagation path between equivalent sources on a train and several microphones, is used to streamline the calculation method in Nord2000. For a more accurate prediction of the overall sound power radiation, based on the speed and type of train, a linear regression model, a neural network, and a decision tree model are built, trained and evaluated with a dataset of measured train pass-bys. The determined linear equation system of the propagation path, in combination with existing measurement data, is also solved to find the vertical sound power distribution over equivalent sources.

The prediction models are evaluated using a test dataset, that is split from the original dataset and not used in the training phase of the models. Comparison against the predictions with the Nord2000 model shows a potential for improvement of the current prediction model. The linear regression model yields reliable predictions, while the neural network and decision tree are more affected by outliers in the data and, therefore, result in a worse overall prediction. The method to find vertical sound power distribution only yields results at low frequencies. Generally, more sound power contribution from the sources, higher on the train, can be seen around 40 Hz and around 200 Hz.

While the prediction of the sound radiation from a train, based on the speed and type of train, can be improved with the new linear regression model in this thesis, it was not possible to incorporate the rail and wheel roughness into the models, as the wheel roughness could not be derived from the available data. As the roughness of both the rail and wheel is the root cause of rolling noise, the performance of the models might not be limited by the amount of data, but the absence of the determining factor to predict rolling noise, the roughness of the rail and wheel.
The results from the method to find a vertical sound power distribution on a train are contrary to the results according to the literature. Finding an appropriate vertical sound power distribution with measured sound exposure levels at only two microphones might not be at all possible, as transfer paths between sources and microphones are too similar. Finding an accurate vertical sound power distribution might require array measurements. These measurements have to be carefully evaluated, as they can underestimate the sound power contribution from the rail when beam-forming is only carried out in the normal direction to the track.

Keywords: Railway Noise, Prediction Model, Source Model, Nord2000

Acknowledgements

I would like to thank my supervisors Astrid Pieringer, Magnus Källman, and Mikael Ögren for the opportunity to carry out this project. Thank you for giving me the freedom and trust to pursue the project in the direction I found most interesting and suitable for this thesis. Thank you very much!

I would like to express my deepest gratitude to the people in the Division of Applied Acoustics for creating the best learning environment I could have wished for. Thank you for all the five-minute-discussions at the coffee machine and the inspiration that bloomed from them.

Vincent Ratay
Göteborg, June 2024

List of Acronyms

Below is the list of acronyms that have been used throughout this thesis listed in alphabetical order:

LQS	Linear Equation System
RMSE	Root Mean Square Error
SEL	Sound Exposure Level

Nomenclature

Below is the nomenclature of indices and variables that have been used throughout this thesis.

Indices

i	frequency band
j	source
k	microphone
s	segment
A, B	Sources A and B

Acoustic Quantities

E	Sound Exposure
L_{E}	Sound Exposure Level
p_{ref}	Reference Sound Pressure of $2 \cdot 10^{-5}$ Pa
$p(t)$	Sound Pressure
L_{p}	Sound Pressure Level
r_0	Reference Roughness of 1 µm
r	Roughness in µm
L_r	Roughness Level
W	Sound Power
L_{W}	Sound Power Level
$L_{W,1\,\mathrm{m}}$	Sound Power Level per 1 m of Train Length
L_{corr}	Level Corrections
L_{a}	Level Correction for Air Attenuation
lin_{a}	Correction Factor for Air Attenuation
L_{d}	Level Correction for Spherical Divergence
lin_{d}	Correction Factor for Spherical Divergence

L_g	Level Correction for Ground Reflection
lin_g	Correction Factor for Ground Reflection
t_c	Time Correction Factor
f	Frequency in Hz
λ	Wavelength in m
f_c, f_l, f_u	Center Frequency, Lower Bound and Upper Bound of Frequency band

Geometric Quantities

d	Distance between Source and Microphone
l_t	Length of Train
l_seg	Length of Segment

Other Variables

a	Slope of Linear Regression Model
b	Intercept of Linear Regression Model
v_t	Speed of Train
$\boldsymbol{T}$	Transfer Matrix
α	Parameter of Speed Dependency in $L_p \propto \alpha \cdot 10\log(v_\mathrm{t})$
α_a	Air Attenuation of Atmosphere in dB/km
σ_g	Flow Resistivity of Ground in $\frac{\mathrm{kNs}}{\mathrm{m}^4}$

Contents

List of Figures

List of Tables

1. Introduction

The environmental noise model for traffic noise, Nord2000 [1], which is commonly used in the Nordic countries, also includes a prediction model for railway noise. This prediction model, as well as the widely used CNOSSOS-EU [2], both mention imprecision in their source models for trains. The main issue in their source models is the unknown vertical sound power distribution. The source models make use of equivalents sources and while few equivalent sources might be adequate to assess the exposure far away from the track, the assessment is not representative when positions close to the track are considered. As the use of low height noise screens close to the rail is sought after, a more accurate source model is necessary. With the existing models the effect of low height noise barriers can not be predicted accurately and without an accurate prediction of the effect of low height noise barriers, they are hard to justify in the planning phase.
This thesis aims to improve the prediction of the overall sound emission from trains. It is also sought after to improve the source model, to better estimate the effect of low height noise screens. For that purpose, equivalent levels are considered, rather than maximum levels and the main focus lies on the prediction of trains in the Swedish railway network.

1.1. Structure

This thesis approaches the improvement of the prediction model of railway noise in Nord2000 from two angles:

- Predicting the sound emission from a train, based on its speed and its type or category.
- Finding appropriate vertical sound power distribution over equivalent sources.

The model to predict the total sound power emission of a train, based in the speed and type of train, is evaluated. New models are build with different prediction models, based on a dataset of pass-by measurements. The new models to predict the total sound power of a train are build with a linear regression, a neural network, and a decision tree. The new models are then compared to the existing prediction methods in Nord2000 and CNOSSOS-EU.
Another important aspect of the sound emission from trains is the vertical position of equivalent sound sources and the distribution of sound power over them. To find appropriate equivalent sound sources on a train, a linear equation system (**LQS**) that connects the sound power of equivalent sources and the measured sound exposure level (**SEL**) via the transfer paths is formulated and solved.
These two approaches to improve the prediction model in Nord2000 are evaluated and compared to the existing model, as well as to findings in recent literature.

1.2. Common Noise Assessment Characterisics

A measure commonly used to characterise the exposure to sound is the **SEL** L_{E} defined in Eq. (1.1), with $T_0 = 1\,\mathrm{s}$ as the reference time, T as the measurement time, $p(t)$ as the sound pressure, and $p_{\mathrm{ref}} = 2{\cdot}10^{-5}$ Pa as the reference sound pressure. The **SEL** represents

the level of a rectangular impulse of 1 s with the same exposure as the measurement [3, p. 105].

$$L_{\mathrm{E}} = 10 \log\left(\frac{1}{T_0}\int_0^T \frac{p(t)^2}{p_{\mathrm{ref}}^2}\mathrm{dt}\right) \tag{1.1}$$

The emission of a source, independent from its surroundings can be described with the sound power level L_W. The sound power level is defined as seen in Eq. (1.2), with the emitted sound power W of a source and the reference sound power $W_{\mathrm{ref}} = 10^{-12}$ W.

$$L_{\mathrm{W}} = 10 \log\left(\frac{W}{W_{\mathrm{ref}}}\right) \tag{1.2}$$

Note that the commonly used logarithm with base 10 ($\log_{10}$) is abbreviated as log in this thesis.

2. Literature Study

2.1. Sound Emission Mechanisms on Trains

The relevant sound emission mechanisms covered in this thesis are rolling noise, aerodynamic noise, and traction noise. As shown by Thompson et. al. [4], the two dominating sound emission mechanisms, rolling noise and aerodynamic noise contribute to the sound exposure at different speeds and follow different speed dependencies. At an operating speed above 100 km/h the noise emissions from several high-speed trains are shown in Figure 2.1.

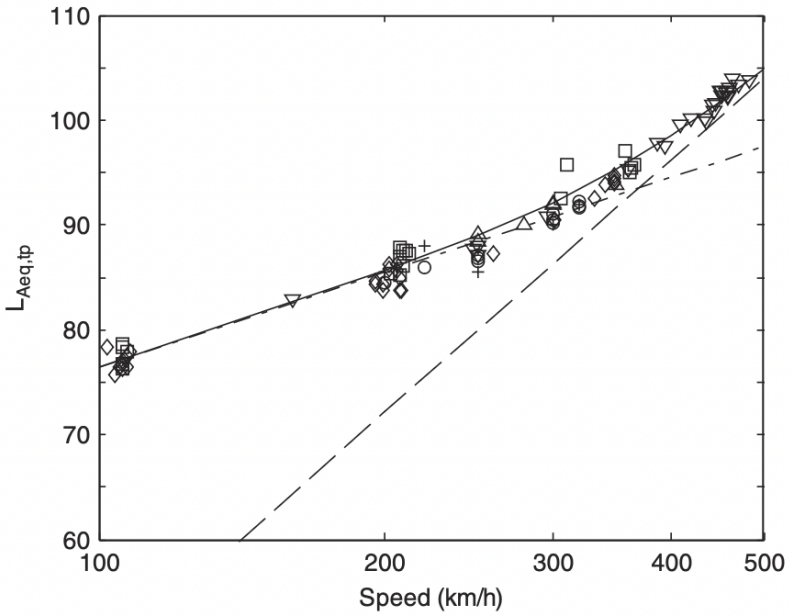

Figure 2.1.: Emission from Different Train Types at a Distance of 25 m
(– – –) Rolling Noise; (- - - -) Aerodynamic Noise [4]

As described by Thompson et. al. [4], the rolling noise generally grows with the speed of the train v_t proportionally to $30\log(v_t)$ and aerodynamic noise follows the proportionality $60\log(v_t)$. At speeds below 250 km/h the rolling noise is the dominant contributor to the total sound radiation of a train, while for trains at high speed the aerodynamic noise has to be considered. At speeds below 60 km/h the traction noise from engines and fans can be dominant, but does not necessarily scale with the speed of the train [5].

Table 2.1.: Noise Emission Mechanism on Trains

Noise Emission Mechanism		Dominant Frequency Range	Speed Relevance
Rolling Noise	Wheel	$> 1.5\,\mathrm{kHz}$	$< 250\,\mathrm{km/h}$
	Rail	$500\,\mathrm{Hz} - 1.25\,\mathrm{kHz}$	
	Sleeper	$< 250\,\mathrm{Hz}$	
Aerodynamic Noise	Pantograph	Speed Dependent	$> 250\,\mathrm{km/h}$
	Flow Separation	Broadband	
Traction Noise	Engines	System Dependent	$< 60\,\mathrm{km/h}$
	Fans		
	Braking System		

The noise emission mechanisms rolling noise, aerodynamic noise, and traction noise have been summarised, with their dominant frequency range and their speed relevance in Tab. 2.1. A more detailed consideration of these noise emission mechanisms is given in the following sections. While other studies take noise from bridges, crossings, and squeal noise into account, these subjects will not be considered in this thesis.

2.1.1. Rolling Noise

Rolling noise is caused by the vibration and sound radiation of the wheel and track and is the most dominant sound emission mechanism in the standard speed range of operation, especially in Sweden, where trains generally do not exceed 200 km/h [6]. The contact between the wheel and rail is crucial in determining the induced vibrations in the wheel and rail, and therefore their radiation. Neither wheel nor rail are perfectly smooth and show unevenness, called roughness, on their surfaces. Even though micro-roughness is desired to benefit the traction of the wheel on the rail, macro-roughness is not sought after [7].
The contact between the wheel and the rail can be modelled with a contact spring and the roughness of both the rail and the wheel, acting as a relative displacement input. For standard ballasted tracks, the rail itself is placed on sleepers, that can be represented as masses, which are in turn connected with springs to the ground, representing the ballast stiffness, as seen in Figure 2.2. Another type of track is referred to as slab track, where the rail is mounted on longer concrete slabs. Especially for high speed train lines slab tracks find an application. The use of slab tracks can reduce the ground vibration [8], while the absorption coefficient can be smaller than for ballasted tracks, reducing the absorption of acoustic energy under the train [9].

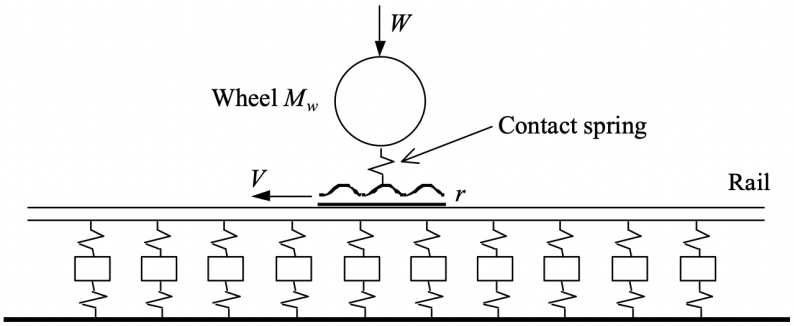

Figure 2.2.: Rail-Wheel Model [10]

A model for the rolling noise is described by Thompson in [7] and can be seen in Figure 2.3. It can be seen that both the wheel roughness and the rail roughness have the same impact on the generated noise and are simply added. A contact filter that corrects for the attenuation of the roughness with a relatively short wavelength compared to the contact patch between the wheel and the rail is also incorporated [7]. The wheel and the rail get excited and radiate sound. Additionally, the rail acts as a wave guide and radiation occurs along the rail. How high the decay rate of the wave is along the rail is highly dependent on the rail pad stiffness, that connects the rail with the sleepers or slabs. Soft rail pads lead to a weak coupling between the rail and the sleepers, resulting in the rail to vibrate more freely and therefore act as a more efficient wave guide [7].

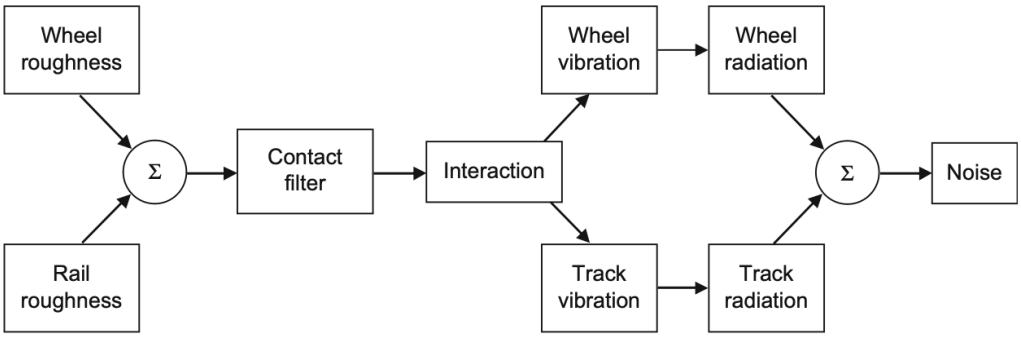

Figure 2.3.: Model for Rolling Noise [7]

As the wheel is a finite structure, its radiation is dominated by its resonances. Thompson compares the wheel to a wine glass or a church bell, as the wheel is very lightly damped, due to its axi-symmetric structure [7] and the low material loss factor of steel. Therefore the radiation of the wheel is dominated by modes. Several modes are shown in Figure 2.5 where n represents the nodal diameters. One-nodal-circle axial and radial modes are the most important modes in rolling noise, due to the relatively high displacement at the web. Both axial and radial modes exhibit vibration in axial and radial direction. As the vibration in axial and radial direction is coupled, the radial excitation by the roughness leads to a radiation at the large surface of the web, due to its axial motion. A straight web results in a weaker coupling of the directions of vibration and is therefore generally quieter [7].

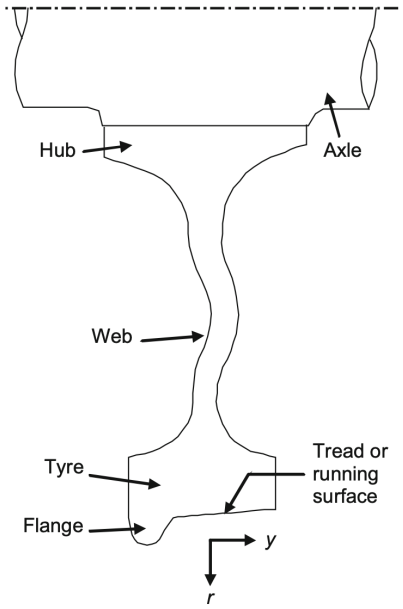

Figure 2.4.: Cross-section of UIC 920 mm Freight Wheel [7]

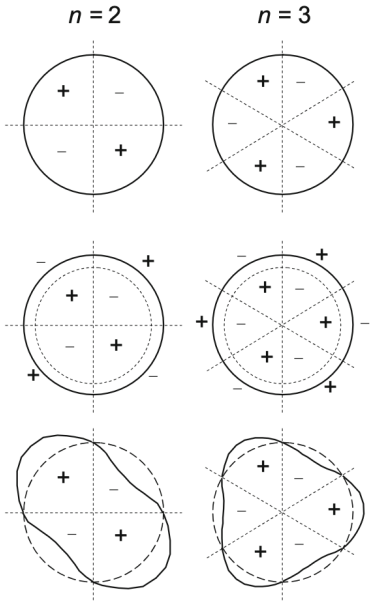

Figure 2.5.: Modes of Wheel [7];
Top: Zero-nodal-circle Axial Modes;
Middle: One-nodal-circle Axial Modes;
Bottom: Radial Modes

Using the TWINS prediction model, one example of noise contributions in rolling noise was calculated by Thompson [7] and can be seen in Figure 2.6. It is noticeable that the contribution to the radiation from the rail is rather dominant between 500 Hz and 1.25 kHz, which is also the frequency range, in which the highest radiation is measured. The wheel has a significant contribution to the sound radiation above 2 kHz, while sleepers dominate the sound radiation below 250 Hz.

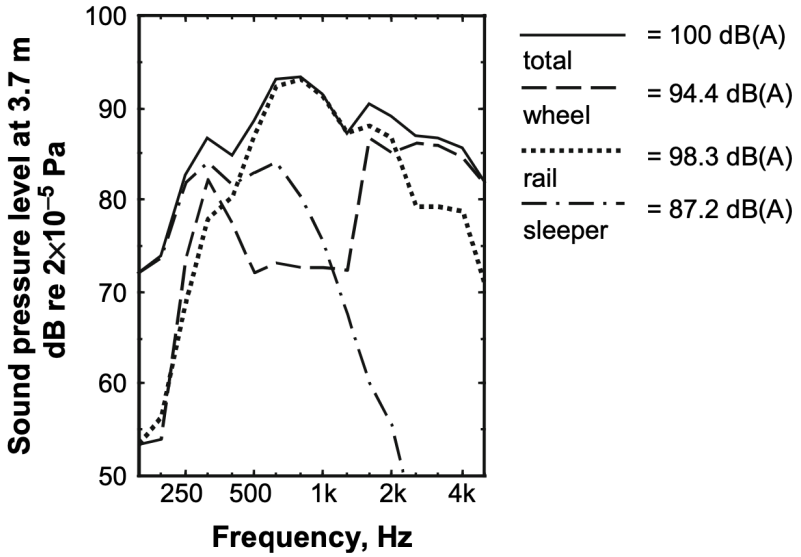

Figure 2.6.: Typical Noise Contribution in Rolling Noise [7]

The TWINS prediction model is, however, only one method to model the rolling noise and most of its calculations are carried out in the frequency domain [11]. A method to

calculate the pass-by emission of the wheel in the time domain has been formulated by Theyssen et. al. [12]. In this method the exposures resulting from the modes of the wheel are calculated separately. The contribution from all modes to the sound exposure leads to the simulated time signal of a train pass-by. A model for the wheel/rail interaction is proposed by Pieringer et. al. [13] and is used to emulate the contact filter effect for different sets of roughness data over the rail. The radiation from the track is modelled efficiently by Theyssen et. al. [14] and is formulated in the wavenumber domain, which reduces the used Boundary Element method from three dimensions (3D) to two dimensions (2D).
The radiation from the wheel and the rail shows significant directivity. The axial modes of the wheel show a particularly high directivity in normal direction to the plane of the wheel. The coupling between the vibration in radial and axial direction is therefore a significant determining factor for the radiation from the wheel. The coupling between radial and axial directions can be reduced with a straight web of the wheel [7] and is generally dependent on the geometry of the wheel. The time domain model, formulated by Theyssen et. al. [12] shows, that the directivity of the wheel is predominantly in axial direction at high frequencies. The directivity of the rail is more frequency dependent. At low frequencies the contribution from the rail can be attributed to the force point, the contact point between the wheel and the rail, and can be modelled as a point source. At higher frequencies the propagating wave along the rail contributes to the sound exposure. The radiation of this propagating part of the rail shows a high directivity and high frequencies are propagated and radiated farther away from the excitation point [7]. It is suggested by Thompson [7] to model the radiation from the rail and wheel as a combination of monopoles and dipoles.

2.1.2. Aerodynamic Noise

Aerodynamic noise is mainly the focus on high-speed trains, as aerodynamic noise only dominates at high speeds. For the Swedish railway network, in which trains generally do not exceed 200 km/h [6], the aerodynamic noise is not significant and the rolling noise is generally more dominant.
Aerodynamic noise is generated by the varying cross section of the train and the occurrence of vortex shedding and turbulence in the boundary layer on the outside of the train and the pantograph [15]. The sound emission from the train as a whole and the different components on the train is described by Kim et. al. [15] using power laws with Eq. (2.1).

$$L_\mathrm{p} \propto \alpha \cdot 10 \log(v_\mathrm{t}) \tag{2.1}$$

The speed dependency of aerodynamic noise of a train as a whole can generally be described with $\alpha = 6$. The speed dependency of the aerodynamic noise is dependent on the train and can be described as a speed dependency of its components. The speed dependency is shown by Kim et. al. [15] for different train types with different α for Eq. (2.1) and can be seen in Tab. 2.2. A more detailed speed dependency for different components on the train is given for the TGV-A in Tab. 2.3 [15].

Table 2.2.: Speed Dependency of Different Train Types [15]

Train system		α
TGV	Locomotive	3 (up to 300 km/h) 7-7.5 (beyond 350 km/h)
	Coach	3 (up to 300 km/h) 6 (beyond 350 km/h)
TGV-A		4.3
ICE		6-8
TR70		6 (fluid separation) 8-9 (turbulent boundary)
Shinkansen		6

Table 2.3.: Speed Dependency on TGV-A [15]

Noise Source (TGV-A)		α
Wheel	Middle Coach	2.9
	Front Locomotive	3.2
	Rear Locomotive	3.0
Pantograph (Rear Locomotive)		5.7
Cooling Fan	Front Locomotive	4.7
	Rear Locomotive	4.6
Front Window (Front Locomotive)		5.1
Between Coaches		4.2
Bogie		6.1
Turbulent Boundary Layer (per m^2)		4.3

Another measurement series regarding high-speed trains in Korea, discussed by Kim et. al. [15], separated the aerodynamic noise from the gaps between carriages and the pantograph. There it has been shown, that the aerodynamic noise from inter-coach gaps grows with $\alpha = 7.7$, while the aerodynamic noise of the pantograph grows with $\alpha = 4.4$ [15].
Microphone array measurements carried out by Kümmritz et. al. [16], also showed that German InterCity trains exhibit more sound power contribution from the pantograph, as the InterCity Express trains, which are designed for higher speeds, leading to the conclusion, that the aerodynamic noise can be reduced notably with design choices [16].
The flow separation and reattachment causes broad band noise, while vortex shedding around the pantographs results in tonal noise [7]. Cavities, as for example gaps between coaches, also lead to tonal noise, due to the resonance of the cavity [7].

2.1.3. Traction Noise

Noise from operating procedures on the train is referred to as traction noise. Common sources of traction noise are therefore the powertrain sources, auxiliary systems and braking systems [5]. These sound sources are not necessarily speed dependent and can be dominant at low speeds below 60 km/h and when idling [5]. Traction noise mechanisms and their relevance for prediction models is shown by Dittrich et. al. [5]. For better illustration common traction noise sources with a high relevance for prediction models are shown in Tab. 2.4. The traction noise of the engine can occur from one engine or multiple power units, distributed along the train.

Table 2.4.: Common Traction Noise Sources with High Relevance for Prediction [5]

Category	Source
Powertrain Sources	Exhaust
	Intake
	Engine Structure
Auxiliary Systems	Cooling Fans
	Cooling Inlets
	Cooling Outlets
Braking Systems	Brake Squeal of Wheels
	Friction of Break Blocks or Disc Breaks

2.2. Previous Studies about localisation of sound sources on trains

The collaboration between different contributors from Germany and Switzerland lead to the formation of sonRAIL to develop a new prediction model for trains [17]. In the project documentation they use the complete propagation model described in ISO 9613-2 [18]. The same propagation model is used in Nord2000 for Sweden and is further described in section 2.4. As meteorological data, an average for Switzerland was used, which will mainly have an effect on the air attenuation of the atmosphere.
In the investigation of different sound sources on a train, two stationary microphone arrays next to the track were used. For low frequencies up to the 1.6 kHz third octave band, a vertical line array with 19 microphones and a respective distance of 240 mm between the microphones was used. For higher frequencies from the 2 kHz third octave band, a 21 microphones vertical line array with respective distances of 80 mm between the microphones was used. As the microphone arrays can overlap, by using several microphones in both arrays, the total number of microphones was 33 [17]. The microphone arrays were focused on 77 vertical positions on the outer wall of the train with a respective distance of 0.1 m between them. The contributing noise emission mechanisms and their respective typical height on a train can be seen in Tab. 2.5, as described in [17].

Table 2.5.: Noise Emission Mechanisms and their Typical Heights on Trains

Noise Emission Mechanism	Typical Height
Rolling Noise	0 m, 0.5 m
Impact Noise	0 m
Bridge Noise	0 m
Curving Noise	0 m, 0.5 m
Secondary Noise	0.5 m, 2 m, 3 m, 4 m
Aerodynamic Noise	0.5 m, 2 m, 3 m, 4 m

The 77 focus points were represented as four replacement sound sources at the heights 0.5 m, 2 m, 3 m, and 4 m, while the sound power was given as sound power per meter of the train length. The replacement sources are modelled as point sources.
In the findings presented in [17], it can be seen that the sound emission from the lowest source dominates for all train types. The noise emitted from the rail and from the wheel are not separated. The locomotives with their pantographs and engines can also be seen

as a significant noise source in the time data. The noise from the lowest source at the height of 0.5 m is still the most dominating.
Similar array measurements with beam-forming were carried out by Kümmritz [16]. In that report the main focus was to differentiate between aerodynamic noise and sound emission from the rail-wheel interaction. In the measurements two microphone arrays were used. One spiral microphone array with a diameter of 3.4 m and 120 microphones was used to capture the whole train, while another ring microphone array with a diameter of 0.7 m and 48 microphones was used to capture the emission from the rail and wheel in detail. As expected, the majority of the sound power is emitted from the lower part of the train, the rail and the wheel. Up to 4 kHz the main contributor for the sound power from the rail and wheel is the contact point between them or rather it can not be distinguished between the rail and the wheel. In the third octave bands of 6.3 kHz and 10 kHz the rail is more dominant than the wheel. These high frequencies have very little to no effect on the total exposure level, as the level in that frequency bands are significantly lower than in the frequency bands with the highest exposure. Another conclusion of the measurements carried out by Kümmritz [16] is that for passenger trains, the locomotives emit more sound power than the rolling noise at higher speeds, with the exception of the train type IC2. In the report it is also described, that the aerodynamic noise from the high speed train InterCity Express (ICE) is barely a factor, while it plays a significant role with the InterCity trains, most likely due to the optimised aerodynamics of the ICE [16].
The two reports [17] and [16] do not go in further detail to describe the differentiation between the radiation from the rail and the wheel, but both show, that the rail-wheel interaction is the main contributor to the sound exposure. Differentiating between the radiation from the rail and wheel might not yield representative values. According to Kitagawa et al. [19] the rail as a contributor to the overall exposure is generally underestimated in array measurements, using horizontal or 2D-arrays. As the rail has a varying radiation angle and these arrays capture the railway noise normal to the rail, the rail is underestimated in the frequency region of wave propagation [19]. At some frequency ranges the noise from the rail is overestimated, but as that overestimation occurs in a frequency range, where the decay rate is relatively high, the rail does not contribute to the overall exposure from the train [19]. One suggestion by Kitagawa et al. [19] is to capture the sound coming from a non-normal direction from the railway using delays in the signal processing with the existing array measurements.
The noise from the different emission mechanisms has also been formulated for the AMTRAK Acela train type in [20] and can be seen in Tab. 2.6. The measurement, the results are based on, is also carried out with a microphone array. A more complete noise assessment for the sub sources can be found in the report *High-Speed Ground Transportation Noise and Vibration Impact Assessment* [21]. In this report by the Federal Railroad Administration of the U.S., the **SEL**s from sub sources on a train are estimated with a speed dependency, similarly to Eq. (2.1). The speed dependency α for several trains is shown in Tab. 2.7 and it can be seen that the speed dependency differs from the values in Tab. 2.2. Finding the exact speed dependency of aerodynamic noise might not be always practical, as it depends on the design of the train.

Table 2.6.: Contribution from Noise Emission Mechanisms at 241 km/h (150 mph) [20]

Emission Mechanism	Relative Power
Rolling Noise	72%
Traction Motors	17%
Pantograph	8%
Fans	2%

Table 2.7.: Speed Dependency of Sub Source according to [21]

Train type	Sound Emission Mechanism		Speed Dependency α
TGV X2000 ICE3	Rail/Wheel		2
	Aerodynamic Noise	Train Nose Wheel Region Pantograph	6

2.3. Current State of Prediction Models

This section discusses Nord2000: New Nordic Prediction Method for Rail Traffic Noise [1], as well as the Common Noise Assessment Methods in Europe (CNOSSOS-EU) [2]. The focus in this section is on the source model and prediction of sound power in these two models. The purpose of these models is to estimate and model the sound emission from trains for practical use, i.e. for noise mapping. The models are therefore not necessarily perfect representations of railway noise, but model it, so the environmental exposure can be assessed.

2.3.1. Nord2000

The Nord2000 prediction model for railway noise [1], published in the year 2001, follows up and improves on Railway traffic noise: the Nordic prediction method [22], revised in 1996.
The train is modelled as a number of point sources along the train. The source positions on a train split into sources for the wheel and contact point between the rail and wheel, as well as the carriage itself. The source positions for the engine, exhaust and aerodynamic contribution have to be determined from case to case. The general source positions can be seen in Tab. 2.8. The source positions for the engine, exhaust and aerodynamic noise have to be determined for each case. For more convenient use of the method the principle source locations are broken down into default values, as seen in Tab. 2.9.

Table 2.8.: Principle Source Locations [1]

	Height above top of rail	Horizontal Location
Source 1: Wheel/Rail	0.01 m	Evenly distributed along train
Source 2: Wheel/Rail	0.35 · wheel diameter	Evenly distributed along train
Source 3: Wheel/Rail	0.70 · wheel diameter	Evenly distributed along train
Source 4: Engine	Actual Height	Centre of engine openings
Source 5: Exhaust	Actual Height	Exhaust outlet
Source 6: Aerodynamic	Determined in each case	To be determined in each case

Table 2.9.: Default Source Locations [1]

	Height above top of rail (m)	Frequency Range (Hz)	Horizontal Location
Source 1: Wheel/Rail	0.01	200 - 10,000	Evenly distributed along train
Source 2: Wheel/Rail	0.35	200 - 10,000	Evenly distributed along train
Source 3: Wheel/Rail	0.70	200 - 10,000	Evenly distributed along train
Source 4: Engine/Exhaust	2.5	25 - 160	Centre of engine openings

The sources described in Tab. 2.9 are point sources. In the Nord2000 method, a non-omnidirectional directivety of the sources is described. As the directivety of the sources as described in Nord2000 [1] is designed to not change the measured **SEL** at a receiving point, it is left out here. With a propagation model, further described in section 2.4, the sound power of the whole train coming from the sub sources can be connected to the **SEL** at a receiving point. In this process it is determined, that the sub sources have the same sound power. Going forward, the sound power of a train is described in sound power level per meter of the train, with the units dB/m. The total sound power level of a train L_{W} can be calculated with the sound power level per meter $L_{\mathrm{W},1\,\mathrm{m}}$ and the length of the train l_{t}, as seen in Eq. (2.2) [1].

$$L_{\mathrm{W}} = L_{\mathrm{W},1\,\mathrm{m}} + 10\log(l_{\mathrm{t}}) \tag{2.2}$$

As the distribution of sound sources is fixed, as seen in Tab. 2.9, the total sound power of the train in third octave bands is sought after. For that purpose the Nord2000 method [1] uses linear regression models for different train types.
The linear regression model to estimate the total sound power of a train has a form as seen in Eq. (2.3), where $L_{\mathrm{W},1\,\mathrm{m}}$ is the sound power of a train per meter, v_{t} is the speed of the train in km/h, and a and b are parameters that have been determined empirically for different train types.

$$L_{\mathrm{W},1\,\mathrm{m}} = a \cdot \log\left(\frac{v_{\mathrm{t}}}{100}\right) + b \tag{2.3}$$

Originally the train specific parameters a and b have been determined from measurements from the years 1993 - 1995. This old dataset limited the parameters to be calculated in octave bands. With linear interpolation between the octave bands, the parameters were expanded to third octave bands. Originally the parameters were also not complete and did not describe all train types. The parameters have since been revised by Ögren et. al [23] with a more up-to-date dataset. The described train types in the report for the updated parameters a and b can be seen in Tab. 2.10.

Table 2.10.: Updated Train Types for Nord2000 [23]

Train Types	Code
X2, X2C, X2U	X2
X11 - X14	X11
X31	X31
X40	X40
X50 – X54, X55	X50
X60 – X62	X60
X74	X74
Y31, Y32	Y31
ER1	ER1
Locomotive Hauled Passenger Trains	PT
Freight train, Cast Iron Block Brakes	GT
Freight train, K-block, Disc Brakes	GTK

The parameters a and b for the train types in Tab. 2.10, can be seen in appendix B.
It has to be noted, that this method does not take the rail roughness or wheel roughness into account. As shown in section 2.1.1, the roughness of both the wheel and the rail are significant determining factors. Incorporating the rail and wheel roughness into the Nord2000 method might therefore be advisable.

2.3.2. CNOSSOS-EU

The Common Noise Assessment Methods in Europe (CNOSSOS-EU) [2] gives general guidelines in how to assess noise from trains. For that purpose vehicles are classified according to their vehicle type, number of axles, brake type, and noise reduction measure at the wheels. The classifications for the vehicle can be seen in Tab. C.1 in appendix C. Generally, CNOSSOS-EU tries to differentiate between common train types, axle loads and wheel diameters and gives values for the calculation of their sound emission. Incorporating the rail roughness and wheel roughness into the calculation of the sound emission of a train is very appropriate, as it is known to be root cause of the sound emission. CNOSSOS-EU provides default values for the wheel, depending on the brake type of the wheel and for the rail, depending on whether the rail is well maintained or not. In the standard SS-EN 15610:2019 [24], a method to measure the rail and wheel roughness is described. For the number and positions of equivalent sources that describe the train, two line sources (A and B) along the train are chosen. The sources are positioned in the middle between the two rails. The height of the source lines are $h_{\mathrm{A}} = 0.5\,\mathrm{m}$ and $h_{\mathrm{B}} = 4\,\mathrm{m}$ above the top of the rail and can be seen in Figure 2.7. The approach to only use two line sources is a simplification compared to the Nord2000 method. For predictions far away from the railway, this simplification is not problematic. It is also not clear if the approach to model the line sources in the middle between the two rails is a significant factor. Modelling the sound sources on the outside wall of the train might be more appropriate, but requires information about the dimensions of the train.

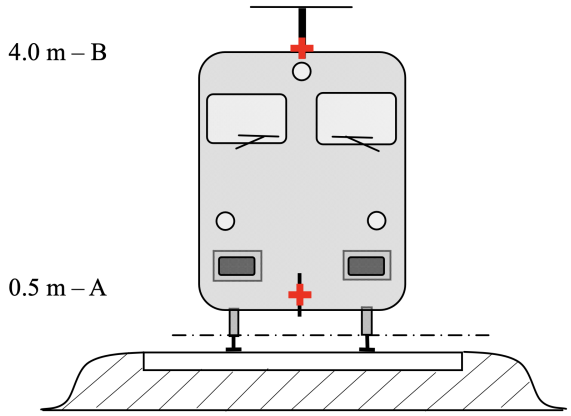

Figure 2.7.: Position of Equivalent Sources [2]

The two positions are chosen to represent different sound emission mechanisms:

Table 2.11.: Sound Emission Mechanisms According to CNOSSOS-EU [2]

Category	Description	Source
Rolling Noise	Vibration from track, wheel, sleepers, and superstructure of freight trains	A
Traction Noise	Engines, Transmission, Exhaust, Cooling Outlets, Fans, etc.	A and B Determined in each case
Aerodynamic Noise	Shrouds and Screens (source A) Pantograph (source B)	A and B
Impact Noise	Crossings, Switches, and Junctions	A
Squeal Noise		A
Bridge Noise		A

Rolling Noise

Contrary to the Nord2000 method, the roughness level of the rail and the wheel is taken into account in CNOSSOS-EU. The roughness level is usually given as a spectrum of wavelengths λ. Depending on the speed of the train, the added roughness of the rail and the wheel excites different frequencies. The roughness level L_r is defined with the roughness r in µm and the reference roughness $r_0 = 1\,\mu\mathrm{m}$, as seen in Eq. (2.4) [2].

$$L_\mathrm{r} = 10 \log\left(\frac{r}{r_0}\right)^2 \tag{2.4}$$

The roughness level spectrum can be converted from a wavelength spectrum to a spectrum of frequencies f with the speed of the train v_t, as seen in Eq. (2.5).

$$f = \frac{v_\mathrm{t}}{\lambda} \tag{2.5}$$

The frequency bands obtained from that calculation will not match up with the standard centre frequencies for octave bands or third octave bands. To calculate the roughness level in a frequency band, the contribution from each calculated frequency band should be considered. This is shown in Figure 2.8. The two calculated roughness levels L_1 and L_2

contribute to the standard frequency band (in red), with o_1 and o_2 as the overlap. The roughness level L of the standard frequency band, can then be calculated with a weighted average, seen in Eq. (2.6).

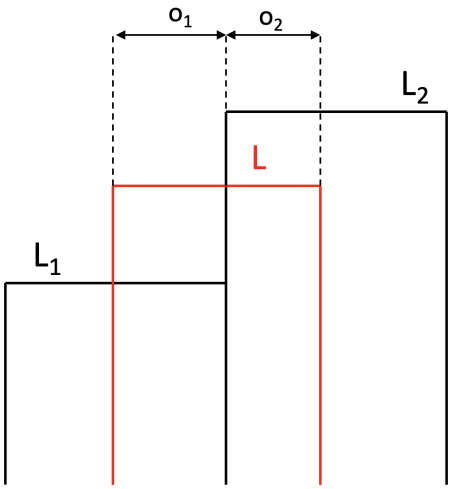

Figure 2.8.: Overlap of Frequency Bands

$$L = 10 \log\left(\frac{o_1 \cdot 10^{L_1/10} + o_2 \cdot 10^{L_2/10}}{o_1 + o_2}\right) \tag{2.6}$$

The total roughness is calculated with the roughness of the wheel and the rail taken into account. Their interaction is adjusted by a contact filter A_c. The total roughness level $L_{\mathrm{R,Total},i}$ of the i-th frequency band can then be calculated with the roughness level of the wheel $L_{\mathrm{R,Wheel},i}$ and the roughness level of the rail $L_{\mathrm{R,Rail},i}$ in the i-th frequency band, as well as the contact filter $A_{c,i}$ (see Eq. (2.7)) [2]. The roughness filter for common cases is shown in CNOSSOS-EU and can be seen in Tab. C.2 in appendix C.

$$L_{\mathrm{R,Total},i} = 10 \log\left(10^{L_{\mathrm{R,Wheel},i}/10} + 10^{L_{\mathrm{R,Rail},i}/10}\right) + A_{\mathrm{c},i} \tag{2.7}$$

At constant speed of the train, the sound power level of the corresponding sources A and B, as seen in Figure 2.7 can be calculated with the total roughness level $L_{\mathrm{R,Total},i}$ and provided transfer functions for rail $L_{\mathrm{H,Rail},i}$ and the vehicle $L_{\mathrm{H,Veh},i}$. The transfer functions are given in CNOSSOS-EU [2] and can be seen in Tab. C.3 and Tab. C.4 in appendix C. The sound power level $L_{\mathrm{W,A},i}$ and $L_{\mathrm{W,B},i}$ of the sources A and B in i-th frequency band are calculated with Eq. (2.8) and Eq. (2.9) [2], with N_{a} as the number of axles per wagon.

$$L_{\mathrm{W,A},i} = L_{\mathrm{R,Total},i} + L_{\mathrm{H,Rail},i} + 10 \log(N_{\mathrm{a}}) \tag{2.8}$$

$$L_{\mathrm{W,B},i} = L_{\mathrm{R,Total},i} + L_{\mathrm{H,Veh},i} + 10 \log(N_{\mathrm{a}}) \tag{2.9}$$

Aerodynamic Noise

In CNOSSOS-EU it is suggested, that aerodynamic noise should only be taken into account above the speed of 200 km/h and for networks that are limited to 250 km/h it might not need to be considered as well. The speed dependency of the aerodynamic noise should be determined with one or two measurements [2]. The default parameters suggest a speed dependency of $\alpha = 5$ in Eq. (2.1).

2.4. Propagation Model

The propagation model used in Nord2000 is described in Nord2000: *Comprehensive Outdoor Sound Propagation Model. Part1: Propagation in an Atmosphere without Significant Refraction* [25]. The aim is to connect the sound power level L_{W} of a source with the sound pressure level L_{p} at a receiver position. For a point source this can be done with Eq. (2.10).

$$L_{\mathrm{p}} = L_{\mathrm{W}} + L_{\mathrm{corr}}, \tag{2.10}$$

where L_{corr} includes corrections for the ground reflection L_{g}, the air attenuation L_{a}, and the spherical divergence L_{d} (see Eq. (2.11)) [25].

$$L_{\mathrm{corr}} = L_{\mathrm{g}} + L_{\mathrm{a}} + L_{\mathrm{d}} \tag{2.11}$$

The correction for the air attenuation and the spherical divergence is simply calculated with the distance d between the source and the receiver. The effect of the ground reflection is more complicated.
The propagation model in CNOSSOS-EU uses a similar approach but formulated differently, as it corrects for the spherical divergence, the air attenuation and the ground reflection.

2.4.1. Correction Terms for Propagation

Air Attenuation

The absorption of sound in an atmosphere is described in ISO 9613:1 [26] and given in an attenuation α_{a} in dB/km. With a distance d in m, the attenuation can be described as seen in Eq. (2.12).

$$L_{\mathrm{a}} = -\alpha_{\mathrm{a}} \frac{d}{1000}. \tag{2.12}$$

Spherical Divergence

The spherical divergence term L_{d} is merely the spherical divergence from a propagation of a spherical wave. It is calculated with Eq. (2.13).

$$L_{\mathrm{d}} = 10 \log\left(\frac{1}{4\pi d^2}\right) \tag{2.13}$$

Ground Reflection

As described in Nord2000: *Comprehensive Outdoor Sound Propagation Model. Part1: Propagation in an Atmosphere without Significant Refraction* [25], sound that directly radiates from the source S to the receiver R interferes with sound that propagates on a secondary path that reflects from the ground as seen in Figure 2.9.

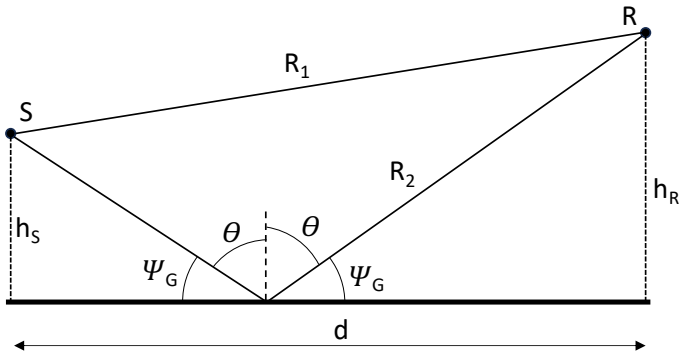

Figure 2.9.: Propagation on Flat Ground

The sound pressure p at the receiver position can be calculated with Eq (2.14), where $k = 2\pi f/c$ is the wave number calculated from the frequency f and the speed of sound c, R_1 is the length of the direct path, and R_2 is the length of the reflective path between the source and the receiver [25].

$$p = \frac{e^{jkR_1}}{R_1} + Q\frac{e^{jkR_2}}{R_2} \tag{2.14}$$

The factor Q is a function dependent on the ground impedance Z_g, the grazing angle Ψ_g and R_2. The calculation of Q is also described in [25] and defined in Eq.(2.15), with the plane wave reflection coefficient $R_p(\theta)$ described in Eq.(2.16) and the function $E(\rho)$ calculated with Eq.(2.18). The reflection angle θ is calculated from the grazing angle Ψ_g as: $\theta = \pi/2 - \Psi_\mathrm{g}$. The ground impedance, can be calculated with the flow resistivity σ_g and the frequency f in Hz, as seen in Eq. (2.17).

$$Q = R_\mathrm{p}(\theta) + (1 + R_\mathrm{p}(\theta))E(\rho) \tag{2.15}$$

$$R_\mathrm{p}(\theta) = \frac{\cos(\theta) - \frac{1}{Z_\mathrm{g}}}{\cos(\theta) + \frac{1}{Z_\mathrm{g}}} \tag{2.16}$$

$$Z_\mathrm{g} = 1 + 9.08\left(\frac{1000f}{\sigma_\mathrm{g}}\right)^{-0.75} + j11.9\left(\frac{1000f}{\sigma_\mathrm{g}}\right)^{-0.73} \tag{2.17}$$

$$E(\rho) = 1 + j\sqrt{\pi}\rho w(\rho) \tag{2.18}$$

The factor ρ is calculated with the length of the reflective path R_2 with Eq.(2.19).

$$\rho = \frac{1+j}{2}\sqrt{kR_2}\left(\cos(\theta) + \frac{1}{Z_g}\right) \tag{2.19}$$

The $w(\rho)$ function is defined with the factor ρ and the error function erfc in Eq. (2.20). This function can approximated with Algorithm 2 in appendix A.

$$w(\rho) = e^{-\rho^2}\mathrm{erfc}(-j\rho) \tag{2.20}$$

The correction of the sound pressure with ground reflection compared to the sound pressure in free field can then be calculated with

$$L_\mathrm{g} = 20\log\left(\left|1 + \frac{R_1}{R_2}Qe^{jk(R_2-R_1)}\right|\right). \tag{2.21}$$

The sound pressure level at a receiving point can then be calculated with the corrections in Eq. (2.12), (2.13), and (2.21) and the sound power level of a source in Eq. (2.10). Typical flow resistivity for the calculate of the ground impedance (see Eq. (2.16)) for different ground conditions is given in [25] and can be seen in Tab. 2.12.

Table 2.12.: Typical Flow Resistivity of Ground [25]

Flow Resistivity σ_g in $\frac{kNs}{m^4}$	Ground Description
12.5	Very Soft (snow or moss-like)
31.5	Soft Forest Floor (short, dense heather-like or thick moss)
80	Uncompacted, loose ground (turf, grass, loose soil)
200	Normal uncompacted ground (forest floors, pasture field)
500	Compacted field and gravel (compacted lawns, park area)
2000	Compacted dense ground (gravel road, parking lot)
20000	Hard Surface (dense asphalt, concrete, water)

2.4.2. Track Sections

For modelling moving sources, the two propagation models Nord2000 [1] and CNOSSOS [2] make use of the source line segment method. This method introduces source line segments that explain the movement of a source as seen in Figure 2.10. The sound exposure $L_{E,ij}$ at a receiving point from j-th source moving along s-th segment can be calculated with Eq. (2.22), where T_0 is the reference duration of 1 s, t_1 is the point in time when the source enters the segment, t_2 is the point in time when the source exits the segment, and $L_p(t)$ is the sound pressure level at the receiver in time.

$$L_{E,js} = 10 \log \left(\frac{1}{T_0} \int_{t_1}^{t_2} 10^{L_p(t)/10} dt \right) \tag{2.22}$$

Assuming a constant speed v_{source} of the source and the length $l_{seg,s}$ of the segment s this can be simplified. Additionally the sound pressure level at the receiver, induced by the sound power of a source, can be assumed to be constant, if the distance between the source and the receiver does not change significantly. With this assumption the source line segment can be modelled as a single point source in the middle of the segment that radiates for the duration the source passes through the source line segment. With these assumptions the **SEL** $L_{E,js}$ can be calculated with Eq. (2.23), whereas L_W is the sound power level of the source and L_{corr} is term for the corrections, due to air attenuation, spherical divergence and ground reflection. [1]

$$L_{E,js} = 10 \log \left(\frac{l_{seg,s}}{v_{source}} 10^{(L_W + L_{corr})/10} \right) \tag{2.23}$$

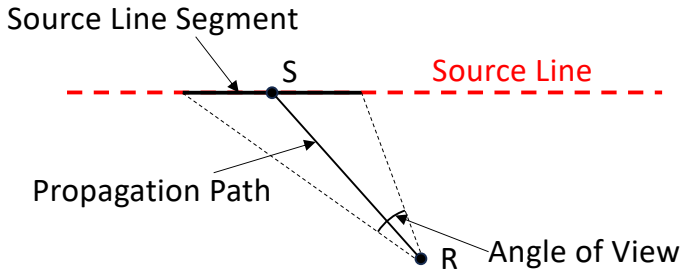

Figure 2.10.: Source Line Segment

The sound exposure $L_{\mathrm{E},j}$ at the receiver from the exposure of j-th source is then calculated with Eq. (2.24), where n is the number of segments.

$$L_{\mathrm{E},j} = 10 \log \left(\sum_{s=1}^{n} 10^{L_{\mathrm{E},js}/10} \right) \tag{2.24}$$

General requirements for segments are described in CNOSSOS [2] as:

- The speed and emission characteristics of the source may not change significantly within a segment.
- The terrain shape and surface properties should be consistent in the angle of view (see Figure 2.10) between the receiver and the source line segment
- The size of the segment should be smaller than the shortest distance between the receiver and the track
- The closest point of approach should be an end point of a segment

In Nord2000 [1] a specific methodology of finding appropriate segments sizes is described, while CNOSSOS refers to Nord2000 for the methodology to find segment sizes. The method to find the segment sizes introduces three boundaries:

$$\begin{aligned} l_{\mathrm{seg,max}} &= 5 - 10 \text{ m}, \quad \text{lower figure may be used when close to the track} \\ \beta_{\mathrm{max}} &= 10^\circ \text{ (0.175 rad.)}, \\ RD_{\mathrm{min}} &= 0.75. \end{aligned}$$

To find the appropriate size of segments Algorithm 1 can be performed, where l_{seg} is the length of the segment, β is the angle of view, and RD is the ratio between the distance from the receiver to the closest point of the segment and the distance from the receiver to the farthest point of the segment.

Algorithm 1 Segmentation of Source Line

if $l_{seg} \leq l_{seg,max}$ **then**
  Do not split segment;
end
else if $l_{seg} > l_{seg,max}$ ***AND*** $(\beta > \beta_{max}$ ***OR*** $RD < RD_{min})$ **then**
  if $\beta > \beta_{max}/2$ **then**
    Split segment such that angles of view of new segments are equal;
  end
  else
    Split segment at midpoint of segment
  end
end
Repeat for all newly created segments until no new segments are created;

The position of the source within a segment is on the line that bisects the angle of view β equally, IF β is bigger than $\beta_{\max}/2$, otherwise the source is positioned in the middle of the segment. [1]
This procedure can be repeated for all sources and the total **SEL** of all sources L_{E} can be added with Eq. (2.25), where m is the total number of sources.

$$L_{\mathrm{E}} = 10 \log \left(\sum_{j=1}^{m} 10^{L_{\mathrm{E},j}/10} \right) \tag{2.25}$$

This procedure can be performed for a whole spectrum or any type of frequency bands.

2.5. Machine Learning Algorithms

This section gives a short overview of statistic models and machine learning algorithms that are relevant for the modelling approach.

2.5.1. Linear Regression

This section gives an introduction to linear regression models with one independent input variable, also called simple linear regression. Considering a dataset with two variables x_i and y_i with an arbitrary relationship a linear relationship can be formulated as seen in Eq. (2.26) [27], where β_0 is the intercept, β_1 is the slope, and ε the error of each data entry.

$$y_i = \beta_0 + \beta_1 x_i + \varepsilon \tag{2.26}$$

The error between the regression curve and the data entries is evaluated with the least square method and minimised for all data entries [27]. The least square error criterion for a dataset with N number of entries can be formulated with Eq. (2.27) [27].

$$S(\beta_0, \beta_1) = \sum_{i}^{N} (y_i - \beta_0 - \beta_1 x_i)^2 \tag{2.27}$$

For better illustration, some dummy data has been created, that follows the function $y = 2x + 3$. Additionally random noise is induced. Creating the 100 entries the linear relationship between x and y can be estimated quite well with a linear regression model, as seen in Figure 2.11. More data would lead to a better approximation of the linear relationship between x an y, as it is assumed, that the noise is uncorrelated.

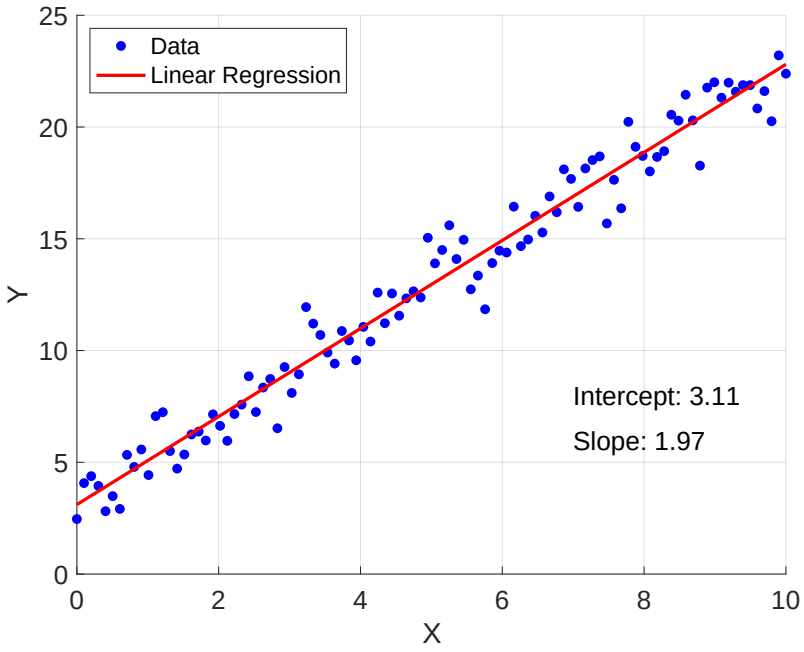

Figure 2.11.: Linear Regression on Dummy Data

2.5.2. Neural Network

A neural network is another method that can be used to model the relationship between two variables. A neural network is composed of several neurons in several layers that are connected with transfer functions. The simplest neural network with one neuron is shown in Figure 2.12. Multiple inputs $x_1 ... x_n$ with certain weights $w_1 ... w_n$ and the bias b are added in the neuron. A transfer function $f(x)$, or activation function, is performed on the sum and given as output. Multiple options for the transfer function are possible and used. Common transfer functions are the Sigmoid-function $\sigma(x)$ (see Eq. (2.28)) and the $\tanh(x)$-function [28].

$$\sigma(x) = \frac{e^x}{1 + e^x} \tag{2.28}$$

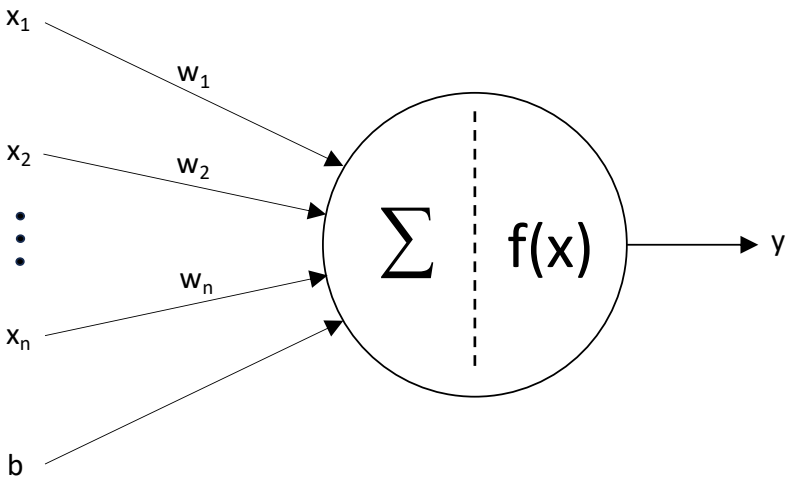

Figure 2.12.: Single Neuron Network [29]

A more complex neural network can be built by connecting several neurons in multiple layers as seen in Figure 2.13. Input parameters and a bias are given to each neuron with weighting in the first hidden layer 'Layer 1'. The neuron performs the same calculation as mentioned before, summing up its inputs and applying a transfer function on the sum. The output of that neuron is given with weighting to all neurons in the second hidden layer 'Layer 2' and the same procedure is followed. It is possible to introduce a bias in each layer. The last layer represents the output layer. The number of neurons and hidden layers is variable and the number of input neurons in the input layer and the output layer is dependent on the data structure at hand.
When training a neural network, the weighting factors are trained to fit the output to real values from a dataset.

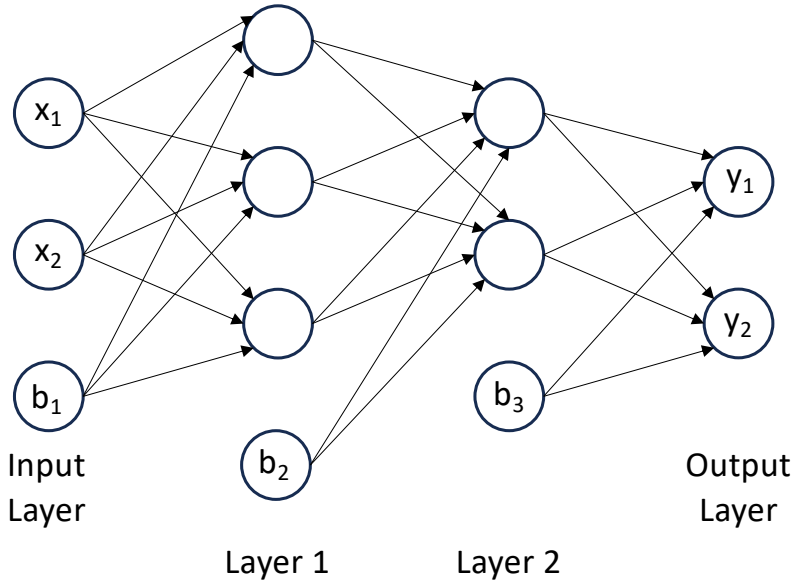

Figure 2.13.: Feed Forward Neural Network [29]

2.5.3. Decision Tree

Another approach to estimate the relationship is a binary decision tree. Again, two variables x and y in a dataset are considered and it is sought after to predict the output y with an input x. To build a decision tree, the values of x in the dataset are split up into two non overlapping sets of data. For example all entries in the dataset, where $x < 5$ is fulfilled are gathered in dataset A, while the other entries are gathered in dataset B. The prediction of y from the two datasets are then just the mean-averages of the responses y in each dataset. The datasets A and B can then be further split up into more branches. [30]
Considering the same dummy data, used in section 2.5.1 the prediction can be seen in Figure 2.14. To find the prediction from a certain input, one follows the decision tree seen in Figure 2.15. In this example one numerical variable was used to predict another, even though it is also possible to use categorical inputs and multiple variables to build a decision tree.

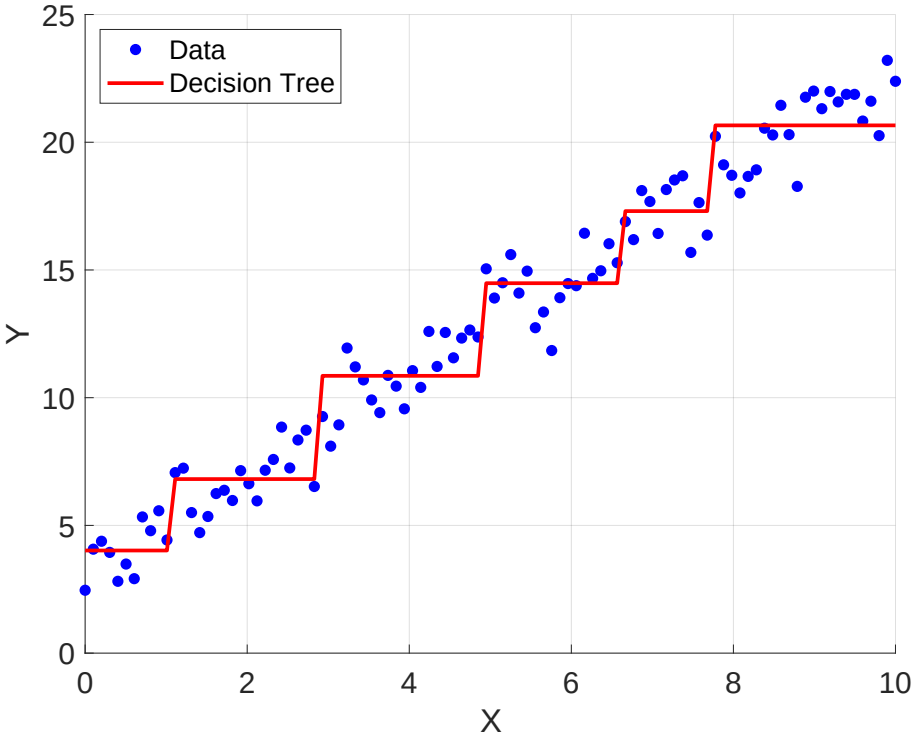

Figure 2.14.: Prediction of Decision Tree

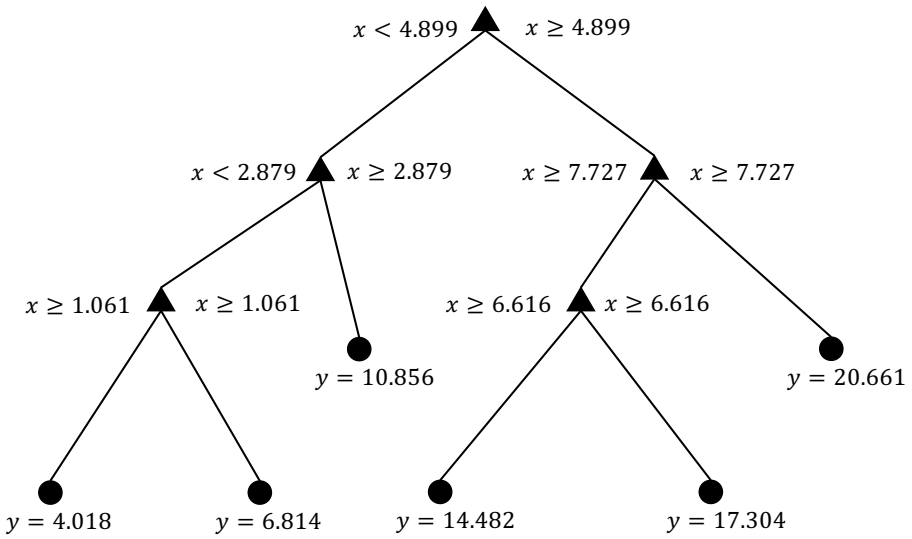

Figure 2.15.: Nodes and Leaves of Decision Tree

3. Methodology

3.1. Available Data

Two main datasets of pass-by measurements of trains have been used for this thesis. All datasets either include the **SEL** of train pass-by measurements or data that can be converted into the **SEL**, measured according to SS-EN ISO 3095:2013 [31]. In this measurement procedure the microphone is placed at a distance of 7.5 m from the center point between the two rails and at a height of 1.2 m above the top of the rail.
The two datasets are here referred to as

- Trafikverket data, and
- ProRAIL data.

The data in these datasets is available in third octave bands in a wide frequency range. It was decided that the third octave bands of interest for all calculations are the third octave bands from 40 Hz to 6.3 kHz.

3.1.1. Trafikverket Data

This dataset is a result of several measurement series and therefore an accumulation of many unrelated measurements. Additionally to the microphone height of 1.2 m the sound pressure level was also measured at a height of 4 m, while maintaining the horizontal distance from the track. This dataset contains descriptive and quantitative data, like the length of the train, speed, number of axis, and train type. After pre-processing the dataset, to exclude incomplete data entries, the number of measured train pass-bys is 293. In this dataset the train types are described with an abbreviated code. The codes for the train types and the number of measurements of each train type can be seen in Tab. 3.1

Table 3.1.: Train Types contained in Trafikverket Dataset

Train Type	Nr. of Measurements	Train Type	Nr. of Measurements	Train Type	Nr. of Measurements
ER1	8	PT	5	X50	25
FLIX	5	X11	12	X55	8
GTD	8	X2	36	X60	46
GTE	25	X31	55	X74	15
GTK	2	X40	24	Y31	19

3.1.2. ProRail Data

This dataset is provided by ProRail and results from several permanent measurement stations in the Netherlands. These measurement stations also automatically read the train parameters i.e. length, speed, and type. They were in service for several years and therefore a big number of measurements were accumulated. The dataset is already pre-processed to exclude incorrect measurements, measurements with extreme weather conditions, etc.. The final dataset contains roughly 200000 measurements.

3.2. Connecting Sound Power to Measured Data

The measurement data contains the exposure from the trains in the from of the **SEL**. As the radiation from the trains, independent of the surrounding, is of interest, the measurement data is transformed to source-describing values, the sound power level L_{W} of a train. In the propagation model in section 2.4 a method to calculate the **SEL** at a microphone position from the sound power of a moving source is described. Calculating the sound power from the **SEL** is done by formulating a **LQS**, that connects the sound power of several moving sources with the **SEL** at several microphones.
General assumption were made: The flow resistivity σ_g of the ground is constant (see Eq. (3.1)), as the ground is assumed to be compacted dense ground. With the yearly average temperature and humidity in Sweden (10 °C, 80%) the attenuation of the atmosphere is according to ISO 9613-1 [26].

$$\sigma_g = 2000 \, \frac{\mathrm{kNs}}{\mathrm{m}^4} \tag{3.1}$$

The moving sources along the track are modelled as following a path between the two rails, at a horizontal distance of 7.5 m from the microphones. If the moving sources were modelled on microphone-facing outer surface of the train, the geometry of the train would have to be taken into account. With the approach of modelling the sources between the rail, this can be avoided.

Linear Equation System

While the calculation of the **SEL** at a given position is possible with known sound power levels of equivalent sources, calculating the sound power levels from measured **SEL** inverses the problem and the calculation procedure is not straight-forward anymore. For this reason the propagation model described in section 2.4 is formulated as a **LQS**. A similar approach has been carried out by Taraldsen [32], where the emission from cars was connected to the exposure level at receiving points. The measured **SEL** is then a result from the emitted sound from the different sources on the train. The goal is to have a **LQS** as seen in Eq. (3.2), where the sound power of the sub sources in $\vec{W}$ is connected with a transfer matrix $\boldsymbol{T}$ to the measured sound exposure $\vec{E}$ at the microphone positions.

$$\boldsymbol{T}\vec{W} = \vec{E} \tag{3.2}$$

The transfer matrix $\boldsymbol{T}$ contains the transfer paths from each source j to each microphone k. The terms in the transfer matrix are constructed from the linear correction terms in section 2.4. The linear correction terms are lin_{a} for the air attenuation (see Eq (3.3)), lin_{d} for the spherical divergence (see Eq. (3.4)), and lin_{g} for the ground reflection (see Eq. (3.5)). The time the exposure is present from one segment is incorporated into the model with the time correction factor t_{c}, seen in Eq. (3.6), with l_{seg} as the segment length in m and v_{t} as the speed of the train in m/s.

$$lin_{\mathrm{a},jk} = 10^{(\frac{-\alpha d}{1000})/10} \tag{3.3}$$

$$lin_{\mathrm{d},jk} = \frac{1}{4\pi d^2} \tag{3.4}$$

$$lin_{\mathrm{g},jk} = \left|1 + \frac{R_1}{R_2} Q e^{jk(R_2 - R_1)}\right|^2 \tag{3.5}$$

$$t_c = \frac{l_{\mathrm{seg}}}{v_{\mathrm{t}}} \tag{3.6}$$

The transfer path between the source and the microphone is then described purely with the factors in Eq. (3.3) - (3.6). The exposure E_k at a microphone k is then the combination of the exposure from the sub sources j when passing through all segments s. Assuming that the sound power of the sources is the same in each segment leads to Eq. (3.7).

$$E_k = \sum_j^J \Big(\sum_s^S (lin_{\mathrm{a},jks}\ lin_{\mathrm{d},jks}\ lin_{\mathrm{g},jks} \cdot t_c) \Big) W_j \tag{3.7}$$

With Eq. (3.7) the transfer matrix $\boldsymbol{T}$ can be constructed to connect the sound power directly to the measured exposure. The element at position $[k, j]$ in the transfer matrix $\boldsymbol{T}$ is then:

$$\mathbf{T}_{k,j} = \sum_s^S (lin_{\mathrm{a},jks}\ lin_{\mathrm{r},jks}\ lin_{\mathrm{g},jks} \cdot t_c). \tag{3.8}$$

With this method the exposure $\vec{E}$ at several microphones can be connected to the sound power $\vec{W}$ of many sources that are moving along a path. A visual representation can be seen in Figure 3.1.
This procedure is repeated for all third octave bands from 40 Hz to 6.3 kHz to calculate the levels in third octave bands. The number of segments is a less crucial part of the calculation, as long, as the furthest segment does not have a significant influence on the total **SEL**. The number of segments was chosen, so that the furthest segment is one train-length away from the microphone.
When calculating the ground reflection correction (see. Eq. (3.5)), it is possible that the center frequency of the third octave band of interest results in a sharp reduction of sound pressure at the receiver position. This is not necessarily representative for the whole range of the third octave band. In [25] a method with Fresnel-zones was used to address this issue. In this case, several frequencies within the range of the third octave band were used to calculate the ground reflection. For that purpose the centre frequency of the third octave band f_c was used to calculate the range of the third octave band, with the lower bound f_l and upper bound f_u as seen in Eq. (3.9) and (3.10).

$$f_{\mathrm{u}} = f_c \cdot 10^{0.05} \tag{3.9}$$

$$f_{\mathrm{l}} = f_c / 10^{0.05} \tag{3.10}$$

Then the ground reflection correction for 10 frequencies between the upper and lower bound for the third octave band of interest were calculated. The resulting ground reflection corrections were averaged to find a more representative ground reflection correction for the whole third octave band.

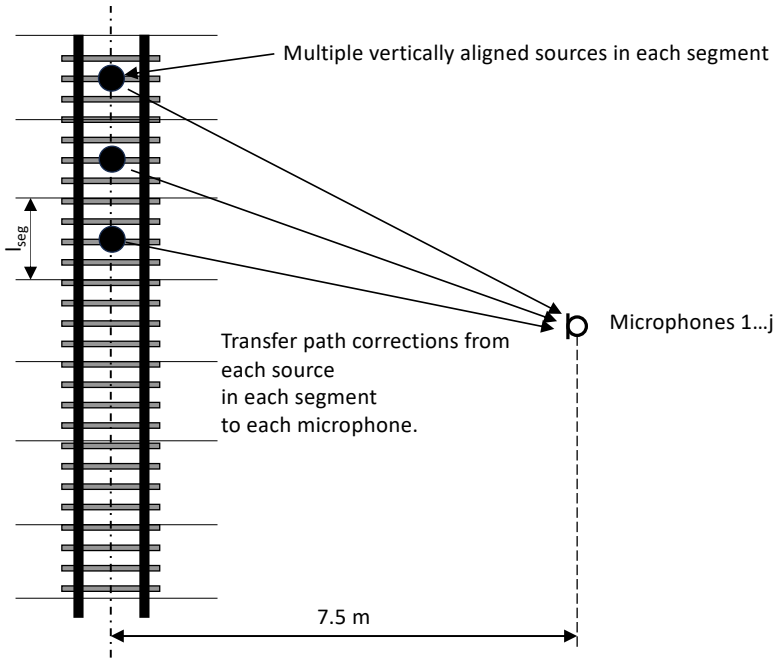

Figure 3.1.: Top-down View of Model

3.3. Estimation of Total Sound Power

For the estimation of the total sound power of a train, it has to be constructed from the measured **SEL**. In section 3.2 the procedure is explained in detail. As it is sought after to use the default source positions in Nord2000 (see Tab. 3.2) a similar assumption as in Nord2000 is made: The sound power level of the sub sources is equal.
In the context of the transfer matrix $\boldsymbol{T}$, this results in an addition of the columns of $\boldsymbol{T}$. The sound exposure E at a microphone can then be calculated with the sum of its corresponding row in $\boldsymbol{T}$ and the sound power W_j of one sub source. Solving for the sound power of sub source gives the sound power of all other sub sources, as it is assumed, that their emission equal. The height of the top of the rail above the ground is assumed to be 0.2 m.

Table 3.2.: Assumed Source Heights

Source	Height above top of rail (m)
Source 1	0.01
Source 2	0.35
Source 3	0.70
Source 4	2.5

To predict the sound power of a train from known train parameters, like the train type and train speed, different prediction models were used and tested for their performance. The implemented prediction models are:

- Linear Regression Model,
- Neural Network,

- Decision Tree.

The performance of the models is measured with the root-mean-square-error (**RMSE**), defined in Eq. (3.11), where y_i are the measured values, $\hat{y}_i$ are the predicted values, and N is the number of datapoints. A lower **RMSE** represents a better fit of the predicted values to the measured values.

$$\mathbf{RMSE} = \sqrt{\frac{\sum_{i=1}^{N}(y_i - \hat{y}_i)^2}{N}} \tag{3.11}$$

This evaluation was only performed on a test dataset, that is not used to train the models.

3.3.1. General Data Preparation

As the Trafikverket Dataset contains measurement from Swedish train, this dataset is prioritised in this section. It should be noted, that when a sound power of a train is described in this section, that it is sound power per length of the train. The unit of that measure is then dB/m.
The Trafikverket dataset contains a large number of measurements, as well as descriptive data. After pre-processing the dataset to exclude incomplete entries, the dataset is further split up into subsets for each train type. Some train types only occur very seldomly in the dataset, therefore building a whole dataset out of very little data entries is undesired. For that purpose five additional datasets are built, that categorise the trains into five categories:

- High-speed Trains,
- Inter-city Trains,
- Regional Trains,
- Freight Trains with Cast Iron Block Brakes,
- Freight Trains with K-Block, Disc Brakes.

It is chosen, that the minimum amount of entries required to build a dataset for the train type is 10. With that constraint the trains can be categorised as seen in Tab. 3.3.

Table 3.3.: Train Categories

Train Types	Dataset
ER1, X2, X31, X40, X50, X55, X74	High-speed Trains
FLIX, PT, X60	Inter-city Trains
X11, Y31	Regional Trains
GTE	Freight Trains with Cast Iron Block Brakes
GTK, GTD	Freight Trains with K-Block, Disc Brakes
X11	X11
X2	X2
X31	X31
X40	X40
X50	X50
X60	X60
X74	X74
Y31	Y31

The subsets are further split up randomly into a training dataset and a test dataset. The ratio for this procedure is 90%/10%. The splitting up of the dataset into train types allows

the use of different models for each train type or category. It also ensures that all train types and categories contribute to the test dataset, that is not used for the training of the various prediction models. The test dataset is then representative for the whole dataset, as each train type occurs with the same ratio in the test dataset as in the whole dataset. The splitting of the dataset is only done for the linear regression model and the decision tree. A different method was used to distinguish between train types, when training the neural network, which is further described in section 3.3.3.
For convenience the input data that is used in each model is shown in Tab. 3.4. It is noted that v_t is the speed of the train in km/h.

Table 3.4.: Prediction Models and their Input

Model	Input
Linear Regression Model	$\log(v_\mathrm{t}/100)$
Neural Network	$\log(v_\mathrm{t}/100)$ Train Categories as Dummy Variables
Decision Tree	$\log(v_\mathrm{t}/100)$

3.3.2. Linear Regression Model

The linear regression model is similar to the current Nord2000 method, that predicts the sound power of a train from its speed v_t. Similarly to the Nord2000 method, the logarithmic value v_t is taken, as the generated sound power is closely coupled to $\log(v_\mathrm{t})$. As described in section 3.3.1, the data is split up into subsets for train types and categories. For each subset and each third octave band a linear regression model is build with inbuilt Matlab functions. For the training stage, only the training dataset is used, while the test dataset is set aside. The predominant Matlab functions to train and predict the linear regression model can be seen below. Feature and target are commonly used terms to describe the properties and variables of a specific case (**Feature**) and the response from these properties and input variables (**Target**).

```
% training a linear regression model with data
linear_regression_model = fitlm(feature, target);
% predicting with linear regression model
prediction = predict(linear_regression_model, feature);
```

The target variable represents the target values, that are to be predicted. In this case the targets are the sound power levels per meter of the train in each third octave band.
The feature variable describe known parameters about the train. As it is sought after, that the linear regression model has the same form as in Nord2000, as seen in Eq. (3.12), the feature variable contains information about the speed of the train v_t. The updated parameters a and b in Nord2000 (see. Tab. B.1) are based on the same dataset as used here.

$$L_{\mathrm{W,1\,m}} = a \cdot \log\left(\frac{v_\mathrm{t}}{100}\right) + b \tag{3.12}$$

With a linear regression of the training sets of the datasets seen in Tab. 3.3 the slope a and the intercept b are optimised for each third octave band.

3.3.3. Neural Network

Before training the neural network, the issue of the train types as qualitative data is addressed. This is done by encrypting the train types into binary dummy variables. This gives the neural network a quantitative value to detect which train type each case is. As described in section 3.3.1, the dataset is split into a training dataset and a test dataset, with the ratio 90%/10%.
For the neural network a feed forward network with two layers is used. The layer size is 8 neurons for the first layer and 8 neurons for the second layer. In each layer the transfer functions to the next layer are logarithmic Sigmoid functions. During the process of training the neural network a validation takes place. For that validation another 10% of the training dataset is used. This validation checks how close the predicted values are to the actual values, while not training with the validation data.
Contrary to the linear regression model described in section 3.3.2, where the sound power of each third octave band is predicted with a different linear regression model, the neural network predicts the whole spectrum in the trained frequency range. The input data for the neural network is then only the speed of the train v_t as $\log(v_t/100)$ and the dummy variable for the train category.
The neural network is then trained with the training dataset, while the test dataset is used to evaluate the performance with the **RMSE**, according to Eq. (3.11). The neural network is build entirely with in-built Matlab functions. The most important aspects of the implementation can be seen below.

```
% define neural network with the size of the layers
neural_network = feedforwardnet([8, 8]);
% define logarithmic Sigmoid transfer functions in the layers
neural_network.layers{1}.transferFcn = 'logsig';
neural_network.layers{2}.transferFcn = 'logsig';
% training the neural network
neural_network = train(neural_network, feature, target);
% make prediction with neural network
prediction = neural_network(feature);
```

3.3.4. Decision Tree

For the prediction of the total sound power of a train a decision tree was build for each dataset and each frequency band. Similarly to the linear regression model, the decision tree model uses the $\log(v_t/100)$ as input. The decision tree is build with in-built Matlab functions. The functions to build a decision tree and make predictions with a trained tree can be seen below.

```
% train decision tree
decision_tree = fitrtree(feature, target);
% make prediction with decision tree
prediction = predict(decision_tree, feature);
```

3.4. Sound Power Distribution over Equivalent Sources

A method to find an appropriate vertical sound power distribution is described in this section. The method makes use of a determined **LQS**, that connects the sound power of

equivalent sources to the exposure level at the microphone position. The linear factors are only dependent on the transfer path between the sub sources and the microphone positions, as described in section 3.2.
Defining as many sub sources as microphones results in a determined **LQS**. The **LQS** (see Eq.(3.13)) can then be solved with measured sound exposures $\vec{E}$, as seen in Eq. (3.14), with the $\boldsymbol{T}^{-1}$ as the inverse of the transfer matrix.

$$\boldsymbol{T} \cdot \vec{W} = \vec{E} \tag{3.13}$$

$$\vec{W} = \boldsymbol{T}^{-1} \cdot \vec{E} \tag{3.14}$$

The source heights in the construction of the transfer matrix are assumed and can be seen in Tab. 3.5. This procedure was carried out for the Trafikverket dataset.

Table 3.5.: Assumed Source Heights, Localization of Sources

Source	Sound Emission Mechanism	Height above Top of Rail (m)
Source1	Wheel/Rail	0.5
Source2	Aerodynamic Noise Traction Noise	2.5

For solving the **LQS** (see Eq. (3.14)) it was determined that the minimum sound power level of a sub source is 60 dB. This value acts as a lower bound that ensures the resulting sound power to be positive and non-zero.
Another issue arises when the rows of the transfer functions are almost co-linear. In this case, the **LQS** becomes under-determined and no vertical sound power distribution can be deducted.

4. Results

4.1. Estimation of Total Sound Power

As explained in section 3.3.1, the trains are categorised for their types. The train types that have very few entries on the dataset are collected in datasets for high-speed trains, intercity trains and regional trains. The train categories for the train type that were used can be seen in Tab. 3.3.

4.1.1. Linear Regression

The linear regression makes use of the same form as in Nord2000, as seen in Eq. (4.1). The updated parameters a and b in Nord2000 are based in the same database used here, although the parameters found here were different. The categorization of the data is done differently as well.

$$L_{\mathrm{W,1\,m}} = a \cdot \log\left(\frac{v_{\mathrm{t}}}{100}\right) + b \tag{4.1}$$

The factors a and b can be seen in Tab. 4.1. As the parameter a is the slope of the linear regression it is referred to as the speed dependency of the model. For each dataset notable aspects of the linear regression model are pointed out. Generally the speed dependency is quite frequency dependent. The intercept b can hardly be interpreted without the slope a as context.

- In the linear regression with the **High Speed Dataset**, it can be seen that the speed dependency is greater at frequencies around 80 Hz and 2 kHz, while there is very little speed dependency in the third octave band of 500 Hz.
- The linear regression with the **Inter-city Dataset** results in a very high speed dependency, especially for the frequencies around 2 kHz. While there is still a strong speed dependency at the frequencies around 630 Hz, the intercept is significantly higher than in other frequency bands.
- The dataset of **Regional Trains** yields parameters for the linear regression, that suggest a stronger speed dependency for the frequencies around 100 Hz, while there is a mild speed dependency in other frequency bands.
- In the linear regression with the dataset for **Freight Trains with Cast Iron Block Brakes** it can be seen that the speed dependency is relatively high at frequencies below 80 Hz. Between the frequencies of 100 Hz and 400 Hz the speed dependency is even negative. Above 500 Hz the speed dependency is again positive.
- In the linear regression model with the dataset for **Freight Trains with K-Block, Disc Brakes**, the speed dependency is relatively low between up to 200 Hz. Between 250 Hz and 1 kHz the speed dependency is negative and again slightly positive above 1 kHz.
- The linear regression with the **X11**-dataset yields speed dependencies that are either slightly positive or slightly negative.
- The linear regression resulting from the **X2**-dataset gives a high speed dependency at lower frequencies, below 160 Hz. In the frequency bands from 250 Hz to 800 kHz

the emission is almost not speed dependent. At frequencies above 800 Hz the speed dependency is again more apparent.

- The linear regression with the **X31**-dataset results in a model, that has a high speed dependency below 200 Hz and above 630 Hz. In the frequencies around 400 Hz the speed dependency is reduced.
- The **X40**-dataset and its linear regression shows a significant speed dependency between in all frequency bands but is reduced at 50 Hz and around 630 Hz
- The linear regression of the **X50**-dataset yields a model that shows a positive speed dependency in all frequency bands. The speed dependency is strongest around the frequency bands of 80 Hz and 2 kHz, while being relatively low around 630 Hz.
- The linear regression resulting from the **X60**-dataset shows a negative speed dependencies below 500 Hz and above 2 kHz, with the exception of the 50 Hz frequency band. Strong positive speed dependency can be observed around 800 Hz.
- The linear regression with the **X74**-dataset shows a high speed dependency in all frequency bands, except for the 50 Hz and 400 Hz. The speed dependency is particularly high at 2 kHz
- The linear regression model resulting from the **Y31**-dataset yields strong positive speed dependencies in all frequency bands. The speed dependency is very high at 100 Hz.

Table 4.1.: Parameters of Linear Regression

Dataset		Parameters																						
	f in Hz	40	50	63	80	100	125	160	200	250	315	400	500	630	800	1000	1250	1600	2000	2500	3150	4000	5000	6300
High-speed	*a*	39.3	30.5	49.8	54.6	44.6	43.4	39.2	35.5	25.6	19.4	18.1	9.2	22.5	28.2	39.0	43.1	49.7	57.5	49.0	36.6	38.0	36.9	38.4
	b	85.4	87.9	82.8	81.2	80.7	79.1	79.7	81.1	83.4	85.4	86.9	90.2	89.7	91.6	90.7	87.9	85.8	84.0	83.4	82.1	79.8	78.6	77.0
Inter-city	*a*	44.6	26.4	37.8	46.5	39.6	37.9	41.1	46.3	42.1	37.3	34.7	32.1	32.6	45.0	62.5	54.9	73.0	91.8	74.7	76.3	59.3	58.3	51.4
	b	84.0	90.0	84.5	81.4	80.4	79.1	78.8	78.4	79.4	81.7	83.0	85.3	90.5	92.3	89.2	86.5	84.3	80.2	78.6	74.9	76.2	74.7	75.0
Regional	*a*	36.4	11.2	8.5	28.5	59.1	39.3	31.1	29.4	21.8	36.4	32.2	23.6	4.1	12.0	14.9	7.3	12.4	17.8	18.6	19.2	7.5	21.5	28.1
	b	88.7	93.9	92.1	90.7	87.2	87.3	85.5	84.7	86.0	85.6	88.3	91.7	97.2	100.2	97.8	95.7	95.5	93.8	90.9	86.4	86.3	84.3	81.8
Freight Trains Cast Iron Block Breaks	*a*	43.1	45.0	27.0	9.7	-1.1	-10.0	-11.2	-12.8	-20.8	-20.7	-16.6	10.5	30.9	35.1	35.0	40.8	46.9	39.6	25.7	20.2	21.0	23.5	25.8
	b	91.0	89.6	87.0	85.2	83.4	82.1	82.4	83.3	85.3	87.8	92.2	99.4	103.5	104.9	103.8	100.8	102.1	98.8	96.7	93.0	91.6	89.3	87.5
Freight Trains K-Block/Disc-Breaks	*a*	18.3	27.3	10.1	16.4	15.7	21.7	16.3	5.8	-7.5	-15.4	-18.0	-15.6	-10.9	-15.7	-12.8	6.6	2.9	5.5	1.4	2.1	6.7	9.5	13.4
	b	88.1	92.2	86.6	87.4	86.6	85.5	85.1	84.9	86.1	87.6	88.8	89.2	92.8	91.1	90.5	92.7	90.8	90.7	88.7	86.3	85.0	83.4	81.5
X11	*a*	1.6	7.0	7.3	7.9	-6.4	-3.9	-4.4	-3.3	-7.1	-9.5	-8.9	-6.5	0.6	0.9	-4.2	-3.0	-3.6	-12.2	-7.7	-9.4	-7.4	-1.7	-2.7
	b	88.7	97.0	93.9	90.4	86.8	87.3	86.7	85.7	87.3	86.3	88.7	93.4	101.5	105.4	101.2	98.1	98.7	96.5	93.4	88.8	88.1	85.7	82.7
X2	*a*	50.0	39.1	41.8	44.0	45.9	36.3	27.4	18.7	11.9	6.3	11.1	12.9	2.1	10.1	18.3	30.7	44.6	51.6	49.9	44.0	29.9	29.0	32.5
	b	82.1	85.2	84.1	82.4	79.8	79.8	81.9	85.7	87.2	89.0	88.5	90.3	95.9	99.1	98.4	94.6	91.5	89.0	85.9	83.6	84.1	82.1	79.6
X31	*a*	42.1	34.5	59.6	62.4	48.7	47.1	41.6	33.7	22.3	16.0	19.7	7.2	32.4	41.8	53.5	54.2	55.3	58.3	48.0	29.0	36.9	40.4	40.7
	b	86.3	87.3	82.2	81.2	81.1	79.2	79.9	81.1	83.9	85.7	86.8	90.7	88.5	89.7	89.2	86.6	83.8	82.3	82.5	82.1	78.8	77.9	76.3
X40	*a*	43.3	12.3	37.4	54.5	45.7	44.0	44.3	32.3	38.8	35.9	19.6	16.1	14.3	14.0	20.5	30.1	37.7	45.8	41.8	39.4	36.4	37.8	34.1
	b	84.5	91.8	85.9	82.9	81.4	79.8	79.4	82.1	83.3	84.3	87.8	88.3	90.0	93.0	93.6	89.5	88.2	86.1	83.8	80.2	79.2	77.7	77.0
X50	*a*	38.8	21.4	42.7	45.2	41.9	36.0	35.2	37.8	23.7	19.2	18.2	15.2	9.5	12.0	34.2	25.2	26.9	41.9	35.8	38.1	26.8	25.0	29.4
	b	85.6	90.7	85.0	81.9	80.4	79.4	79.4	78.9	80.5	82.6	85.3	88.2	93.0	96.4	92.4	90.4	90.2	87.3	86.1	81.6	81.9	81.4	78.8
X60	*a*	-22.2	21.2	-7.1	-23.3	-17.4	-19.9	-23.5	-19.7	-17.0	-11.1	-4.3	11.0	37.7	42.9	8.2	6.1	10.4	-18.4	-26.3	-24.2	-16.1	-26.2	-7.5
	b	88.1	91.1	87.1	85.3	83.7	82.4	82.7	82.2	82.7	84.5	85.2	86.4	90.1	92.7	92.3	89.3	87.8	85.9	83.7	80.1	80.2	79.3	78.2
X74	*a*	58.6	9.7	43.2	64.8	48.8	50.7	54.4	45.9	38.5	30.1	6.8	25.5	32.3	27.2	31.3	29.9	37.9	61.1	51.7	50.6	29.2	46.5	42.7
	b	82.7	91.2	83.5	79.0	80.1	77.6	76.2	77.8	79.0	82.0	89.1	87.4	89.3	93.4	94.4	91.0	89.1	84.8	83.3	79.0	80.4	76.8	76.8
Y31	*a*	25.3	24.5	24.2	37.2	66.1	40.2	35.0	35.0	28.1	38.1	39.3	38.0	36.7	49.1	39.0	25.8	35.7	34.7	31.3	29.6	17.0	28.9	30.2
	b	91.2	91.4	89.6	90.7	89.2	88.4	85.5	84.8	85.8	87.0	89.3	90.8	92.0	94.4	94.7	93.1	92.2	91.7	89.1	84.8	84.9	83.5	81.9

The speed dependency of the different models is also shown by using the parameters from Tab. 4.1 in combination with the Eq. (4.1). The speed dependent prediction is then plotted for speeds between 50 km/h and 200 km/h. One such visualization can be seen in Figure 4.1 for X2-trains in the X2-dataset. There it can be observed, that the speed dependency of the emission is relatively weak in the frequency bands around 500 Hz. The contribution from these frequency bands is already high at low speeds, while the main sound power contribution shifts to the frequency bands around 1 kHz at higher speeds. Another aspect is the low emission in the frequency bands around 50 Hz at low speed, while at higher speed significant emission can be observed in these frequency bands.

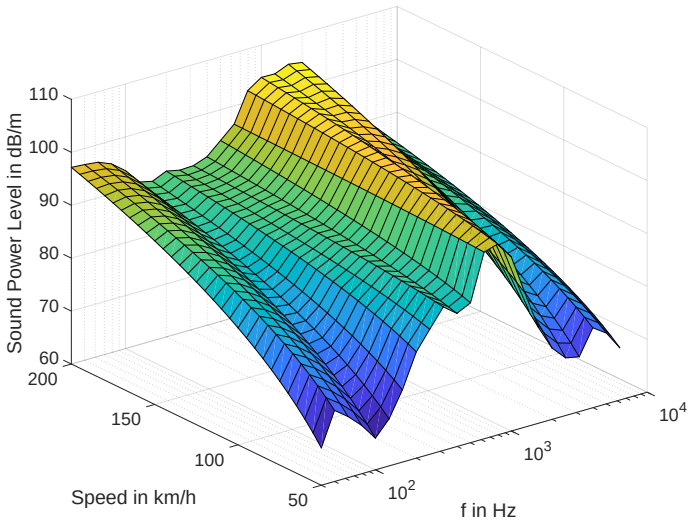

Figure 4.1.: Speed Dependency of Linear Regression for X2-Trains

Similar predictions can be observed for the linear regression calculated with the high-speed train dataset, seen in Figure 4.2. The emission at low speeds is more dominated by the 500 Hz frequency band, while more emission can be observed around 1 kHz and at low frequencies at high speeds. All visualizations of the linear regression models can be found in appendix D.

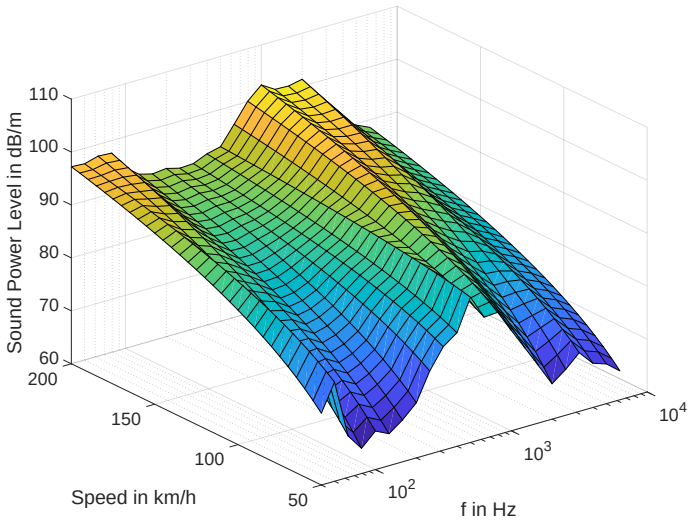

Figure 4.2.: Speed Dependency of Linear Regression for High-Speed-Trains

4.1.2. Neural Network

The weighting values and biases of the neural network to predict the total sound power of the train in dB/m are difficult to visualise and interpret. Nevertheless the weighting parameters are shown in Figure 4.3 for the weighting functions from the input to the Neurons in the first layer, in Figure 4.4 for the weighting functions from the neurons in layer 1 to the neurons in the layer 2, and in Figure 4.5 for the weighting functions from the neurons in layer 2 to the output neurons, the sound power level in third octave bands. Similarly the biases are shown in Figure 4.6 for layer 1 neurons, in Figure 4.7 for layer 2 neurons, and in Figure 4.8 for the output neurons.

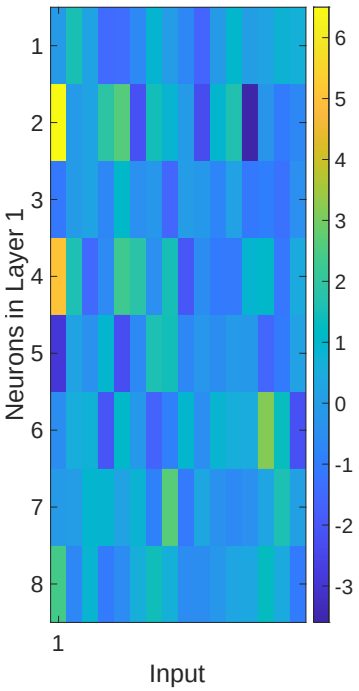

Figure 4.3.: Weights, Input to Layer 1 Neurons

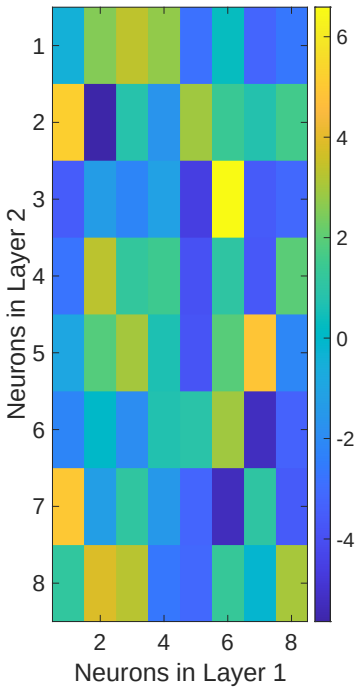

Figure 4.4.: Weights, Layer 1 to Layer 2 Neurons

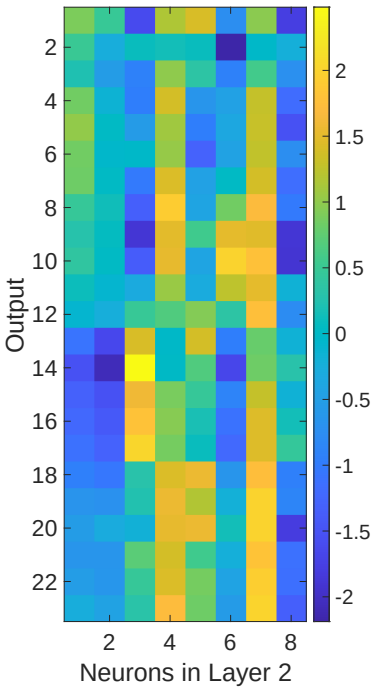

Figure 4.5.: Weights, Layer 2 to Output

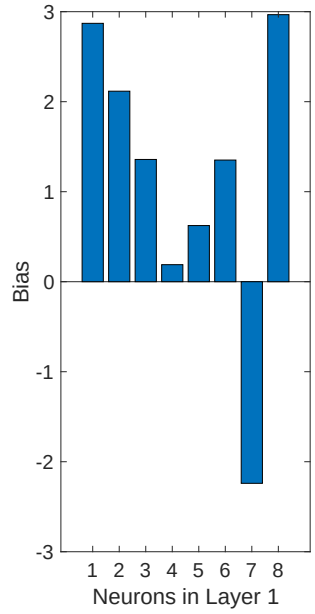

Figure 4.6.: Bias, Layer 1

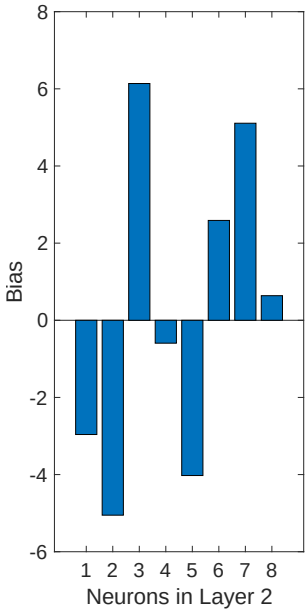

Figure 4.7.: Bias, Layer 2

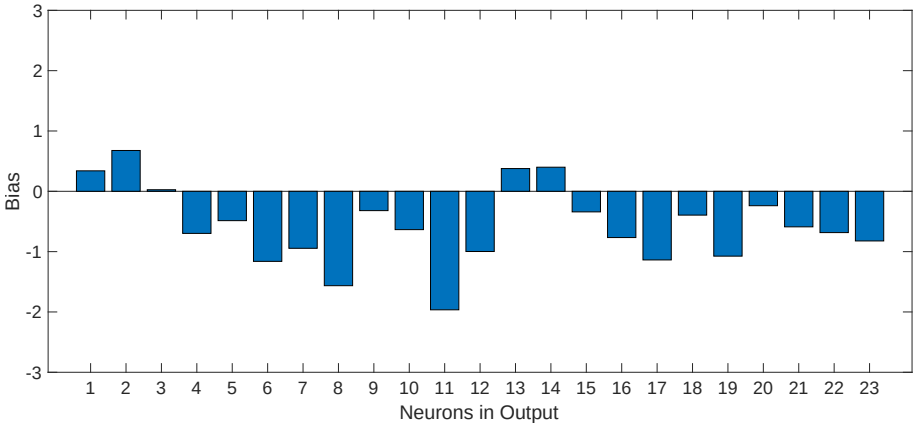

Figure 4.8.: Bias, Output

4.1.3. Decision Tree

As explained in section 3.3.4, several decision trees are built and trained. Showing all decision trees (for each dataset and each third octave band) is completely unfeasible. Interpreting the decisions of the decision tree is also not as straight forward as for example in the case of the linear regression model. Therefore the performance and predictions of the decision tree is the main result of the decision tree.

4.2. Comparison of Models and Current Prediction Models

In this section the **RMSE** (see Eq. (3.11)) for each model and the Nord2000 Method with each dataset is shown, as well as some specific cases of the test dataset and the prediction of the models on it. This evaluation of each model is done with the test dataset, that was not used to train the models.
For the calculation of the sound power with Cnossos, some assumptions are made. The

contact filter A_3 is for example dependent on the wheel diameter and wheel load, while the track transfer function $L_{\mathrm{H,tr}}$ is dependent on the pad stiffness and sleeper type. The following assumption are made in the Cnossos prediction model to calculate the sound power level of a train:

- A_3: Wheel Diameter: 920 mm, Axle Load: 100 kN
- $L_{\mathrm{H,tr}}$: Mono-block Sleeper on Medium Stiffness Railpad
- $L_{\mathrm{H,veh}}$ Wheel with Diameter 920 mm:
- $L_{\mathrm{R,Rail}}$: Averaged maintained network
- $L_{\mathrm{R,Wheel}}$: Depending on Train type

With these assumptions the sound power level from a train can be calculated. Generally the Cnossos prediction model gave significantly worse predictions than all other models. The **RMSE** of the Cnossos Method is also consistently higher than for other models. Two examples of the calculated sound power level with the Nord2000 method, linear regression model and Cnossos method can be seen in Figures 4.9 and 4.10. There it can be seen that the Cnossos method gives a significantly worse fit than both the Nord2000 method and the linear regression model, especially at low frequencies. The deviation as **RMSE** of the Cnossos model from the measured values is also generally higher. As the Cnossos method performs significantly worse than the Nord2000 Method and the models described above, it is not further considered.

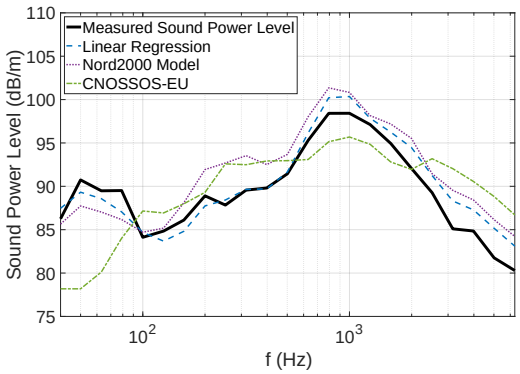

Figure 4.9.: Prediction of Total Sound Power of X2-train, $v_{\mathrm{t}} = 128\,\mathrm{km/h}$
RMSE Linear Regression: 1.8
RMSE Nord2000 Method: 3.0
RMSE Cnossos Method: 5.2

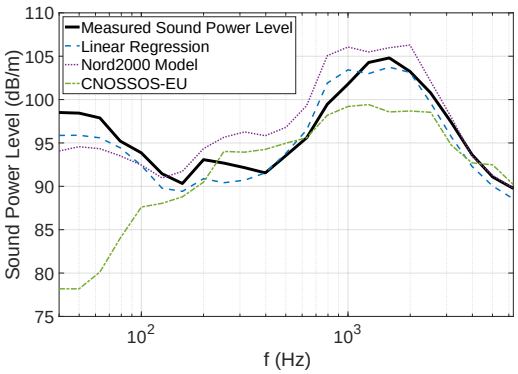

Figure 4.10.: Prediction of Total Sound Power of X2-train, $v_{\mathrm{t}} = 188\,\mathrm{km/h}$
RMSE Linear Regression: 1.6
RMSE Nord2000 Method: 2.9
RMSE Cnossos Method: 7.9

Table 4.2.: **RMSE** of Prediction Models

Dataset	**RMSE** in dB			
	Linear Regression	Neural Network	Decision Tree	Nord2000 Method
High-speed	2.8	1.9	2.9	3.0
Inter-city	6.0	5.6	6.1	5.3
Regional Trains	3.4	3.2	3.2	3.0
Freight Trains K-blocks and Disc Breaks	1.9	1.1	2.2	3.5
Freight Trains Cast Iron Block Breaks	4.0	6.2	4.0	4.9
X11	1.0	1.8	1.0	2.5
X2	1.8	1.7	2.0	3.0
X31	3.1	3.7	4.2	3.8
X40	2.3	5.3	2.3	3.8
X50	2.0	2.0	2.0	2.4
X60	5.2	6.2	5.9	3.5
X74	1.5	2.5	2.4	2.3
Y31	3.0	3.4	3.2	4.0

In Tab. 4.2 the **RMSE** of each model for each dataset is shown. It should be noted, that a lower **RMSE** represents a good performance of the model.
When considering the datasets, that combine the trains into categories (High-speed, Inter-city, Regional Trains) the neural network stands out for high-speed trains, while the other models still yield a good **RMSE**. For inter-city trains the **RMSE** are very high for all models. The Nord2000 method has a slightly lower **RMSE** than the other models. For regional trains all models perform similarly, with the Nord2000 method performing slightly better.
The performance of all models is relatively good for freight trains with K-Block or disc breaks. Especially the neural network stands out with its very low **RMSE**, while the **RMSE** of the Nord2000 method is higher than the other models. For freight trains with cast iron block breaks the neural network yields a very high **RMSE**. The linear regression model and the decision tree perform similarly, while the Nord2000 method performs slightly worse.
It can be seen, that the performance of the prediction models on the datasets of the specific train types of passenger trains (X11, X2, X31,...) is varying. The linear regression model performs relatively well in all these datasets, especially for the X11-, X2-, and X74-datasets, while only being significantly outperformed by the Nord2000 method in the prediction of X60-trains.
The neural network shows a similarly good performance for the X11-, X2-, and X50-datasets as the linear regression, though its **RMSE** are generally higher. The performance of the neural network is very bad for trains of the type X40, X60, and Y31.
Similar to the performance of the neural network, the decision tree shows a similar performance as the linear regression for the trains types X11, X2, and X50. Its performance is similar to the neural network, although its does yield an good **RMSE** for X40-trains. The **RMSE** of the decision tree in the X60- and X31-datasets is relatively high. The performance of the linear regression model and the neural network is also rather unsatisfactory in these datasets.

Comparing the Nord2000 method to the other models shows, that the Nord2000 method only outperforms all other models when predicting X60-trains. The Nord2000 method yields high **RMSE** for the X40- and Y31-datasets and shows higher **RMSE** in the datasets for X11, X2, and X50 trains than the other models. For trains of the type X31 and Y31 the Nord2000 method yields similar **RMSE** as the neural network or decision tree, while being outperformed by the linear regression.

Now the measurements and predictions of the test data are considered in more detail. For that purpose some cases in the test data are shown here. All cases of the test dataset are plotted in appendix D. The prediction of the sound power of a X2-train in the high-speed dataset can be seen in Figure 4.11. It can be observed, that all prediction models roughly follow the graph of the measured sound power level. The Nord2000 method slightly overestimates the sound power in the frequency bands form 100 Hz to 4 kHz. The linear regression model, neural network, and decision tree slightly underestimate the sound power level around 315 Hz and at high frequencies above 2 kHz. Generally all models give an adequate prediction of the sound power level and perform similarly. The overestimation from the Nord2000 method, especially in the frequency bands, where the maximum sound power level can be observed, around 1 kHz yields a higher total sound power level of the train when using the Nord2000 method.

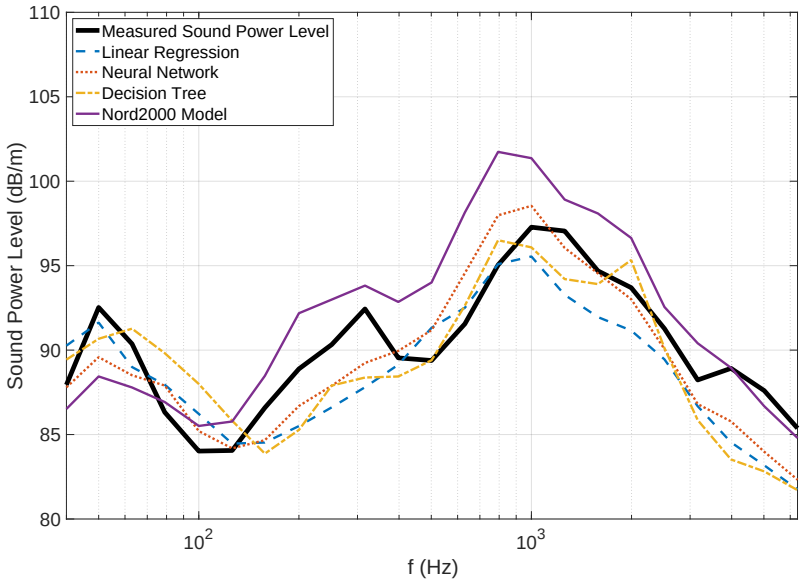

Figure 4.11.: X2-Train in High-speed Dataset, $v_t = 133\,\mathrm{km/h}$

Considering the prediction and measurement of a X2-train in the X2-dataset, as seen in Figure 4.12, it can be seen that all prediction models yield very good predictions of the sound power level of the train in each third octave band. A slight overestimation of the sound power level around 315 Hz from the Nord2000 model can be seen, while all models predict a lower sound power level at high frequencies than the measurement produces.

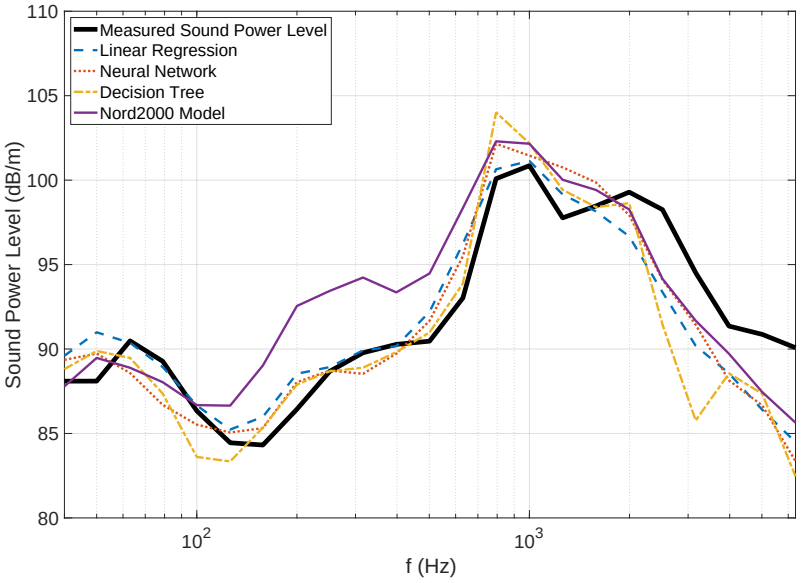

Figure 4.12.: X2-Train in X2-Dataset, $v_t = 141\,\mathrm{km/h}$

In some cases, the predictions from the neural network and decision tree deviate significantly from the prediction from the linear regression model, as well as the Nord2000 method. Comparing two measurements and predictions of X31-trains in Figures 4.13 and 4.14 with a similar speed, it can be seen, that even similar cases behave very differently. For the case shown in Figure 4.13 the linear regression and Nord2000 method yield a good prediction, while slightly overestimating the sound power above 100 Hz for this case. The neural network and decision tree yield a significantly overestimated sound power level, especially in the frequency bands around 800 Hz, where both of these models show a sharp peak in sound power level. In the case shown in Figure 4.14, the neural network and decision tree give an excellent prediction of the sound power level in all frequency bands, while the linear regression model and Nord2000 method significantly underestimate the sound power level, especially in the frequency bands around 800 Hz.

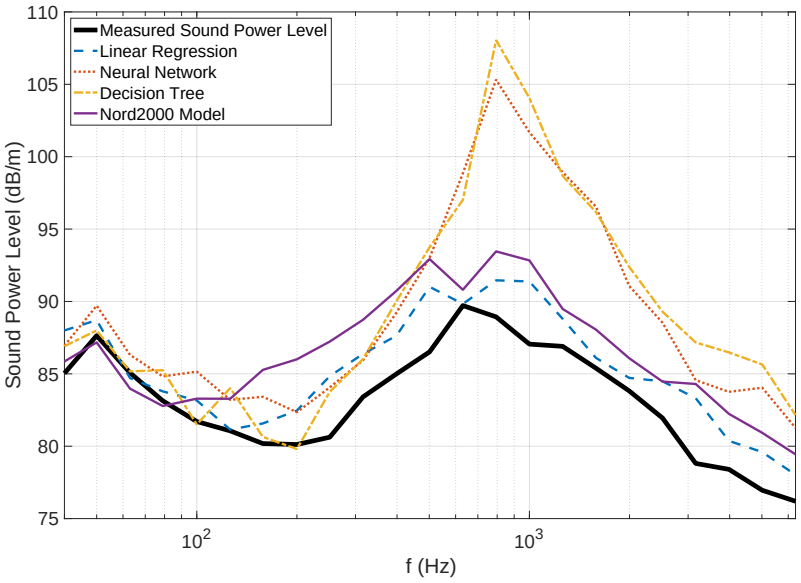

Figure 4.13.: X31-Train in X31-Dataset, $v_t = 110\,\mathrm{km/h}$

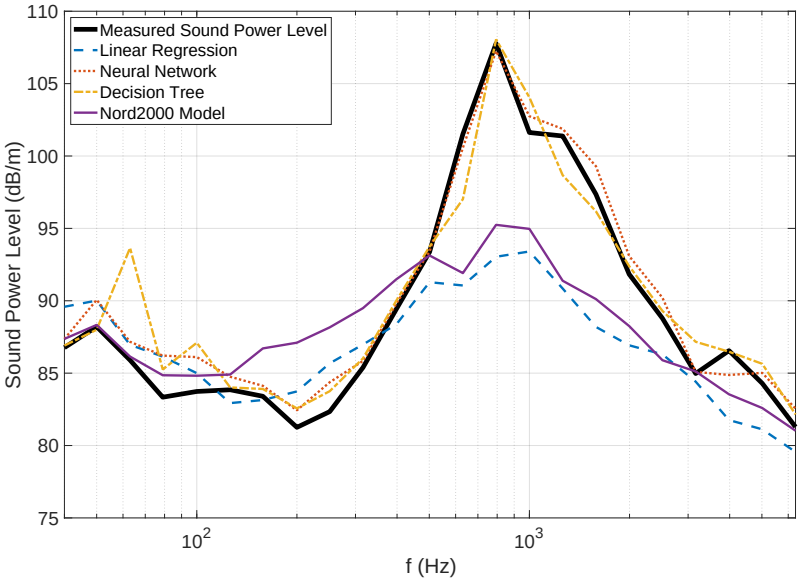

Figure 4.14.: X31-Train in X31-Dataset, $v_t = 120\,\mathrm{km/h}$

Considering the case of a X60-train shown in Figure 4.15, it can be seen that all models give a similar prediction of the sound power level and overestimate the sound power level around 800 Hz. The Nord2000 method also overestimates the sound power level around 315 Hz, while the other models give a good fit in this frequency range.

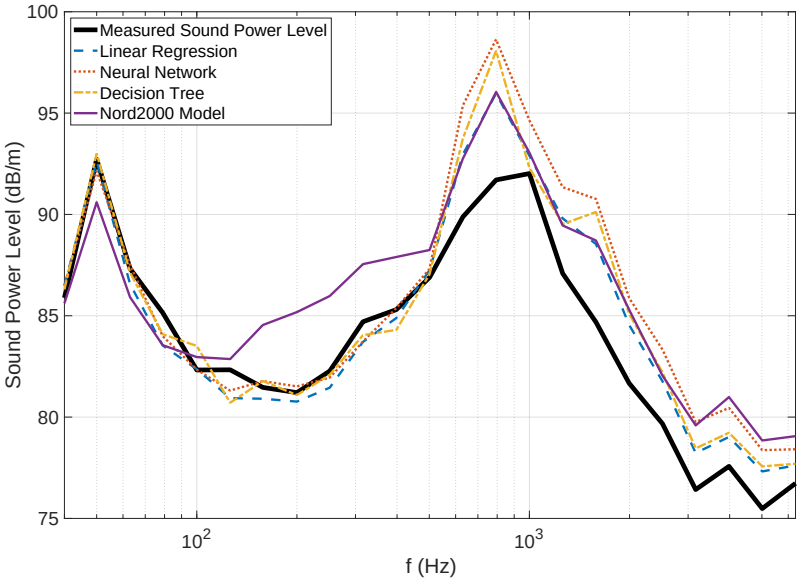

Figure 4.15.: X60-Train in X60-Dataset, $v_t = 119\,\mathrm{km/h}$

The overestimation of the sound power by the Nord2000 method in the frequency bands around 315 Hz can be observed in many cases. In the case of a X60-train, shown in Figure 4.16, the prediction of the sound power is quite good from all models. The prediction from the Nord2000 model overestimates the sound power around 315 Hz but yields similar predictions in the other frequency bands. This overestimation of the sound power level by the Nord2000 method can be observed throughout most measurements in the test data.

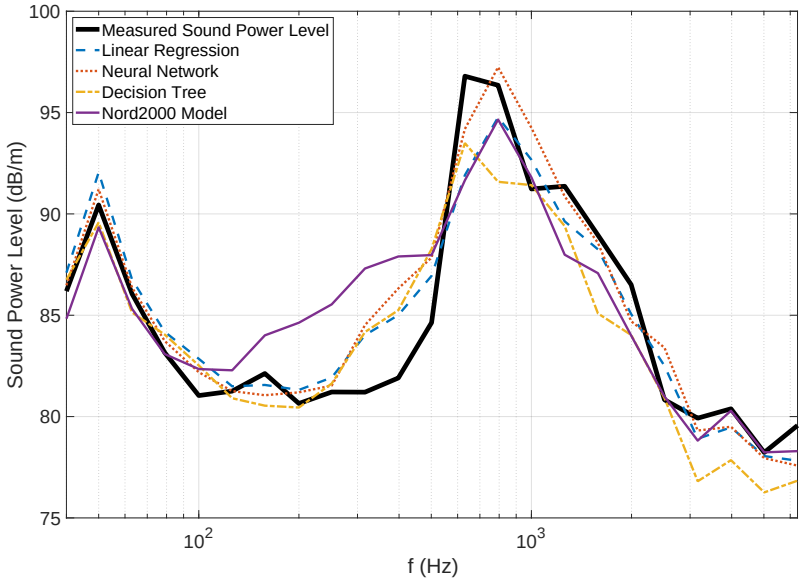

Figure 4.16.: X60-Train in X60-Dataset, $v_t = 112\,\mathrm{km/h}$

One aspect of the neural network and the decision can be seen for the case of a X40-train, seen in Figure 4.17. The prediction form neural network yields sharp peaks at 80 Hz and 2 kHz, while completely overestimating the sound power level around 800 Hz. It has to be noted, that the Nord2000 method also yields a significant overestimation between 1 kHz and 2 kHz, while the linear regression model and decision predict the sound power level from the train adequately. The best fit can be observed from the decision tree.

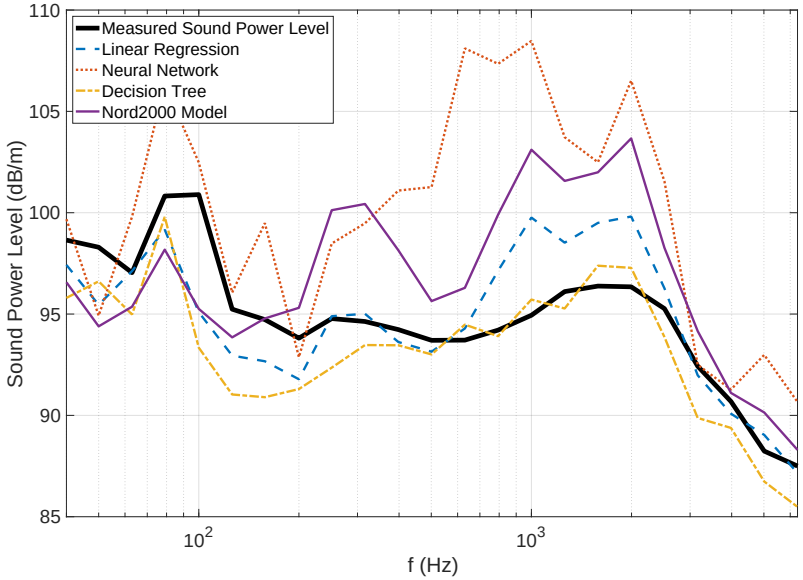

Figure 4.17.: X40-Train in X40-Dataset, $v_t = 199\,\mathrm{km/h}$

Another method to evaluate the models is to show the absolute deviations of each case in the test dataset. The mean, the 95th percentile, and the maximum deviation are shown in Figure 4.19.
Comparing the deviations of the models from the measured sound power level, it can be seen, that the maximum deviation is the lowest for the Nord2000 method, as it is only just

above 10 dB in the frequency bands of 800 Hz and 1.6 kHz. Comparing the 95th percentiles of the deviation of the Nord2000 method and the linear regression model, it can be seen, that they are relatively similar. The 95th percentile of the deviation is around 5 dB for both the linear regression and the Nord2000 method. Around the frequency bands of 1 kHz the 95th-percentile of the deviation is around 10 dB for both models. The maximum deviation is very close to the 95th-percentile of the deviation in case of the Nord2000 method. In case of the linear regression model, the difference between the maximum deviation and the 95th-percentile of the deviation is significantly higher, especially at frequencies below 315 Hz and above 1.6 kHz.
The maximum deviations of the neural network and the decision tree are both significantly higher. The maximum deviation is almost 20 dB around 1.6 kHz for the neural network, and almost 20 dB around 800 Hz for the decision tree. The 95th percentile of the deviations of both these models are both around 13 dB around 1 kHz, while it is comparable to the values of the linear regression and the Nord2000 method at frequencies around 315 Hz. Comparing the average deviation from all models it can be seen that the average deviation is in the realm of 2 dB to 4 dB. Especially noteworthy is the average deviation of the Nord2000 method in the frequency bands around 315 Hz and the increased average deviation at 800 Hz and 1.6 kHz for all models.

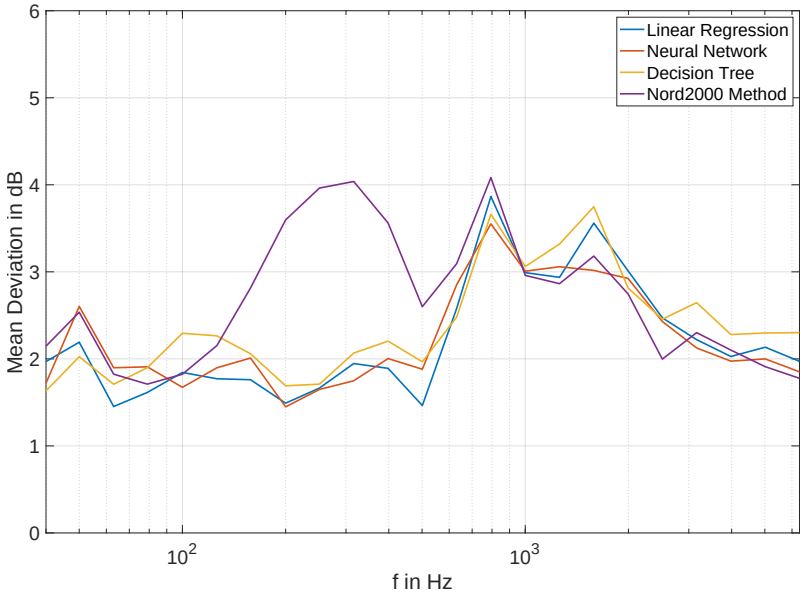

Figure 4.18.: Average Deviation of Prediction Models

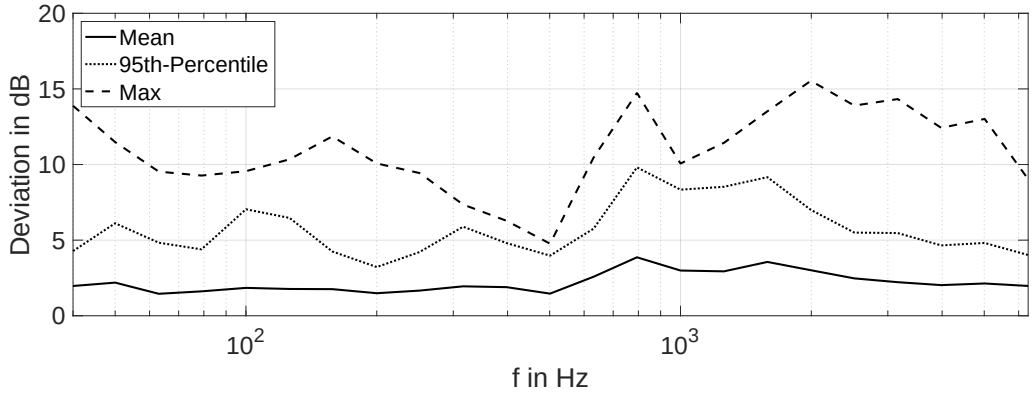

(a) Linear Regression

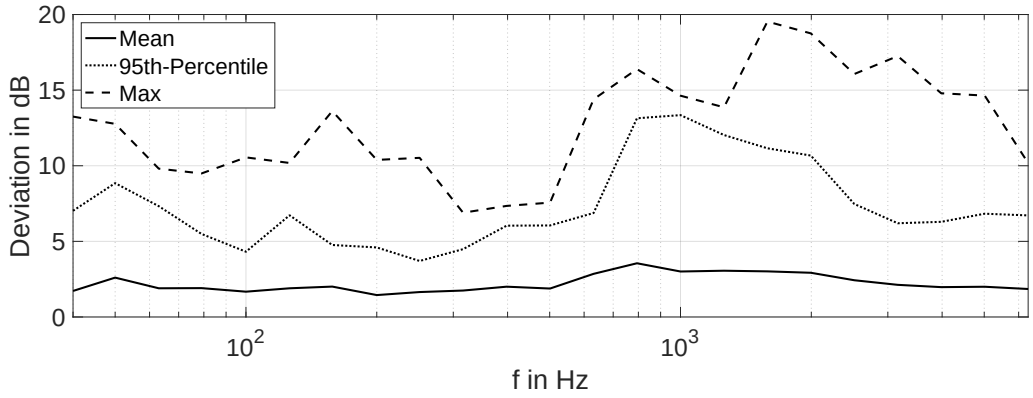

(b) Neural Network

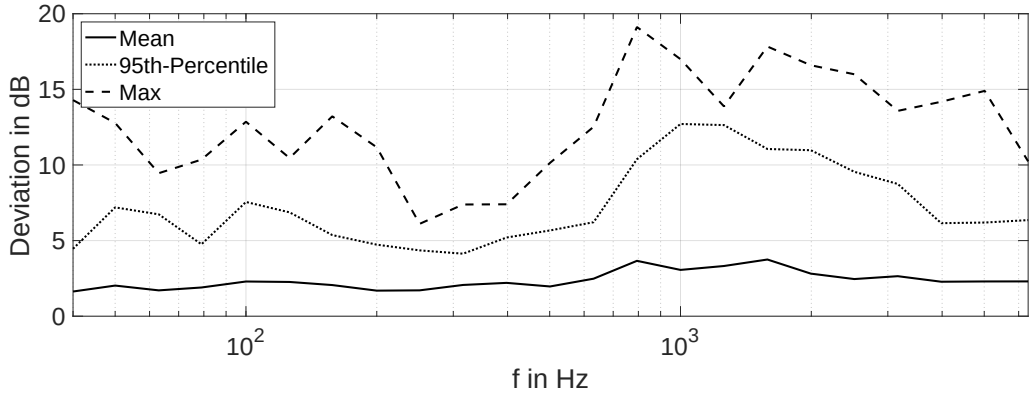

(c) Decision Tree

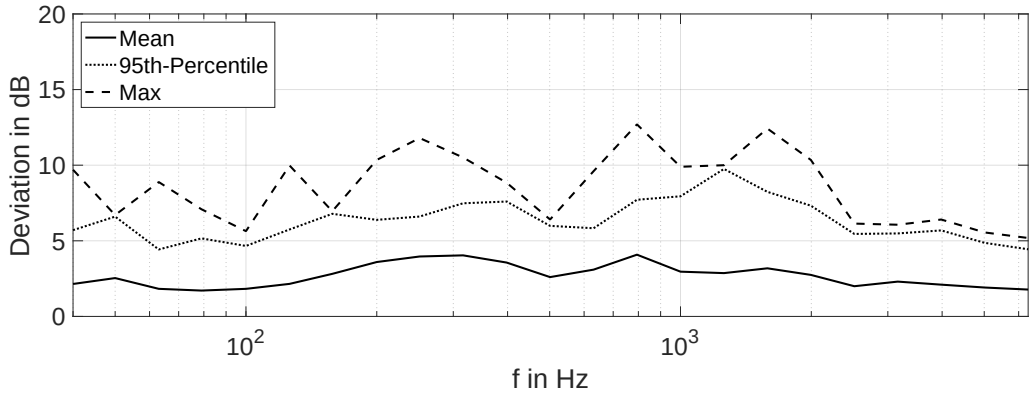

(d) Nord2000 Method

Figure 4.19.: Absolute Deviations of Prediction Models

It can be seen that the emissions of the trains, as sound power level, usually exhibit a maximum level around the 1 kHz third octave band. Calculating the total A-weighted sound power level over all frequency bands gives a single value, that is more easily comparable when assessing the total emitted sound power in the context of environmental noise for humans. For the entire test dataset the difference between the predicted and the measured total A-weighted sound power level is calculated for each case. These results can be used to assess whether the prediction under-estimates or over-estimates the emission of the train. This is done for all prediction models and each case of the test dataset, resulting in a spread around 0 dB, which represents a perfect prediction of the total A-weighted sound power level. The deviation of the total A-weighted sound power level is shown as box plots for all new prediction models and the Nord2000 Model in Figure 4.20. The box itself represents the 25th, 50th (median), and 75th percentile, while the whiskers show the 10th and the 90th percentile. The markers show the outliers, that are beyond the 10th or 90th percentile.
In Figure 4.20 it can be seen, that the boxplots are around 0 dB for the linear regression, neural network, and decision tree. The median of all these models is close to 0 dB. The current Nord2000 model has a median at 2.8 dB and the 75th percentile reaches only slightly below 0 dB.
The spread of the outliers is also noteworthy. The linear regression and the current Nord2000 model have less of a spread of the outliers than the neural network and the decision tree.

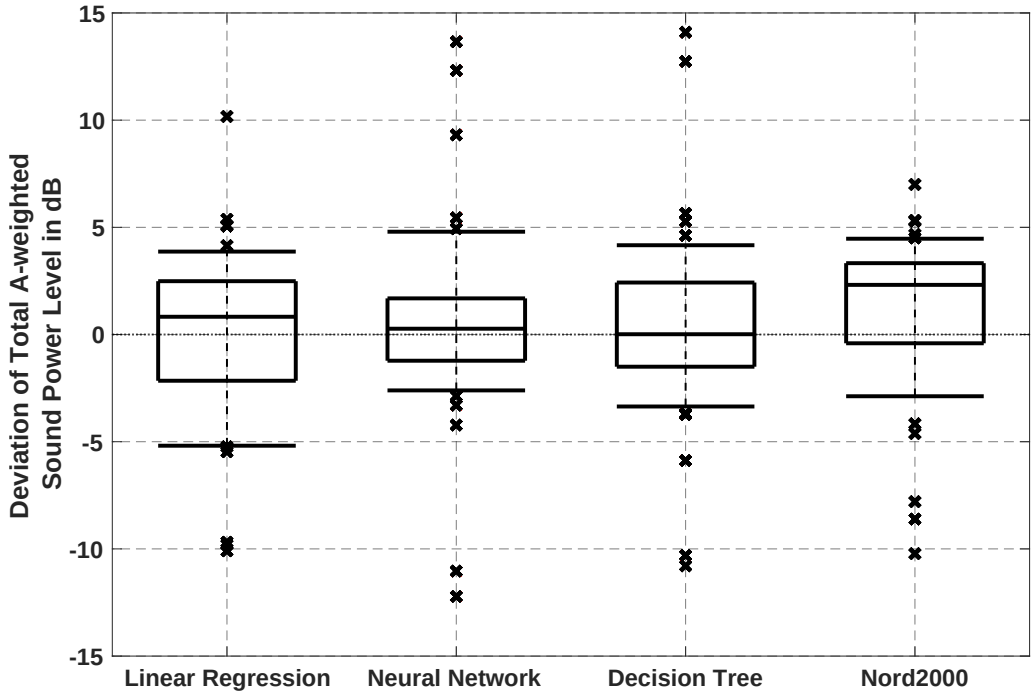

Figure 4.20.: Deviation of Total A-weighted Sound Power Level;
Box: 25th-Percentile, Median, 75th-Percentile;
Whiskers: 10th-Percentile, 90th-Percentile

4.3. Sound Power Distribution over Equivalent Sources

The results from finding the sound power distribution over equivalent sources is shown. The results of the sound power contribution from the two sources are shown as the relative sound power level of the sub sources, relative to the total sound power level of the train. The relative sound power levels are level averaged for each train type.
Considering the relative sound power level of the sub sources of X31-trains, seen in Figure 4.21, it can be seen, that the higher source dominates in the frequency bands below 50 Hz and between 160 Hz and 250 Hz, while the lower source has a higher contribution in the frequency bands of 63 Hz and 80 Hz. Above 250 Hz no sound power distribution over the sources can be deducted from the **LQS**.

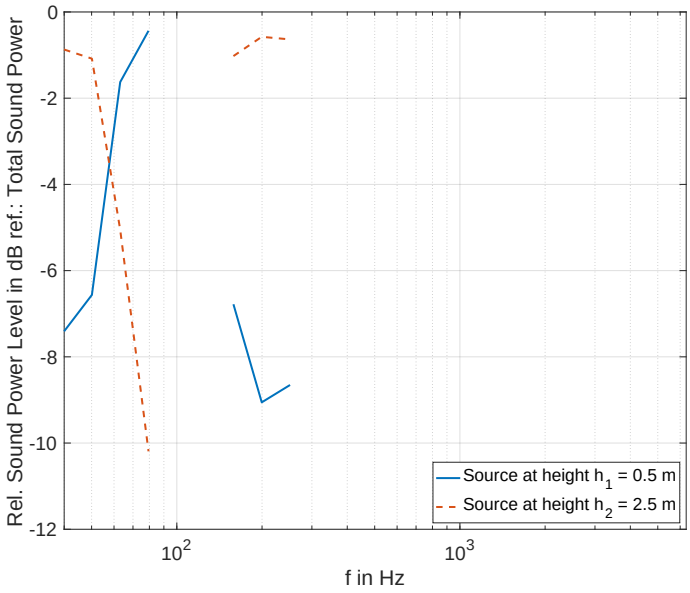

Figure 4.21.: Relative Sound Power Level, X31-trains

The sound power contribution of the sub sources of X2-trains can be seen in Figure 4.22. The contribution of the sources is roughly equal around 63 Hz. In the lowest frequency band of 40 Hz the higher source contributes more to the total sound power level, as well as in the frequency bands of 200 Hz and 250 Hz. Again, no vertical sound power distribution can be found for frequency bands higher than 250 Hz.

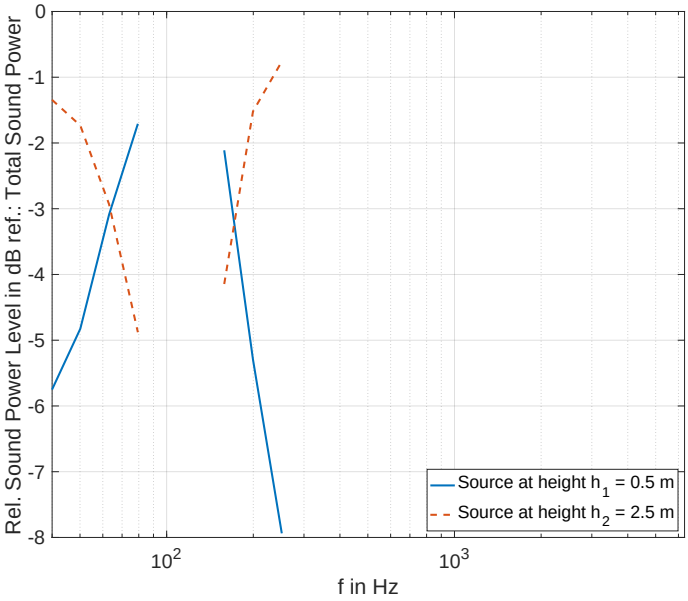

Figure 4.22.: Relative Sound Power Level, X2-trains

For X50 trains the relative sound power level can be seen in Figure 4.23. The higher source is again dominant at 40 Hz, while the lower source has a higher sound power contribution at 80 Hz. The contribution to the sound power from the higher source is very high, compared to the lower source, in the frequency bands of 200 Hz and 250 Hz. The sound power contribution is again not deductible in the frequency bands above 250 Hz.

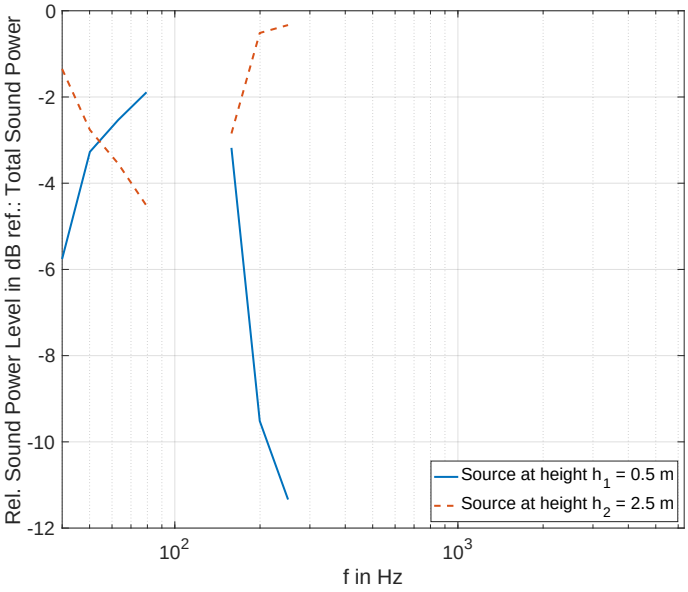

Figure 4.23.: Relative Sound Power Level, X50-trains

The sound power distribution of all other train types can be seen in appendix E.

5. Discussion

In this section the results, shown in section 4 are further discussed. First the performance of the prediction models (see section 4.1) in order to estimate the total emission of the trains are considered. Then the method and the results of finding a sound power distribution over equivalent sources (see section 4.3) on a train are discussed.
Generally it can be seen that the formulation of the calculation procedure of the Nord2000 method as a **LQS** works as intended and emulates the calculation procedure in the Nord2000 method. The formulation as a **LQS** of the method is advantageous, as it is computational less expensive. Using a constant segment length of the track, is also suggested, as it yields a single factor for the time correction, that can be calculated from the segment length and the length of a segment. The segmentation of the source line with Algorithm 1 might be an artifact from the time the Nord2000 method was published, as choosing less segments results in a shorter computing time. On a modern computer this difference is still noticeable, but less of a factor. Formulating the process of the Nord2000 method as a **LQS** might also give the possibility of re-using the transfer function $\boldsymbol{T}$ (see Eq. (3.2)). With the same geometry of source positions and microphone positions and the same amount of segments, the transfer matrix only changes with the time correction t_c, that is determined with the speed of the train. This method would drastically improve the computing time. Re-calculating the transfer matrix is still no heavy task for a modern computer, but noticeable when doing so for a whole dataset of 293 measurements. Therefore it is suggested to use the **LQS**-method to calculate the Nord2000 method with constant segment lengths of the source line.

5.1. Prediction of Total Sound Power of Trains

First the motivation for several modelling decisions is discussed. As the datasets contain descriptive data of the trains, like the number of axles and location of the measurement in the Swedish railway network, the question arises, why only the train type and the speed are used for predicting the sound power level of trains. As the exposure from the trains per 1 m of the train length is considered, information about the length of the train is considered. Including the number of axles of a train would re-introduce information about the train length again, which is undesired. Another approach would be to include the number of axles per 1 m of the train. As the same train type has the same number of axles per 1 m, separating the train types into different datasets already includes information about the number of axles. The number of axles per meter is still a determining factor, but as all cases in one dataset yield the same number of axles per meter, no prediction can be made with it. One instance, where it might be usable is for the datasets for high-speed, inter-city, and regional trains, as there are different train types present. It was decided, that the same modelling approach, as in Nord2000 should be used, so that a simple linear regression can be formulated as in Eq. (4.1).
Including the location of the measurement might give a better fit of the models, but is undesired. The goal of the study is to find a general model, that can be applied to find the sound power of a train, regardless of the location of the train.

The vibration data of the rail was also included in the Trafikverket dataset. It has been tried to include this data, as it is the closest measure in the dataset, that can be related to the rail and wheel roughness. Categorising the roughness of the rail vibration into five quantiles of magnitude did not give a significant better fit for the models. It was decided to not include the vibration data, as it is a variable, that requires measurements. When predicting the emission from a train it is undesirable to require a measurement of the train that is sought after to be predicted. It might be possible to use the categorisation of the magnitude of vibration data to find a range of emission, depending on the roughness of the rail and wheel. This procedure would further subdivide the datasets, leading to an even more limited amount of data being dispersed. Incorporating only the rail roughness into the models is also not representative, as both the rail and wheel roughness have to be taken into account equally. No information about the wheel roughness could be derived from the present data.

Generally all prediction models give adequate predictions of the total sound power in most cases. The evaluation of the different models varies significantly, depending on what train type the prediction is performed on. This is most likely due to the limited amount of data and its variety in the Trafikverket dataset. A separation of the train types leaves limited amount of cases, i.e. 19 cases for Y31-trains, in each dataset for specific train types. This amount of data might not be sufficient to find a well fitting general prediction model of the sound power of the train. Another aspect is that most trains are clustered in speed ranges, meaning the same train is driven with similar speed on the same part of a track. This in turn might give a better fit in these speed clusters, but only mediocre predictions between speed clusters, as there is barely any data available for speed between speed clusters. While a linear regression model gives estimations according to the regression curve, a decision tree might categorise these speed clusters into branches and leafs of itself. A neural network performs quite bad for these kind of cases it has not 'seen'.

The speed dependency according to the linear regression model is varying for each train type or train category. While very high speed dependencies can be observed for train of the type X31, the speed dependency of X11-trains is negative or non-existent. In many sources the speed dependency of rolling noise is described to be proportional to $30\log(v_\mathrm{t})$. Comparing the results of the linear regression to this general rule, it can be seen that it does not hold up for all frequency bands, but rather a quite different speed dependency can be observed for each frequency band. The speed dependency of i.e. X2-trains is around this proportionality, while still fluctuating for each frequency band. The speed dependency of aerodynamic noise or traction noise can be disregarded here, as the speed of the trains is between 50 km/h and 210 km/h. A greater amount of cases in the dataset would give a more accurate speed dependency for each train type.
A model, that fits the data with a negative speed dependency is contrary to results found in literature. This negative speed dependency is most likely due to speed clustering, where all measurements were carried out with similarly fast trains in that dataset. Though a model that yields negative speed dependency is still feasible for some noise emission mechanisms. The roughness of the wheel and rail excite higher frequencies as the train travels faster. Similarly, the tonal aerodynamic noise of the pantograph is shifted into higher frequency bands with increased speed. These two phenomena still do not explain negative speed dependencies in all frequency bands, as some of the frequency bands would still have to yield a positive speed dependency for these phenomena.

Collecting the train categories in the dataset for high-speed, inter-city and regional trains is done, as to give a prediction for the train categories. This is convenient, when the train type is unknown. It is also helpful, when planning a new route i.e. for high-speed trains. In this case it might not be of interest what specific train is driven on the track, but what train category. Collecting the train types in the datasets of train categories poses an issue, as some train types occur more frequently in the dataset. The Inter-city dataset is for example dominated by the amount of measurements of X60-trains, while trains of the type FLIX only occur infrequently.

In the comparison of Figure 4.13 and 4.14 it can be seen, that even for the same train and similar speed very different sound power can be expected. This shows, that the emission is not just a speed dependent variable, but dependent on more factors, not included in the model. One major factor is the rail and wheel roughness, which might be the cause of the high difference in sound power level. Using just the speed as input variable does therefore not give the perfect fit for all cases, but still estimates the sound power level adequately. The neural network or decision tree might detect extreme cases, if they are trained on similar cases. This again means, that more data is required, but also shows the need for information about the roughness in the input data.

Considering the absolute deviations of the models, it can be seen that the current Nord2000 does not yield as extreme outliers as the other models. Especially the neural network and the decision tree are prone to resulting in high deviations. The systemic over-estimation of the Nord2000 model around 315 Hz can be avoided by all other models. Apart from that, the models yield similar average deviations. A more quantified evaluation of the models is done with the **RMSE**. There it can be seen that the linear regression model performs very good in comparison with the other models. The slightly better performance by other models in some datasets is not significant enough to justify their use, with exception of the X60-dataset. In that dataset, the current X60-dataset outperforms all other models significantly. The neural network is either a hit or a miss when being evaluated. In some datasets the neural network gives very good predictions, while in other cases, its prediction is quite unsatisfactory. Even though it might be applicable to use and detect non-linearities in the speed dependency, the amount of data is insufficient to train the model properly. Similar conclusion can be drawn for the decision tree. It might be possible to detect non-linearities and its evaluation is more consistent over all datasets.
The box plots in Figure 4.20 give a good indication of the deviation of the total A-weighted sound power level of a train, when using the prediction models. There it can be seen, that the current Nord2000 model over-predicts the total A-weighted sound power level, while the new models show a spread, that is relatively symmetrical around 0 dB. The outliers of the current Nord2000 method are not as extreme as for the other models. Even though this indicates a more reliable total A-weighted sound power level, the over-prediction is undesired. The spread of the outliers of the neural network and decision tree is significantly higher than for the linear regression model and the Nord2000 model, but their boxes are relatively narrow and the whiskers are close to the box. This shows that for most cases the neural network and decision tree make relatively good predictions, but for a few cases the neural network and decision tree produce heavy outliers, that strongly deviate from the measured total A-weighted sound power level. The occurrence of these heavy outliers of the prediction with the neural network and the decision tree and their insignificant better performance over the linear regression in some datasets, regarding the **RMSE** makes it hard to justify their application.

Another aspect of the linear regression model is the interpretability of the model. The slope and intercept of the linear regression model can be clearly interpreted and related to real measures. This is not the case for the neural network implemented in this thesis. The weighting functions between neurons can not be related to real measures and the neural network has to be treated as a black box. Branches and leaves of the decision tree can be interpreted, as decisions based on the input data can be followed along each decision. Conclusion about i.e. the speed dependency have to be done by analysing the decision tree itself, or considering the prediction of a test dataset.
One way how the neural network and decision tree can be used is by comparing their predictions to the prediction of the linear regression. A high deviation between their predictions might indicate, that the prediction of the linear regression model is rather uncertain.

Similar models were built for the ProRAIL dataset, but not included in this thesis, as for the prediction of sound power of trains in Sweden it is favourable to use models which are based on trains that travel in the Swedish railway network. From the analysis of the models built with the ProRail dataset it was apparent, that the overwhelming amount of data results in good estimations when using a neural network. The uncertainty of the prediction is still present, as the sound power emission of a train is not just dependent on the speed, the train type, the number of axles, etc., but is strongly determined by the rail and wheel roughness.

It is therefore suggested to use the new linear regression model for all datasets except for the dataset of X60-trains. As the Nord2000 model outperforms all other models in this dataset it is suggested to use the existing parameters for X60-trains. Tuning the intercept (factor b in Tab. B.1) of the Nord2000 prediction model might be necessary to avoid the over-estimation in frequencies around 315 Hz.
The use of the linear regression model of high-speed trains is applicable, as it contains a big variety of trains and a large number of cases. The application of the linear regression model in the inter-city dataset does not seem feasible, as it is heavily dominated by one train type. For further improvement of the recommended model it is suggested to incorporate the roughness of the rail and the wheel. Apart from that, more data might give a more accurate speed dependency for each train type.

5.2. Sound Power Distribution over Equivalent Sources on Trains

Considering the sound power distribution over sources on a train, it is apparent, that the method, used in this thesis, does not yield results, that align with literature.
As the **LQS** is a determined system, an exact solution can theoretically be found. The results show a sound power distribution over the two source at the height of 0.5 m and 2.5 m, that do not at all agree with other observations found in literature. A higher sound power distribution from higher sources does not coincide with the findings of other studies, where most of the acoustic energy can be measured from the lower parts of the train, due to the dominance of rolling noise.
Some constraints of solving the **LQS** might limit the solution, but are justified. When the transfer paths are almost identical and the rows in the transfer matrix $\mathbf{T}$ are almost co-linear, no statement about the sound power distribution of the sources can be made, as the **LQS** becomes under-determined. For all frequency bands above 250 Hz no sound

power distribution can be deducted in all measurements. The transfer paths might just be too similar to determine an appropriate vertical sound power distribution over the train. Defining a lower boundary might be appropriate, as minimal emission can be expected from one part of the train. Removing this lower bound would yield a sound power distribution, with negative sound power of one source, in some cases. The difference in **SEL** due to the different transfer paths is very low, only 0.3 dB in some frequency bands. This difference is in the realm of measurement uncertainties of microphones.

Considering the complex measurement setups with microphone arrays and beam-forming in previous studies (see section 2.2), it can be seen that their conclusion is, that most of the acoustic energy is emitted from the lower part of the train. This emission can be attributed to the dominance of rolling noise at normal operating speeds. Even in these studies, the emission from the rail and the wheel can not be differentiated or a power distribution quantified. As explained by Kitagawa et. al [19] even with these complex measurement setups the emission from the rail is under-estimated, when beam-forming in a normal direction to the rail. This means that the exact method of previous studies have to be evaluated critically, as the results of beam-forming in normal direction might under-estimate the contribution from rolling noise in total in some frequency bands, especially where the emission from the rail is dominating. One suggestion to correct for the directivity of the sound emission mechanisms is to angle the beam-forming along the track to find more appropriate results for the distribution of emission of the rail and the wheel. This can be done with the same array measurement and signal processing after the measurement.
Comparing the method to find the vertical sound power distribution on a train in this thesis and the method, using microphone arrays, it can be seen that in this thesis many simplification have been made, that might not represent the complex emissions from different mechanisms properly. The method used in this thesis is based on the calculation method described in Nord2000 [1], which does not claim to yield a perfect representation of railway noise, but is rather a good practical approach to evaluate and compare railway noise. One of those simplifications, is to use point source, while it is described by Thompson [7], that for some sound emission mechanisms it would be more appropriate to use di-poles.

It is most likely not at all possible to find an appropriate vertical sound power distribution on a train with just 2 microphones. Even studies that make use of microphone arrays and beam-forming have difficulties separating the emission from the rail and the wheel, even though it can be seen that a significant portion of the emission originates from the contact point between the rail and the wheel.
With previous studies in mind, it might be possible to find appropriate vertical sound power distributions on trains. One suggestion is to use a more analytic model, that takes the radiation characteristics of the rail and the wheel into account. As the wheel radiation is quite dependent on the geometry of the wheel, this approach demands detailed information about the wheel. As the excitation of the rail and the wheel is strongly determined by their roughness, this aspect should be taken into account as well. Array measurements can then be used to validate an analytical model. When carrying out array measurements and beam-forming, the beam should be angled not just in normal direction to the rail, but along the track, to adjust for the directivity of the different sound emission mechanisms.
Another approach is to just make use of array measurements and build an empirical model

from different measurements. This would require a lot of measurements of a lot of different trains. Information about the wheel geometry would be required to properly evaluate the emission of the train.
The array measurements should be carried out with two microphone arrays, similarly to previous studies. One array with further distances between the microphones could then be used to detect the emission of the whole train, while an array with less distance between the microphones could detect the emission around the rail and wheel in more detail.

6. Conclusion

The aim of this thesis has been to improve the prediction of the overall sound emission from trains. It has also been sought after to improve the source model, to better estimate the effect of low height noise screens. By formulating the propagation path between sources and microphones as a **LQS**, the **SEL** from the sound power of a moving train is calculated in a simplified manner. This formulation of the propagation path could be considered when calculating transfer paths for emission from trains and general noise mapping.

Several models to predict the overall sound emission from a train, based on its speed and type of train have been build with existing measurement data. The new prediction models are a linear regression, a neural network, and a decision tree. These prediction models were evaluated and their prediction was assessed in comparison to the current Nord2000 prediction model. While the neural network and decision tree are sometimes able to detect outlying sound power emissions, the linear regression model yields reliable predictions of the overall emission of a train and is therefore suggested for further use. The predictions from the neural network and the decision tree might be useful to assess the certainty of the linear regression model, when predicting one case. Training the models on more data might result in better prediction models. The root cause of rolling noise, the rail and wheel roughness, are not incorporated in the model, as the wheel roughness could not be deducted from the measurement data. Categorizing the rail roughness might be a feasible method, but would further subdivide the already limited amount of data. As neither the rail roughness nor the wheel roughness are included in the prediction models, they are intrinsically limited. It is therefore advised to incorporate rail and wheel roughness into the models, as it could lead to further improvements of the models.
Finding an appropriate vertical sound power distribution over equivalent sources on trains has been done by solving the propagation path between the equivalent sources and the microphones as a determined **LQS**. The results of this method do not not yield a plausible vertical sound power distribution according to the literature. The difference in transfer paths and the measured **SEL** at the microphone positions might not be significant enough to find the vertical sound power distribution an a train with just two microphones. Therefore it is advised to perform array measurements with beam-forming to find the sound power distribution. This method should be used carefully as it could under-estimate the sound power contribution from the rail, when angling the beam only in normal direction to the track. The beam should therefore be angled along the track, as well as vertically over the train.

The prediction model for railway noise emission in Nord2000 has been improved for the current source positions, used in Nord2000. Finding the vertical sound power distribution on a train was not possible and might not be at all possible without array measurements. The method to formulate transfer paths in a **LQS** might be useful in other areas of application, such as noise mapping.

Bibliography

[1] Hans G. Jonasson, Svein Storeheier. Nord 2000 - New Nordic Prediction Method for Rail Traffic Noise, 2001.

[2] Anfosso-Lédée F, Paviotti M, Kephalopoulos S. Common Noise Assessment Methods in Europe (CNOSSOS-EU), 2012.

[3] Gerhard Müller and Michael Möser. *Taschenbuch der Technischen Akustik*. 01 2003.

[4] Xiaowan Liu Jianyue Zhu David J. Thompson, Eduardo Latorre Iglesias and Zhiwei Hu. Recent developments in the prediction and control of aerodynamic noise from high-speed trains. *International Journal of Rail Transportation*, 3(3):119–150, 2015.

[5] M.G. Dittrich and X. Zhang. The harmonoise/imagine model for traction noise of powered railway vehicles. *Journal of Sound and Vibration*, 293(3):986–994, 2006. Proceedings of the Eigth International Workshop on Railway Noise.

[6] Sj high-speed trains. `https://www.swedentrains.com/sj-high-speed-trains#:~:text=%E2%80%8BSJ%20high%2Dspeed%20train,including%20Gothenburg%2C%20Malmo%2C%20Stockholm`. Accessed on May 14, 2024.

[7] David Thompson. *Railway Noise and Vibration*. 01 2009.

[8] Evangelos Ntotsios, David J. Thompson, and Mohammed F.M. Hussein. A comparison of ground vibration due to ballasted and slab tracks. *Transportation Geotechnics*, 21:100256, 2019.

[9] Xianying Zhang, Hongseok Jeong, David Thompson, and Giacomo Squicciarini. The noise radiated by ballasted and slab tracks. *Applied Acoustics*, 151:193–205, 2019.

[10] David Thompson, Tianxing Wu, and Tristan Armstrong. Wheel/rail rolling noise - the effects of non-linearities in the contact zone. *Proceedings of the Tenth International Congress on Sound and Vibration*, 01 2003.

[11] D.J. Thompson, B. Hemsworth, and N. Vincent. Experimental validation of the twins prediction program for rolling noise, part 1: Description of the model and method. *Journal of Sound and Vibration*, 193(1):123–135, 1996.

[12] Jannik Theyssen, Thomas Deppisch, Astrid Pieringer, and Wolfgang Kropp. On the efficient simulation of pass-by noise signals from railway wheels. *Journal of Sound and Vibration*, 564:117889, 2023.

[13] A. Pieringer, W. Kropp, and D.J. Thompson. Investigation of the dynamic contact filter effect in vertical wheel/rail interaction using a 2d and a 3d non-hertzian contact model. *Wear*, 271(1):328–338, 2011. Proceedings of the 8th International Conference on Contact Mechanics and Wear of Rail / Wheel Systems, Florence, 2009.

[14] Theyssen, Jannik, Pieringer, Astrid, and Kropp, Wolfgang. Efficient calculation of the three-dimensional sound pressure field around a slab track. *Acta Acust.*, 8:4, 2024.

[15] Tae Min Kim and Jung-Soo Kim. Analysis of aerodynamic noise in high speed trains. *International Journal of Railway*, 4, 09 2011.

[16] S. Kümmritz, H. Brammer, C. Jöckle, Deutsches Zentrum für Schienenverkehrsforschung, and gfai tech GmbH. *Emissionsortdetektion im Schienenverkehr mit einer akustischen Kamera*. Berichte des Deutschen Zentrums für Schienenverkehrsforschung. Deutsches Zentrum für Schienenverkehrsforschung beim Eisenbahn-Bundesamt, 2020.

[17] Drangu Sehu, Jean Marc Wunderli, Kurt Heutschi, Thomas Thron, Markus Hecht, Andre Rohrbeck, Thomas Ledermann. SonRail - Projektdokumentation. Technical report, Schweizerische Eidgenossenschaft, 2010.

[18] Swedish Standards Institution. Attenuation of sound during propagation outdoors Part 2: General method of calculation. Standard, International Organization for Standardization, 1996.

[19] T. Kitagawa and D.J. Thompson. Comparison of wheel/rail noise radiation on japanese railways using the twins model and microphone array measurements. *Journal of Sound and Vibration*, 293(3):496–509, 2006. Proceedings of the Eigth International Workshop on Railway Noise.

[20] C. Hanson, B. Barsikow. Noise Sources on Amtrak's High Speed Train. *The 29th International Congress and Exhibition on Noise Control Engineering*, 2000.

[21] C.E. Hanson and Miller & Hanson Inc Harris, Miller. *High-speed Ground Transportation Noise and Vibration Impact Assessment: Final Report*. U.S. Department of Transportation, Federal Railroad Administration, Office of Railroad Policy and Development, 2012.

[22] Matias Ringheim, Hugo Lyse Nielsen, and Nordic Council of Ministers. *Railway Traffic Noise: The Nordic Prediction Method*. Nordic Council of Ministers, Copenhagen, 1996.

[23] Mikael Ögren, Anders Genell, Tomas Jerson, Peter Torstensson, Andreas Gustafson. Svenska emissionsdata för beräkning av buller från spårburen trafik med hjälp av Nord 2000. Technical report, Västra Götalandsregionens Miljömedicinska Centrum, 2023.

[24] European Committee for Standardization. SS-EN 15610:2019: Railway applications – Acoustics – Rail and wheel roughness measurement related to noise generation, 2019.

[25] Nordic Noise Group. Nord 2000. Comprehensive Outdoor Sound Propagation Model. Part1: Propagation in an Atmosphere without Significant Refraction, 2001.

[26] Swedish Standards Institution. Attenuation of sound during propagation outdoors Part 1: Calculation of the absorption of sound by the atmosphere. Standard, International Organization for Standardization, 1993.

[27] D.C. Montgomery, E.A. Peck, and G.G. Vining. *Introduction to Linear Regression Analysis*. Wiley Series in Probability and Statistics. Wiley, 2012.

[28] Activation Functions Neural Networks. `https://towardsdatascience.com/activation-functions-neural-networks-1cbd9f8d91d6`. Accessed on June 25, 2024.

[29] Machine learning space. https://machinelearningspace.com/introduction-to-artificial-neural-networks-anns/. Accessed on May 16, 2024.

[30] Rebecca C. Steorts. Tree Based Methods: Regression Trees.

[31] European Committee for Standardization. SS-EN ISO 3095:2013: Acoustics - Railway applications - Measurement of noise emitted by railbound vehicles, 2001.

[32] Gunnar Taraldsen. Road Traffic: Vehicle Noise Emission. Technical report, Nordic Innovation Centre, 2004.

A. Algorithms

For the purpose of approximating the $w(\rho)$ function with Algorithm 2, x and y are defined as $x = \mathrm{Re}(\rho)$ and $y = \mathrm{Im}(\rho)$.

Algorithm 2 Approximation of $w(\rho)$

if $x > 6$ ***OR*** $y > 6$ **then**
  $w(\rho) = j\rho(\frac{0.5124242}{\rho^2-0.2752551} + \frac{0.05176536}{\rho^2-2.724745})$;
end
else if $x > 3.9$ ***OR*** $y > 3$ **then**
  $w(\rho) = j\rho(\frac{0.4613135}{\rho^2-0.1901635} + \frac{0.09999216}{\rho^2-1.7844927} + \frac{0.002883894}{\rho^2-5.5253437})$;
end
else
  $h = 0.8$
  $A = \cos(2xy)$
  $B = \sin(2xy)$
  $C = e^{-2y\pi/h} - \cos(2x\pi/h)$
  $D = \sin(2x\pi/h)$
  $P_1 = 2e^{-(x^2+2y\pi/h-y^2)}\frac{AC+BD}{C^2+D^2}$
  $Q_1 = 2e^{-(x^2+2y\pi/h-y^2)}\frac{AD+BC}{C^2+D^2}$
  $H = \frac{hy}{\pi(x^2+y^2)} + \frac{2yh}{\pi}\sum_{n=1}^{5}\frac{e^{-n^2h^2}(x^2+y^2+n^2h^2)}{(y^2-x^2+n^2h^2)+4x^2y^2}$
  $K = \frac{hx}{\pi(x^2+y^2)} + \frac{2xh}{\pi}\sum_{n=1}^{5}\frac{e^{-n^2h^2}(x^2+y^2-n^2h^2)}{(y^2-x^2+n^2h^2)+4x^2y^2}$
  if $y > \pi/h$ **then**
    $w(\rho) = H + jK$
  end
  else if $y = \pi/h$ **then**
    $w(\rho) = H + \frac{P_1}{2} + j(K - Q_1/2)$
  end
  else if $y < \pi/h$ **then**
    $w(\rho) = H + P_1 + j(K - Q_1)$
  end
end

B. Nord2000 Parameters

Table B.1.: Updated Nord2000 Parameters [23]

kod	a/b	25	31,5	40	50	63	80	100	125	160	200	250	315	400	500	630	800	1000	1250	1600	2000	2500	3150	4000	5000	6300	8000	10000
X2	a	49,1	48,1	50,2	40,7	43,5	43,8	46,1	34,5	21,6	14,4	17,7	16,3	19,8	18,6	7,7	22,1	31,2	43,7	52,4	64,1	63,4	50,1	30,3	30,5	33,1	32,7	27,4
	b	79,3	80,2	80,3	83,4	82,4	81,5	79,8	81,5	85,8	90,4	90,8	91,8	90,4	91,7	97,2	99,0	97,5	93,5	91,6	88,7	84,7	84,2	85,2	82,9	80,7	78,8	79,0
X11	a	16,5	16,7	22,0	32,2	25,0	20,4	12,6	15,0	10,9	5,7	1,2	4,5	3,5	13,6	43,3	54,2	49,2	52,7	53,8	50,2	44,1	28,4	30,6	31,2	29,4	32,0	33,0
	b	84,7	85,4	85,4	92,1	91,1	88,5	84,9	85,9	87,4	87,9	91,0	90,4	91,9	92,4	95,7	99,2	94,8	90,8	91,5	89,3	87,5	85,0	86,5	83,7	80,8	79,1	78,2
X31	a	46,0	48,7	40,0	30,7	57,4	55,0	40,7	43,0	38,0	29,1	24,8	20,1	20,0	5,4	29,2	47,3	56,4	50,3	54,5	57,5	37,8	21,7	34,6	44,1	42,0	35,7	38,3
	b	83,1	82,8	84,2	85,9	81,6	80,5	81,6	81,5	83,7	84,8	86,2	87,9	89,9	92,7	89,6	91,5	90,5	87,4	85,8	83,7	82,9	83,4	80,8	79,1	77,7	77,2	77,1
X40	a	54,5	57,1	46,4	13,7	33,0	53,8	47,7	44,0	41,1	27,8	39,9	42,6	27,6	18,2	14,7	15,4	26,8	36,7	39,8	55,1	47,4	44,7	36,5	40,3	36,8	42,2	35,5
	b	79,9	79,5	82,7	90,3	85,5	82,1	81,0	80,7	82,5	87,0	88,2	87,7	89,9	90,2	91,9	95,3	95,1	90,6	90,1	87,2	84,1	80,8	80,2	78,1	77,3	74,8	75,2
X50	a	35,6	39,0	36,7	27,6	32,7	37,1	30,9	30,4	27,3	25,0	22,3	18,5	15,2	16,9	18,4	21,2	35,1	36,3	35,0	44,0	37,3	27,1	20,1	22,0	26,3	28,7	29,5
	b	83,7	83,7	84,4	87,5	85,1	82,9	82,3	81,7	83,7	85,1	86,1	88,4	90,1	89,7	91,5	94,5	91,5	88,5	87,9	86,8	85,4	84,5	84,3	82,8	80,1	78,0	77,3
X60	a	30,7	21,7	28,1	45,2	21,5	16,6	22,1	20,8	19,2	19,7	15,6	8,6	0,0	9,9	39,3	49,8	44,5	52,6	58,7	46,5	37,9	27,8	25,1	21,9	27,4	32,0	32,9
	b	83,3	84,1	83,5	87,2	84,3	82,3	81,3	81,3	83,1	83,7	84,8	86,9	87,9	87,5	89,8	92,3	89,7	85,5	84,3	81,8	79,2	77,5	79,1	77,2	77,0	74,8	75,2
X74	a	43,5	58,2	57,1	16,6	41,1	60,1	43,0	49,2	50,2	39,9	41,4	44,0	20,8	29,8	36,9	31,3	38,8	40,6	38,5	68,8	54,6	51,0	26,7	41,3	39,5	46,6	40,5
	b	82,6	80,8	81,4	89,2	82,8	78,9	81,1	78,8	79,4	82,4	83,2	84,5	90,6	89,1	90,8	95,2	95,0	90,8	90,8	85,6	83,8	80,1	81,7	78,2	77,9	74,7	75,9
Y31	a	39,2	25,7	26,6	22,1	19,3	41,2	52,1	26,9	25,0	25,1	28,9	46,9	43,7	43,5	37,9	59,6	41,5	28,9	39,1	38,1	28,0	29,6	14,1	33,2	28,8	33,4	26,7
	b	84,5	87,0	89,3	89,8	88,1	87,8	87,7	88,3	87,6	88,5	89,5	89,9	91,3	91,8	92,8	95,2	95,4	93,8	93,0	93,0	89,8	85,7	85,6	83,5	82,4	79,0	79,3
ER1	a	39,5	40,9	39,0	31,2	39,8	43,4	35,8	35,0	31,5	29,4	28,5	24,1	17,9	14,5	26,3	32,5	44,2	46,0	48,2	57,2	46,1	33,8	30,4	33,7	34,2	34,1	33,8
	b	80,2	80,4	81,1	83,8	80,4	78,9	78,8	78,6	80,5	81,7	83,0	84,9	86,6	87,3	87,0	89,2	87,6	84,1	82,8	81,0	79,5	78,7	78,0	76,2	75,0	73,5	73,4
GT	a	20,8	28,2	26,3	32,2	19,8	9,0	2,3	0,1	0,0	0,0	0,0	0,0	0,0	11,1	28,9	34,3	37,7	47,6	49,8	46,1	32,5	25,5	26,2	24,4	25,9	24,2	23,9
	b	86,9	87,5	87,3	86,7	85,0	84,7	83,9	84,1	85,8	87,7	91,3	94,6	97,6	102,1	105,1	106,4	105,6	103,0	104,2	101,9	98,4	95,7	93,5	90,9	88,8	86,8	85,1
GTK	a	20,8	28,2	26,3	32,2	19,8	9,0	2,3	0,1	0,0	0,0	0,0	0,0	0,0	11,1	28,9	34,3	37,7	47,6	49,8	46,1	32,5	25,5	26,2	24,4	25,9	24,2	23,9
	b	86,9	87,5	87,3	94,7	93,0	92,7	91,9	91,1	83,8	84,7	87,3	89,6	91,6	94,1	97,1	98,4	97,6	95,0	96,2	93,9	90,4	87,7	85,5	82,9	80,8	78,8	77,1
PT	a	18	18	18	19	19	16,3	12	9,3	9,3	11,5	11,5	8,2	0,6	-2,7	2,3	10,9	15,9	19,3	23,9	27,2	23,9	16,8	13,4	13,4	15	15	15
	b	90	90	90	89,9	89,9	90,2	90,2	90,5	92,2	94,4	96,1	97,1	98,1	99,1	99,8	100,8	101,5	100,8	99,9	99,3	97,6	95,8	94,1	90,8	85,9	82,6	82,6

C. CNOSSOS-EU Transfer Functions

Table C.1.: Classifications of Railway Vehicles [2]

Digit	1	2	3	4
Descriptor	**Vehicle type**	**Number of axles per vehicle**	**Brake type**	**Wheel measure**
Explanation of the descriptor	A letter that describes the type	The actual number of axles	A letter that describes the brake type	A letter that describes the noise reduction measure type
Possible descriptors	**h** high speed vehicle (>200 km/h)	**1**	**c** cast-iron block	**n** no measure
	m self-propelled passenger coaches	**2**	**k** composite or sinter metal block	**d** dampers
	p hauled passenger coaches	**3**	**n** non-tread braked, like disc, drum, magnetic	**s** screens
	c city tram or light metro self-propelled and non-self-propelled coach	**4**		**o** other
	d diesel loco	etc.		
	e electric loco			
	a any generic freight vehicle			
	o other (i.e. maintenance vehicles etc.)			

Table C.2.: Contact Filter A_3 [2]

Wavelength (cm)	360 mm / 50 kN	680 mm / 50 kN	920 mm / 25 kN	920 mm / 50 kN	920 mm / 100 kN
1	-8.4	-12	-12	-12	-12
0.8	-12	-12.5	-12.6	-13.5	-14
0.63	-11.5	-13.5	-13.5	-14.5	-15
0.5	-12.5	-16	-14.5	-16	-17
0.4	-13.9	-16	-16	-16.5	-18.4
0.315	-14.7	-16.5	-16.5	-17.7	-19.5
0.25	-15.6	-17	-17.7	-18.6	-20.5
0.2	-16.6	-18	-18.6	-19.6	-21.5
0.16	-17.6	-19	-19.6	-20.6	-22.4
0.125	-18.6	-20.2	-20.6	-21.6	-23.5
0.1	-19.6	-21.2	-21.6	-22.6	-24.5
0.08	-20.6	-22.2	-22.6	-23.6	-25.4
0.063	-21.6	-23.2	-23.6	-24.6	-26.5
0.05	-22.6	-24.2	-24.6	-25.6	-27.5
0.04	-23.6	-25.2	-25.6	-26.6	-28.4

Table C.3.: Transfer Function for Track in CNOSSOS-EU [2]

Frequency (Hz)	$L_{H,tr,i}$										
	Mono-block on soft rail pad	Mono-block on medium stiffness rail pad	Mono-block on hard rail pad	Bi-block on soft rail pad	Bi-block on medium stiffness rail pad	Bi-block on hard rail pad	Wooden sleepers	Wheel with diameter 920 mm	Wheel with diameter 840 mm	Wheel with diameter 680 mm	Wheel with diameter 1200 mm
25	35.1	32.1	31.1	32.1	31.1	31.1	26.1	78.1	78.1	78.1	78.1
32	41.6	38.6	37.6	38.6	37.6	37.6	32.6	77.8	77.8	77.8	77.8
40	49.4	46.4	45.4	46.4	45.4	45.4	40.4	77.9	77.9	77.9	77.9
50	56.2	53.8	53.0	53.8	52.9	52.7	46.9	77.2	77.2	77.2	77.2
63	61.9	60.4	59.8	59.2	58.7	58.5	53.6	79.5	79.5	79.5	79.5
80	63.6	62.9	62.7	60.7	60.5	60.4	56.3	82.1	82.1	82.1	82.1
100	71.0	71.9	72.3	67.4	67.6	67.6	65.9	82.0	82.0	82.0	82.0
125	78.3	80.0	80.7	74.5	74.9	75.0	74.2	83.0	82.5	82.5	82.5
160	82.4	83.9	84.6	79.1	79.7	80.0	77.7	82.1	81.1	81.1	81.1
200	85.6	87.2	87.9	83.2	85.0	85.8	78.6	85.5	83.6	83.4	84.0
250	83.3	84.7	85.4	81.3	83.4	84.4	75.6	88.8	85.6	85.0	89.1
315	86.7	87.3	87.8	84.8	85.3	85.9	81.0	89.0	87.1	87.2	89.6
400	92.0	91.4	91.8	89.4	87.2	87.7	90.0	87.4	88.3	90.6	88.3
500	96.7	95.3	95.5	94.2	90.3	90.5	96.7	84.8	86.9	89.9	86.1
630	101.1	99.3	98.9	99.4	95.7	95.0	100.6	90.1	91.2	92.2	91.0
800	98.7	96.4	95.0	98.7	95.3	92.6	97.5	91.1	90.2	89.6	90.2
1000	103.0	100.3	98.4	103.8	100.6	97.0	101.3	92.3	90.4	87.8	91.0
1250	107.7	105.4	103.6	108.3	105.7	102.8	105.9	97.3	95.6	90.1	97.4
1600	110.7	109.0	107.6	111.0	109.3	107.6	108.6	103.0	100.0	91.9	103.0
2000	112.3	110.9	109.7	112.4	111.4	110.3	110.1	110.6	108.6	100.6	116.6
2500	105.8	104.7	103.7	106.0	105.1	104.3	103.9	113.6	110.6	103.6	114.6
3150	106.9	106.0	105.1	107.0	106.3	105.6	105.3	113.2	112.7	106.2	114.2
4000	110.2	109.6	108.9	110.3	109.9	109.3	108.9	113.7	113.2	109.7	114.7
5000	110.2	109.8	109.3	110.2	109.9	109.5	109.0	113.2	112.7	109.2	114.2
6300	109.0	108.9	108.7	108.9	108.8	108.6	108.1	115.7	115.2	111.7	116.7
8000	104.7	104.9	105.0	104.6	104.6	104.5	104.1	113.4	112.9	109.4	114.4
10000	105.6	106.0	106.4	105.4	105.5	105.6	105.2	113.0	112.5	109.0	114.0

Table C.4.: Transfer Function for Vehicle in CNOSSOS-EU [2]

Wavelength (cm)	$L_{H,veh,i}$									
	Cast iron braked wheel on Dutch typical rail roughness	Disk braked wheel on Dutch typical rail roughness	Disk braked wheel on smooth roughness rail	ISO spectrum	TSI	Very smooth wheel on Dutch typical rail roughness	Composite block on smooth roughness rail	Maximum roughness combined	Minimum roughness combined	Roughness of standard disk braked wheel
63	20	11	20.5	23.5	17.1	11	18.5	25	5	11
50	17	11	18.7	21.7	17.1	11	16.7	20	0	11
40	14	11	16.8	19.8	17.1	11	14.8	20	-5	11
31.5	12	10	15	18	15	10	13	20	-6	10
25	10	9	13.1	16.1	13	9	11.1	20	-7	9
20	10	8	11.3	14.3	11	8	9.3	20	-8	8
16	11	7	9.4	12.4	9	7	7.4	20	-9	7
12	11	6	7.6	10.6	7	6	5.6	20	-10	6
10	11	5	5.8	8.8	4.9	5	3.8	20	-11	5
8	13	3.8	3.7	6.7	2.7	3.8	1.7	20	-12	3.8
6.3	14	2.5	1.6	4.6	0.4	2.5	-0.4	20	-13	2.5
5	14	1.1	-0.7	2.3	-2	1.1	-2.7	20	-14	1.1
4	13	-0.6	-3.2	-0.2	-4.8	-0.6	-5.2	20	-15	-0.6
3.2	10	-2.5	-6	-3	-7.5	-2.5	-8	19	-16	-2.5
2.5	7	-4.8	-9.1	-6.1	-9.4	-4.8	-11.1	17	-17	-4.8
2	3	-7.8	-12.9	-9.9	-12	-7.8	-14.9	15	-20	-7.8
1.6	-2	-11.5	-17.5	-14.5	-15.3	-11.5	-19.5	10	-23	-16
1.2	-7	-15.4	-22.2	-19.2	-18.8	-15.4	-24.2	5	-27	-19
1	-14	-17	-24.7	-21.7	-20	-17	-26.7	0	-30	-22
0.8	-19.5	-19.5	-26.2	-23.2	-22.1	-19.5	-28.2	-5	-31	-25
0.63	-21.5	-21.5	-27.2	-24.2	-23.7	-21.5	-29.2	-10	-32	-28
0.5	-24	-24	-28.7	-25.7	-25.8	-24	-30.7	-15	-33	-31
0.4	-25.5	-25.5	-29.2	-26.2	-26.9	-25.5	-31.2	-20	-34	-34
0.32	-27.7	-27.7	-30.4	-27.4	-28.7	-27.7	-32.4	-25	-35	-37
0.25	-29.6	-29.6	-31.3	-28.3	-30.2	-29.6	-33.3	-26	-36	-40
0.2	-31.6	-31.6	-32.3	-29.3	-31.8	-31.6	-34.3	-27	-37	-43
0.16	-33.6	-33.6	-33.3	-30.3	-33.4	-33.6	-35.3	-28	-38	-46
0.13	-35.6	-35.6	-34.3	-31.3	-35	-35.6	-36.3	-29	-39	-49
0.1	-37	-37.6	-35.3	-32.3	-36.6	-37.6	-37.3	-30	-40	-52

D. Additional Figures

D.1. Visualization of Linear Regression Models

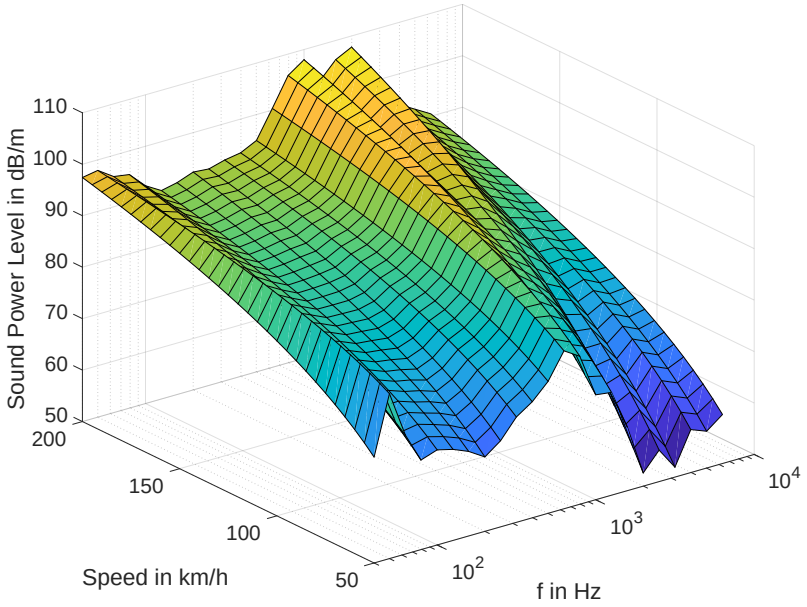

Figure D.1.: Speed Dependency of Linear Regression for Inter-City-Trains

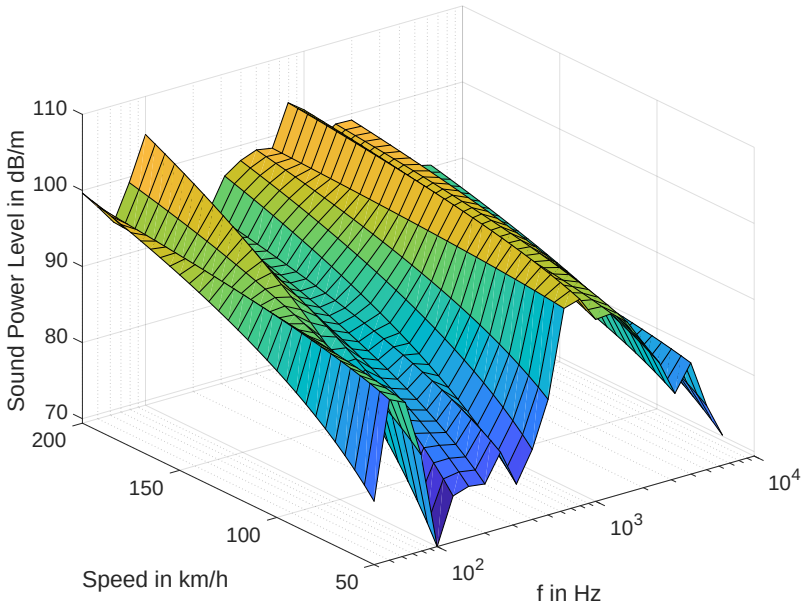

Figure D.2.: Speed Dependency of Linear Regression for Regional-Trains

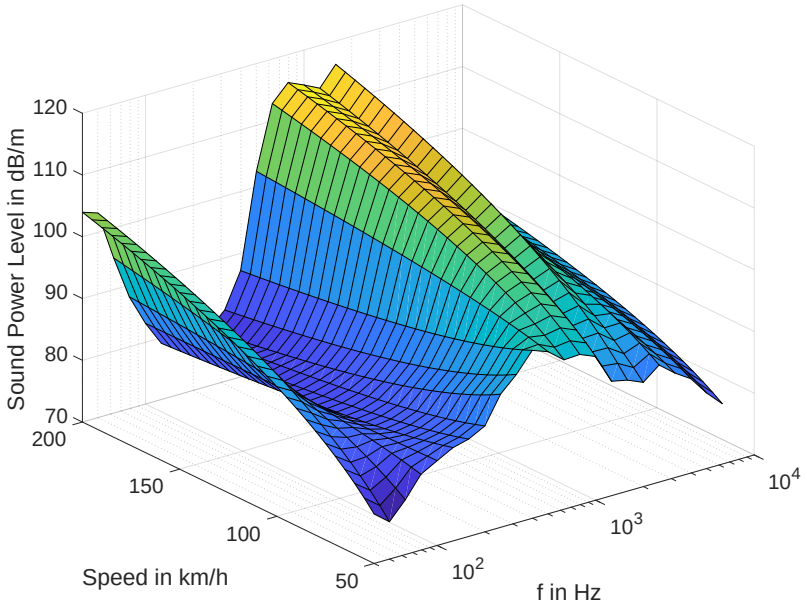

Figure D.3.: Speed Dependency of Linear Regression for Freight Trains with Cast Iron Block Breaks

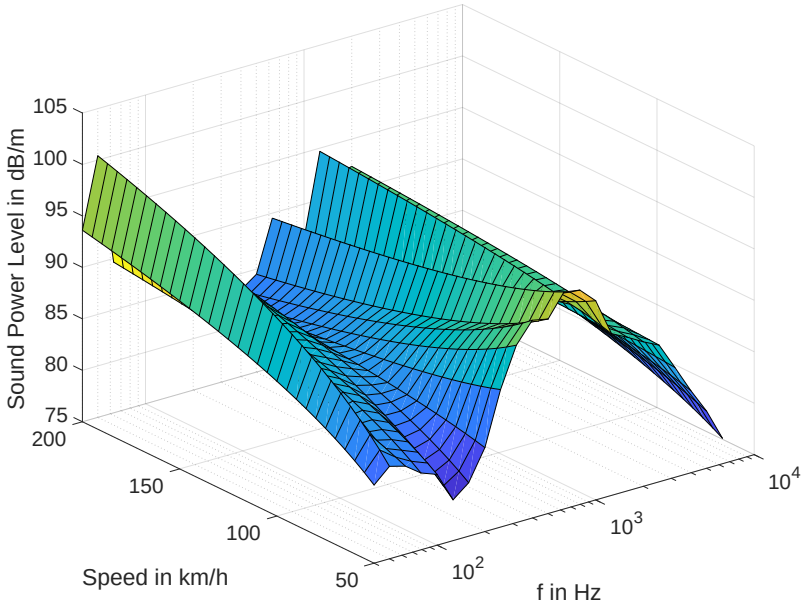

Figure D.4.: Speed Dependency of Linear Regression for Freight Trains with K-Block or Disc Breaks

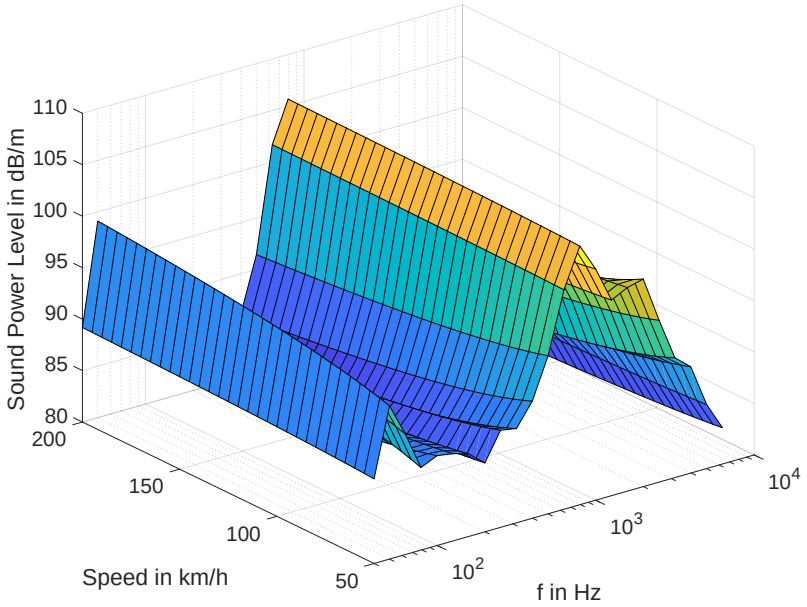

Figure D.5.: Speed Dependency of Linear Regression for X11-Trains

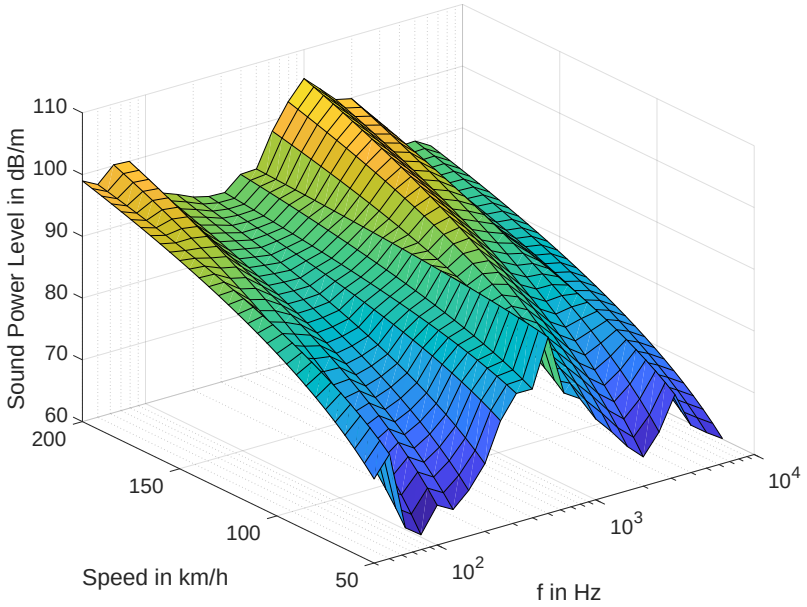

Figure D.6.: Speed Dependency of Linear Regression for X31-Trains

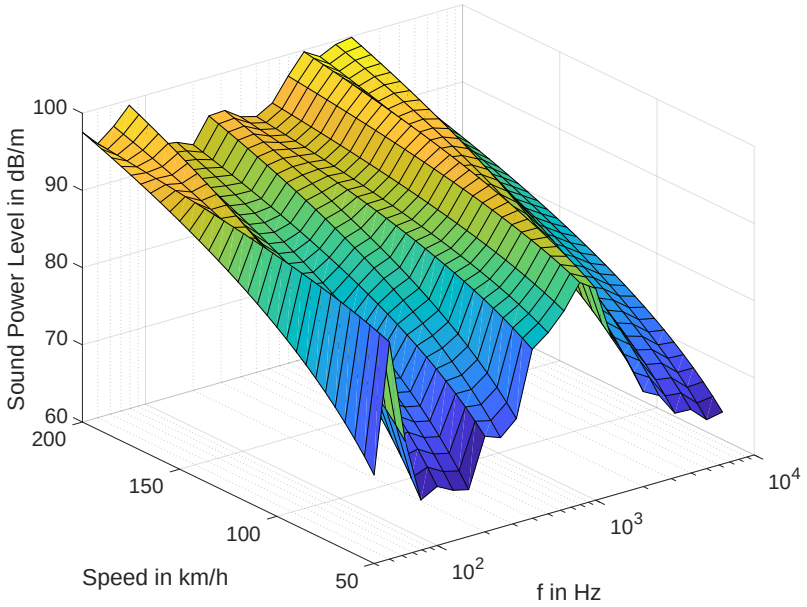

Figure D.7.: Speed Dependency of Linear Regression for X40-Trains

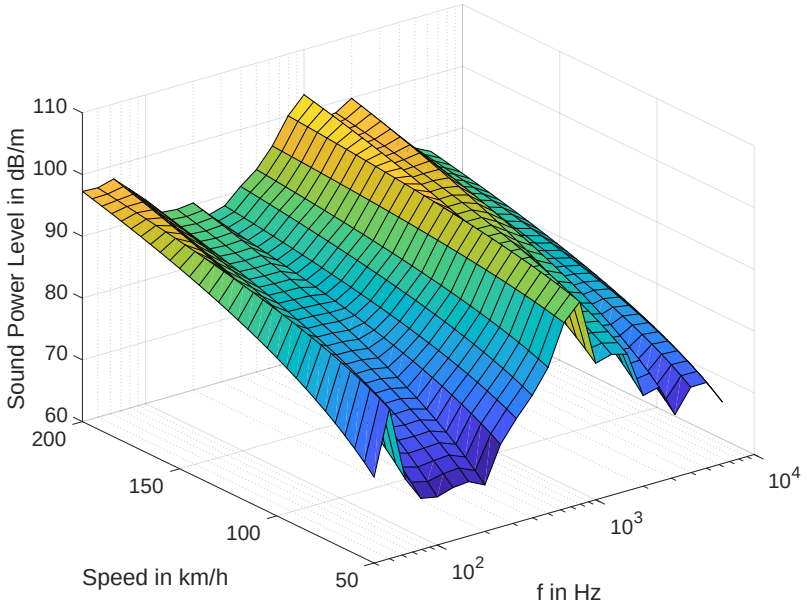

Figure D.8.: Speed Dependency of Linear Regression for X50-Trains

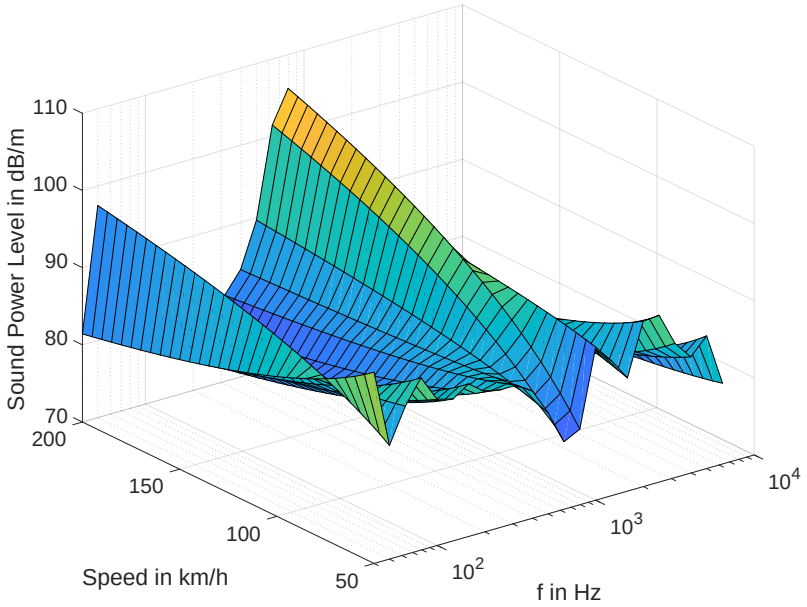

Figure D.9.: Speed Dependency of Linear Regression for X60-Trains

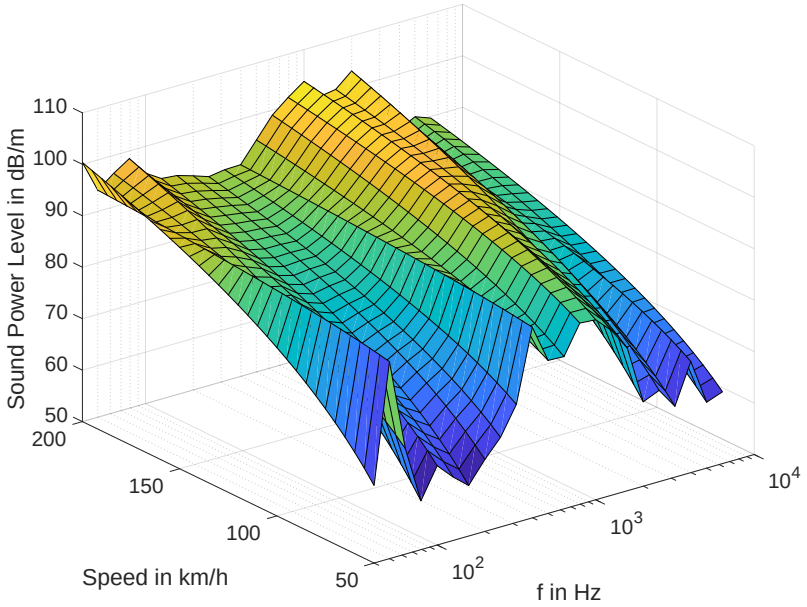

Figure D.10.: Speed Dependency of Linear Regression for X74-Trains

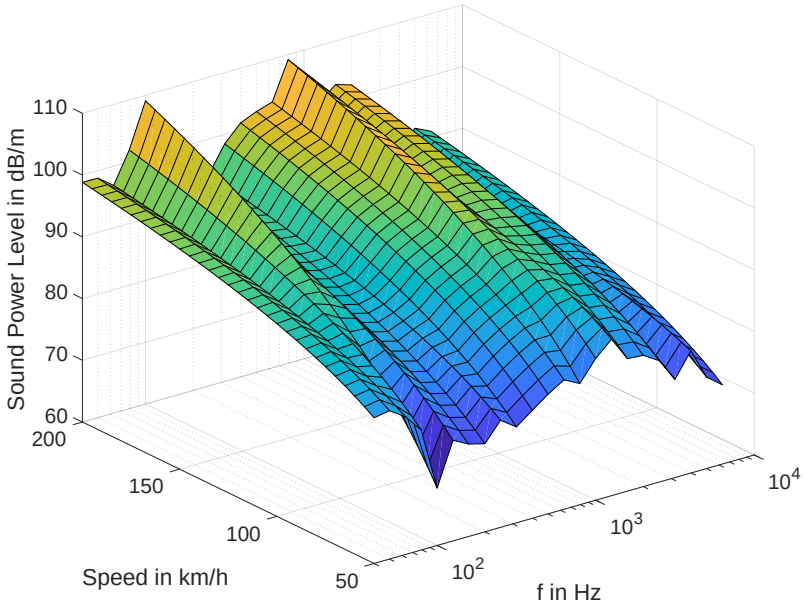

Figure D.11.: Speed Dependency of Linear Regression for Y31-Trains

D.2. Cases from Test Dataset

High Speed Trains

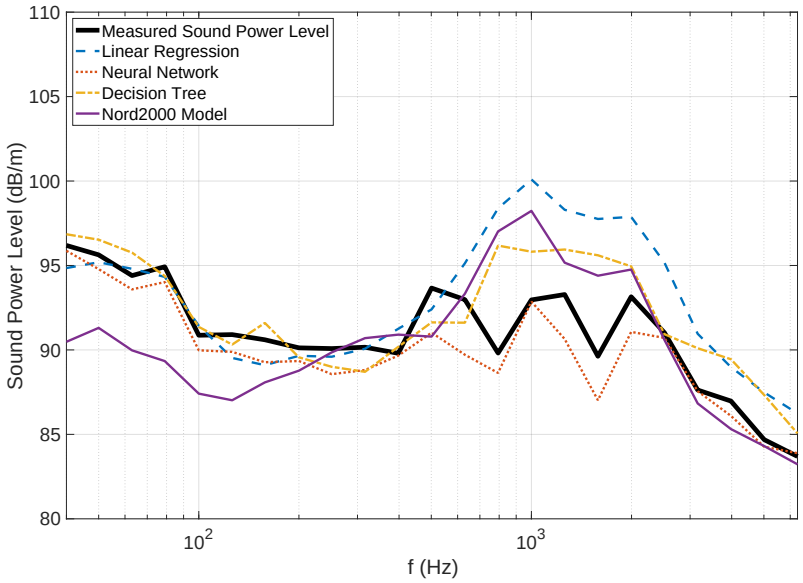

Figure D.12.: ER1-Train in High-speed Dataset, $v_t = 174\,\mathrm{km/h}$

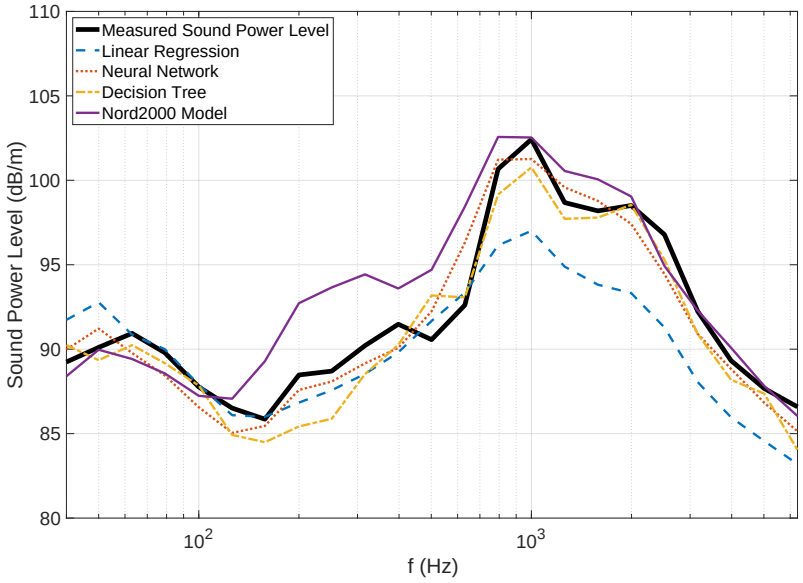

Figure D.13.: X2-Train in High-speed Dataset, $v_t = 145\,\mathrm{km/h}$

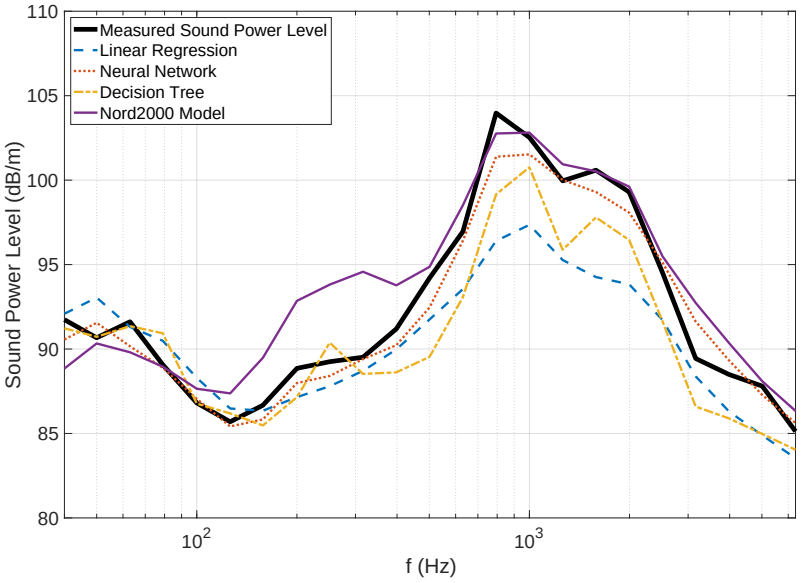

Figure D.14.: X2-Train in High-speed Dataset, $v_t = 148\,\mathrm{km/h}$

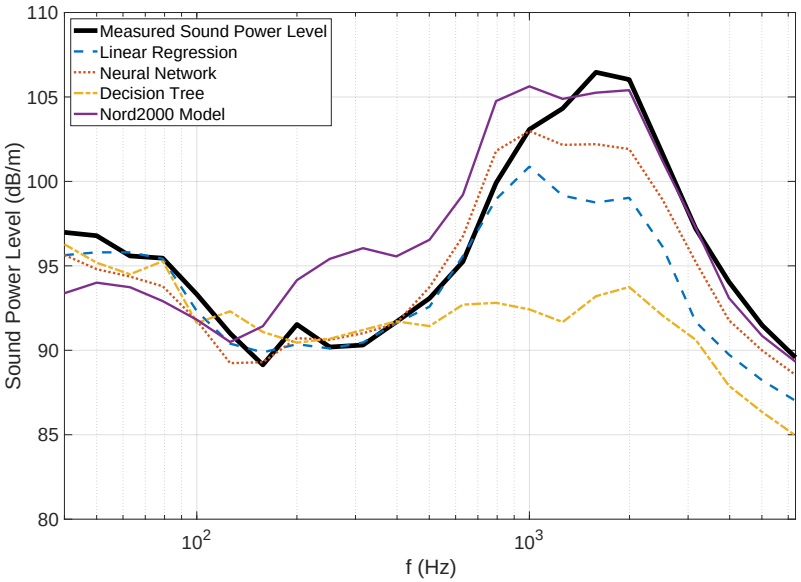

Figure D.15.: X2-Train in High-speed Dataset, $v_t = 182\,\mathrm{km/h}$

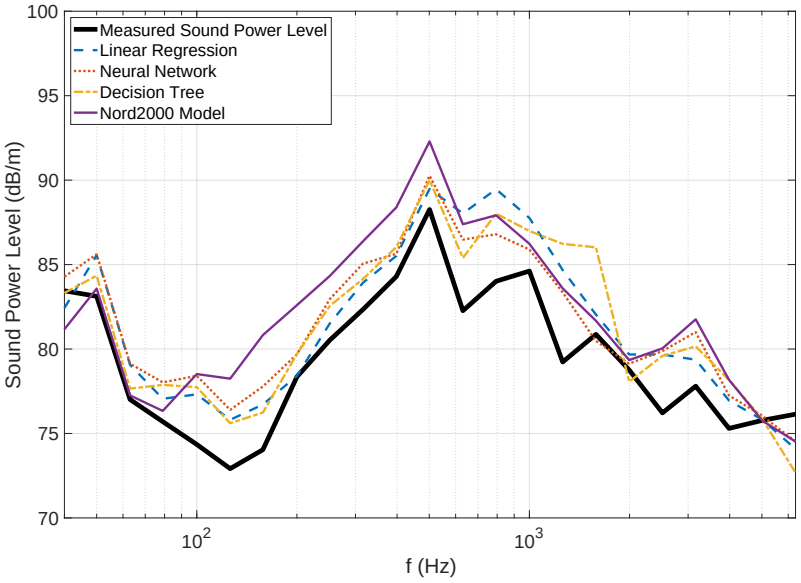

Figure D.16.: X31-Train in High-speed Dataset, $v_t = 84\,\mathrm{km/h}$

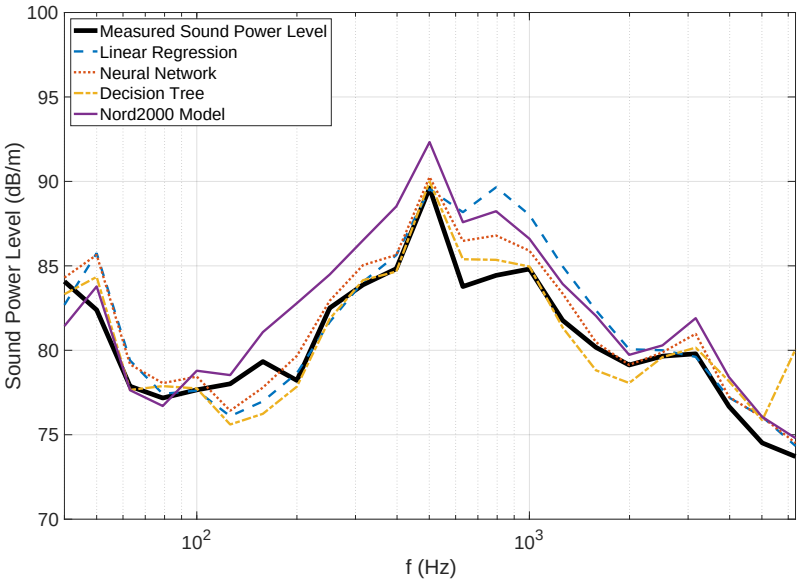

Figure D.17.: X31-Train in High-speed Dataset, $v_t = 85\,\mathrm{km/h}$

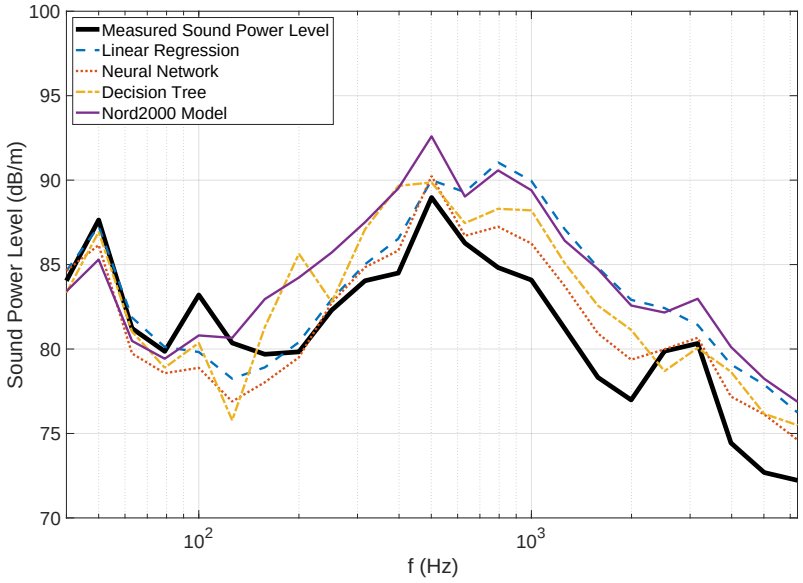

Figure D.18.: X31-Train in High-speed Dataset, $v_\mathrm{t} = 96\,\mathrm{km/h}$

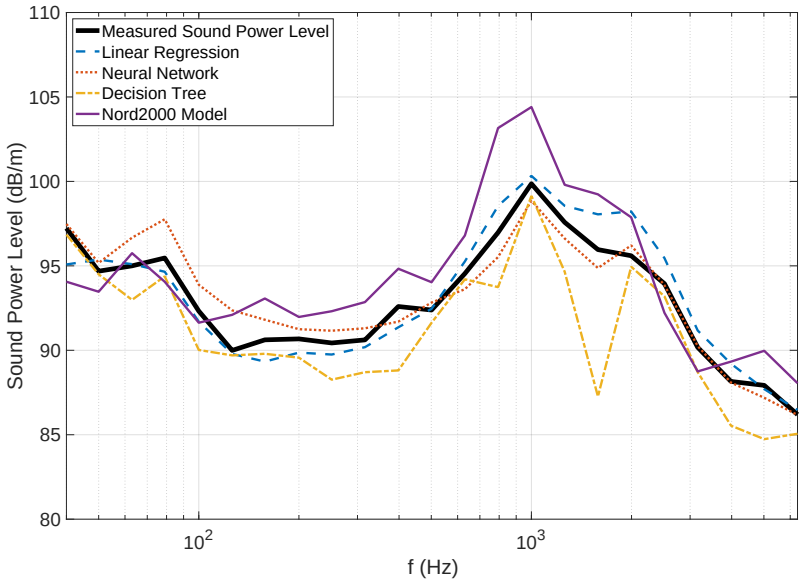

Figure D.19.: X31-Train in High-speed Dataset, $v_\mathrm{t} = 176\,\mathrm{km/h}$

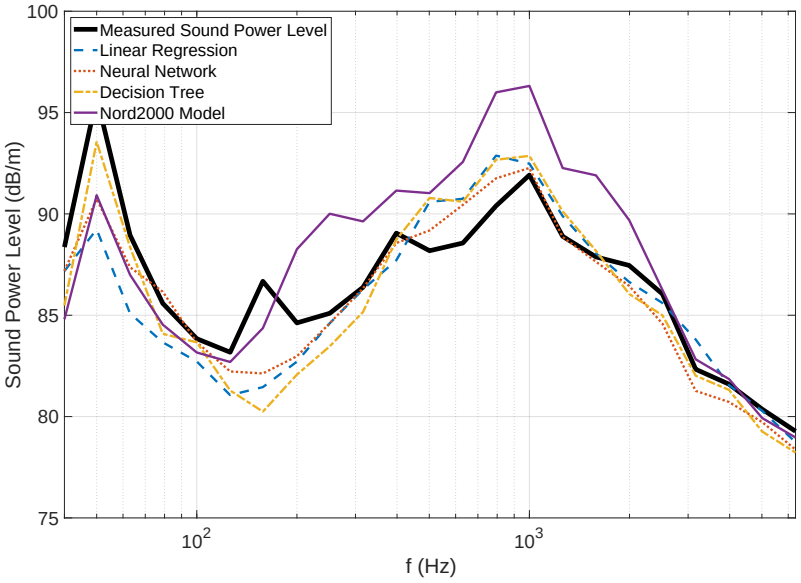

Figure D.20.: X40-Train in High-speed Dataset, $v_t = 111\,\mathrm{km/h}$

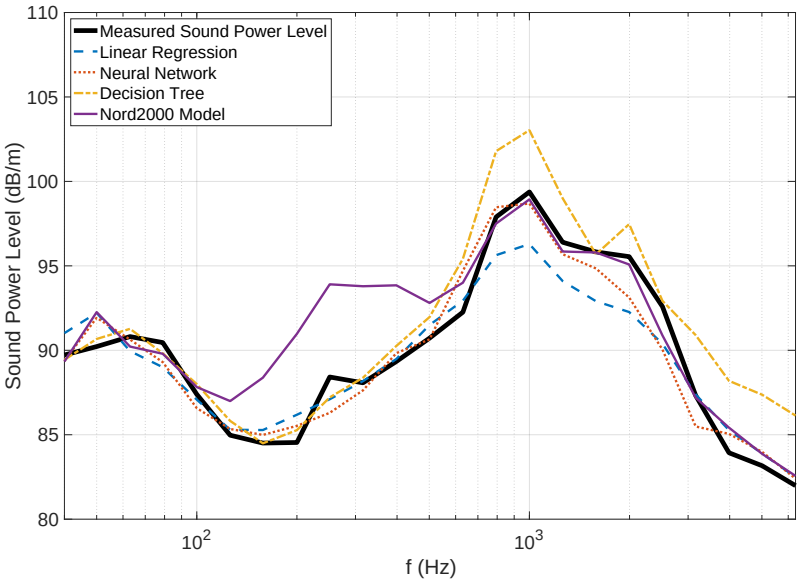

Figure D.21.: X40-Train in High-speed Dataset, $v_t = 139\,\mathrm{km/h}$

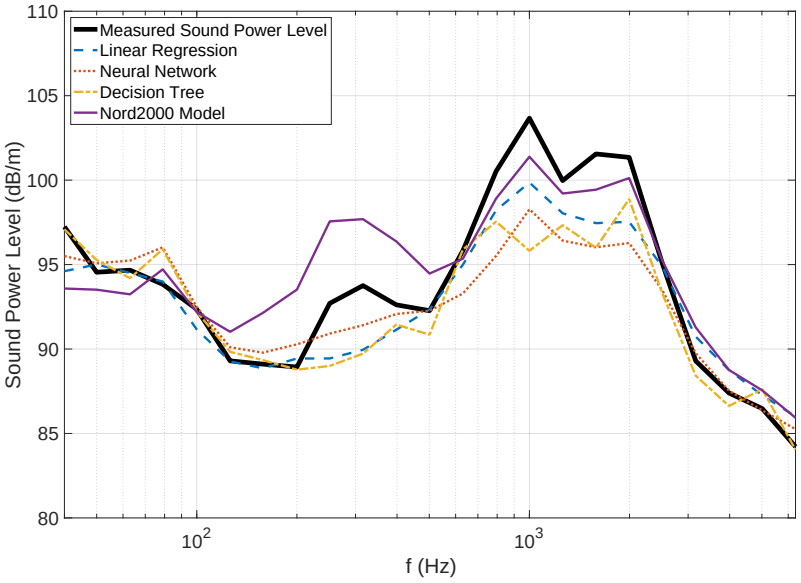

Figure D.22.: X40-Train in High-speed Dataset, $v_t = 172\,\mathrm{km/h}$

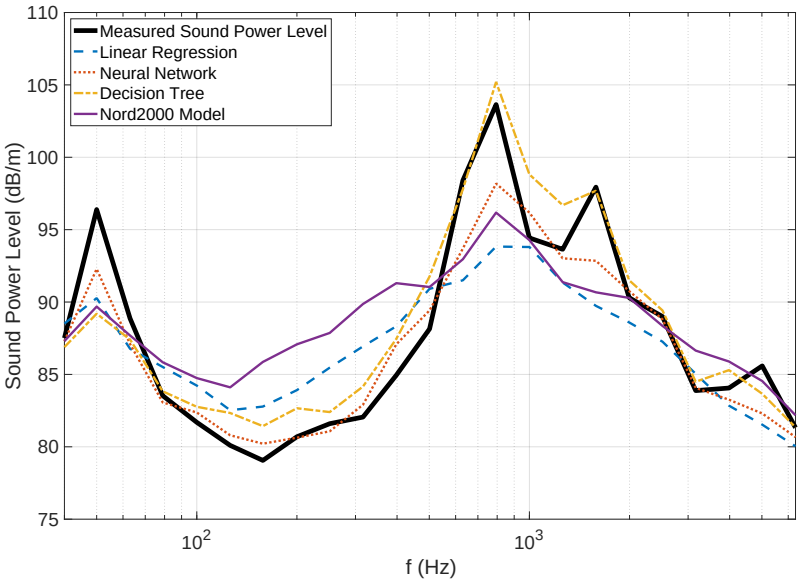

Figure D.23.: X50-Train in High-speed Dataset, $v_t = 120\,\mathrm{km/h}$

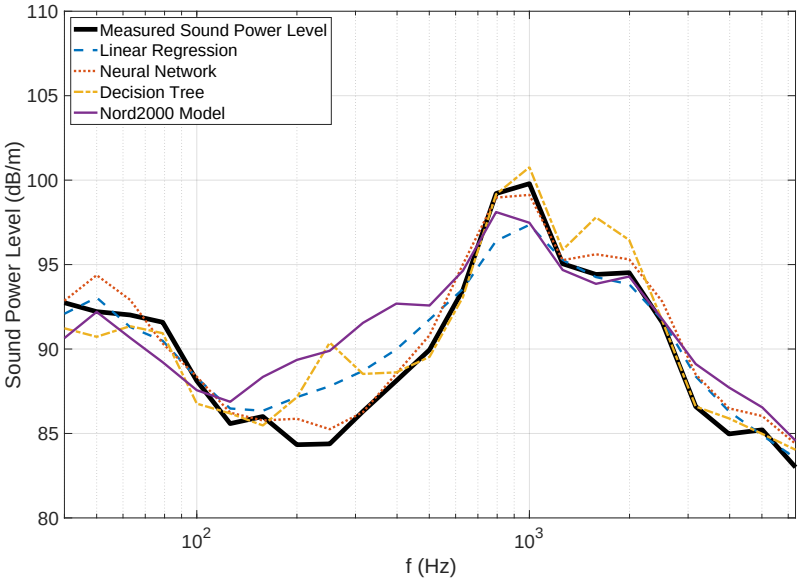

Figure D.24.: X50-Train in High-speed Dataset, $v_\mathrm{t} = 148\,\mathrm{km/h}$

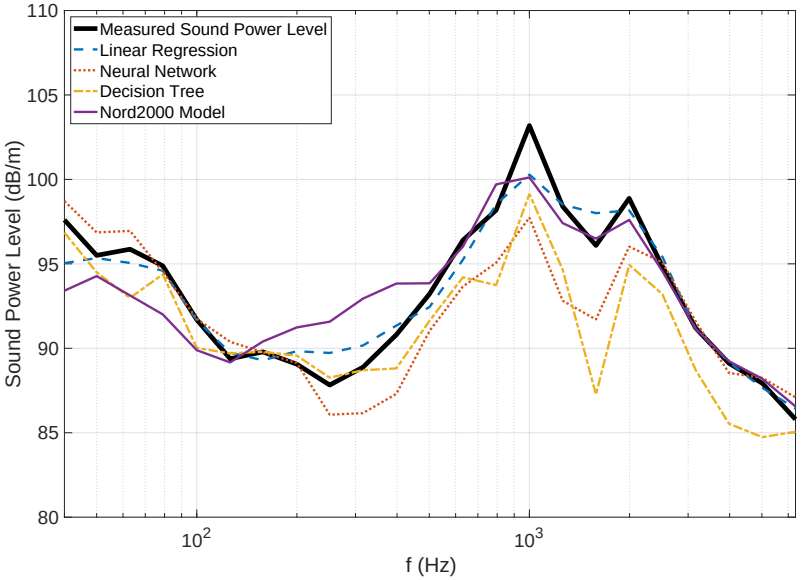

Figure D.25.: X50-Train in High-speed Dataset, $v_\mathrm{t} = 176\,\mathrm{km/h}$

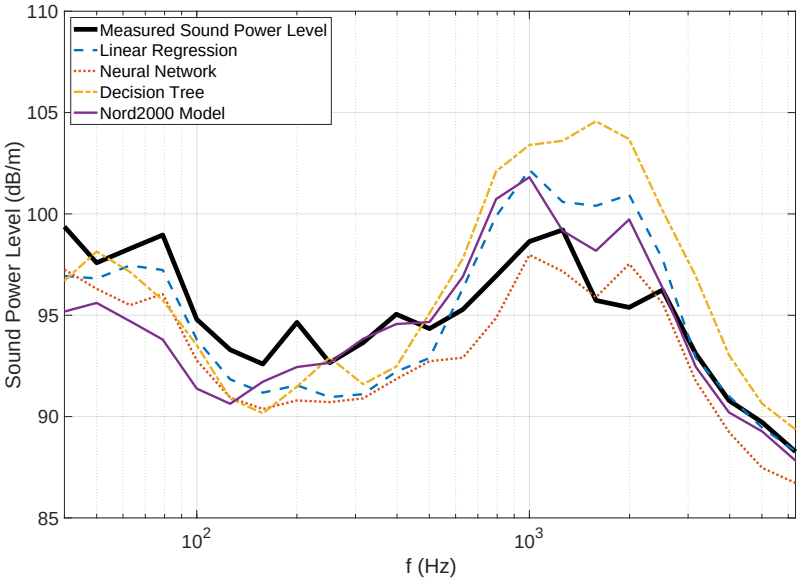

Figure D.26.: X55-Train in High-speed Dataset, $v_t = 197\,\mathrm{km/h}$

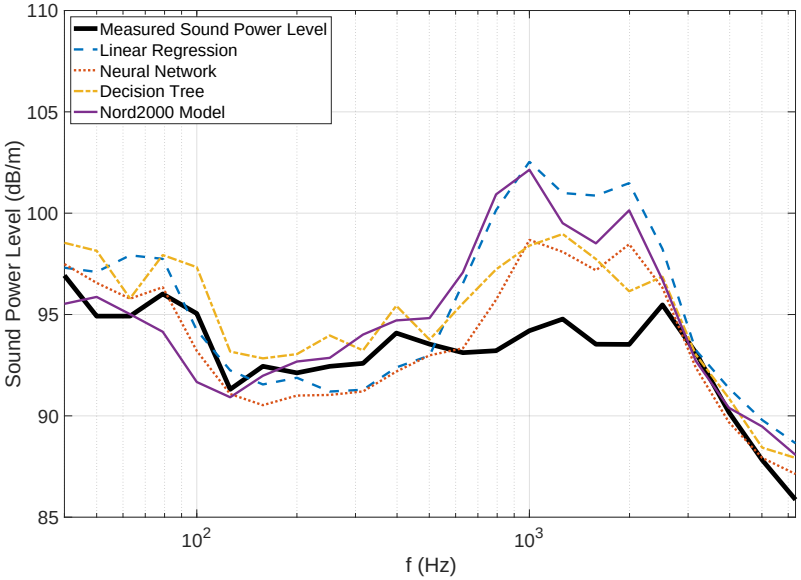

Figure D.27.: X55-Train in High-speed Dataset, $v_t = 201\,\mathrm{km/h}$

Inter-city Trains

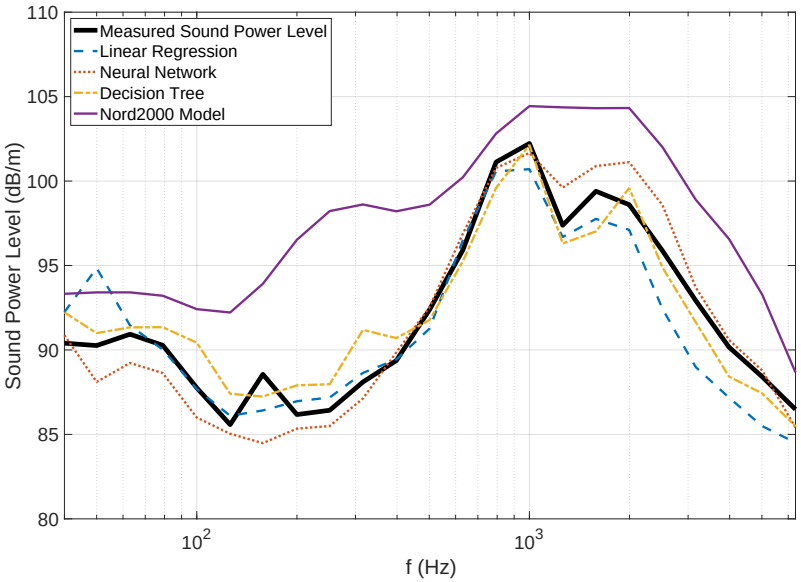

Figure D.28.: PT-Train in Inter-city Dataset, $v_\mathrm{t} = 153\,\mathrm{km/h}$

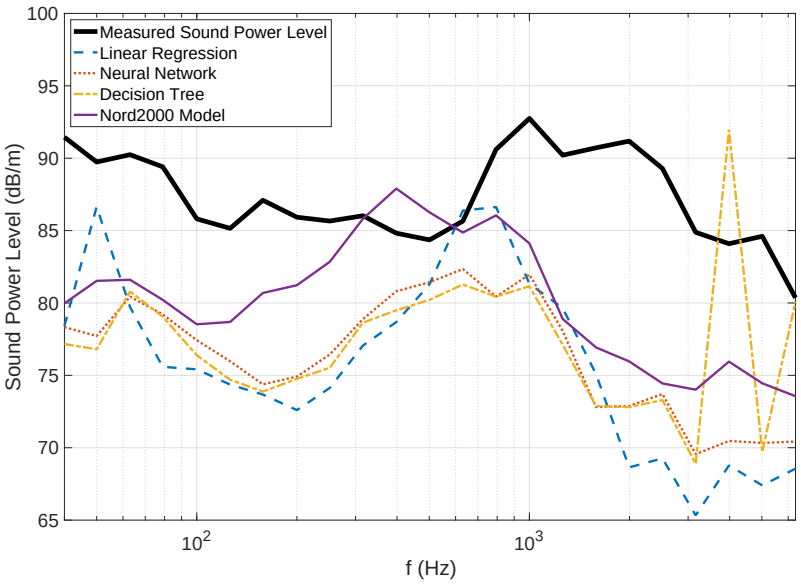

Figure D.29.: X60-Train in Inter-city Dataset, $v_\mathrm{t} = 75\,\mathrm{km/h}$

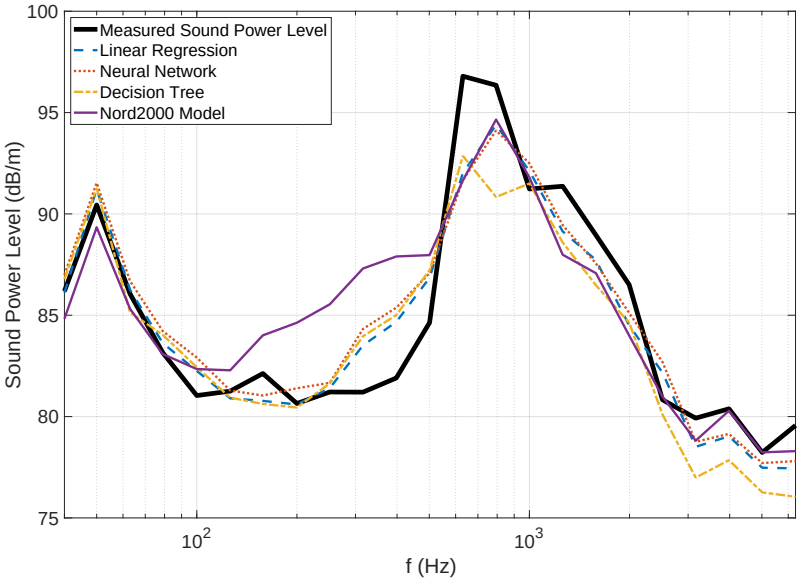

Figure D.30.: X60-Train in Inter-city Dataset, $v_\mathrm{t} = 112\,\mathrm{km/h}$

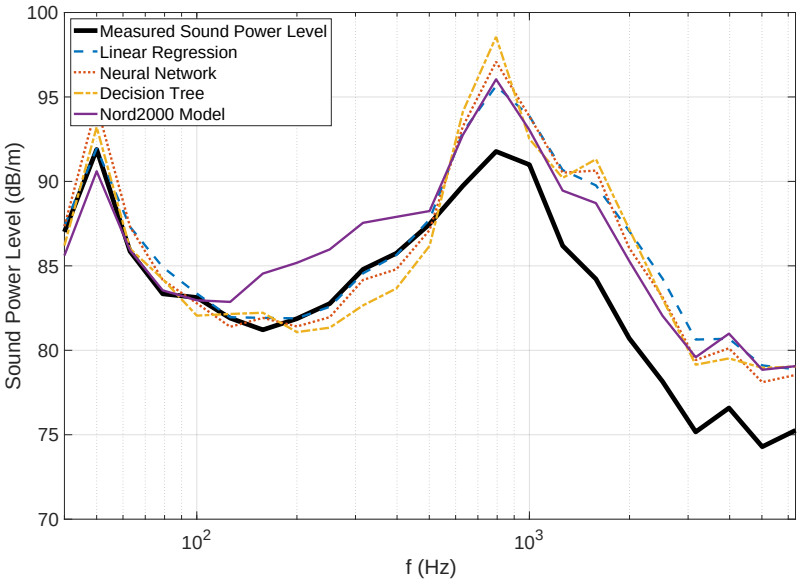

Figure D.31.: X60-Train in Inter-city Dataset, $v_\mathrm{t} = 119\,\mathrm{km/h}$

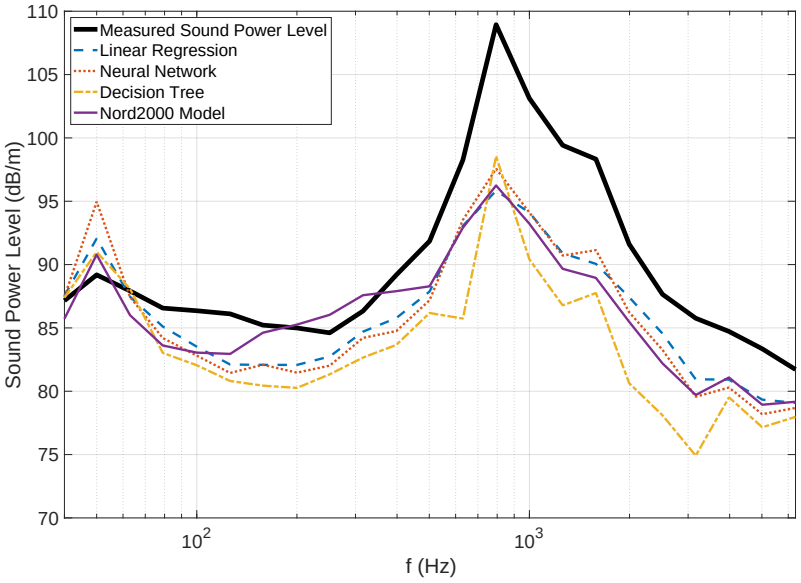

Figure D.32.: X60-Train in Inter-city Dataset, $v_\mathrm{t} = 120\,\mathrm{km/h}$

Regional Trains

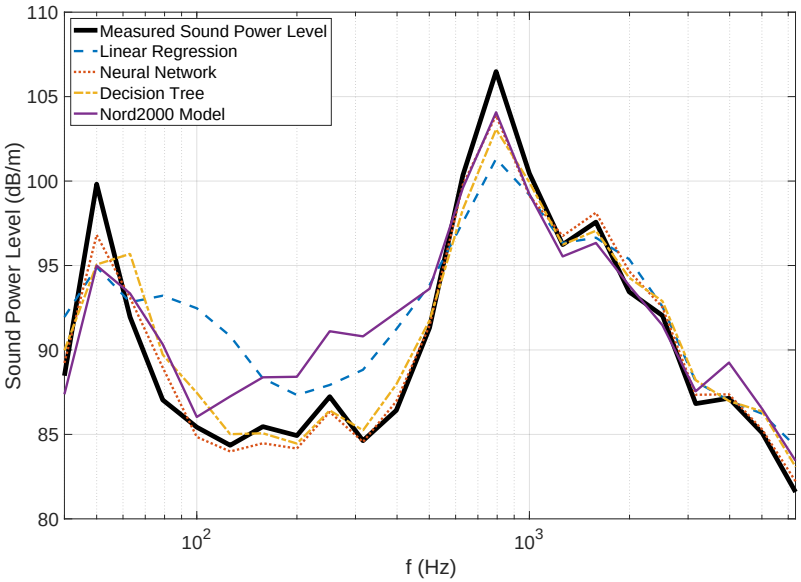

Figure D.33.: X60-Train in Regional Train Dataset, $v_t = 123\,\mathrm{km/h}$

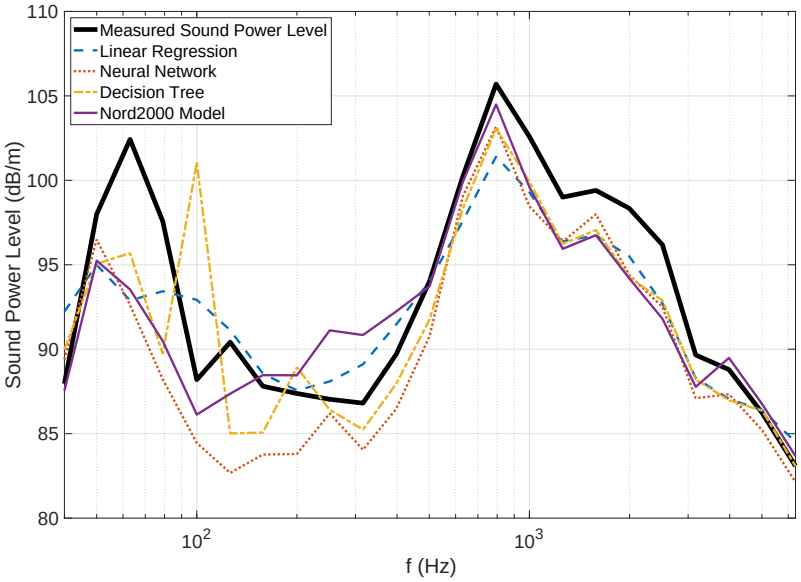

Figure D.34.: X60-Train in Regional Train Dataset, $v_t = 125\,\mathrm{km/h}$

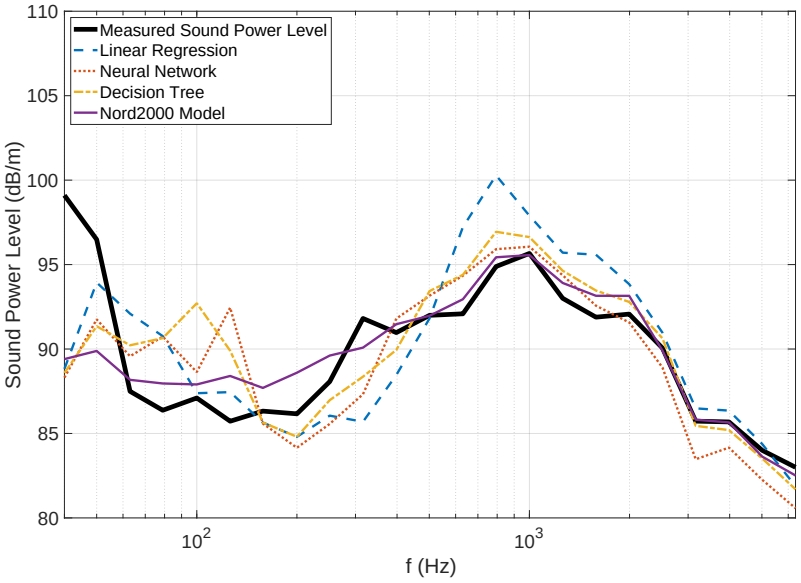

Figure D.35.: Y31-Train in Regional Train Dataset, $v_t = 101\,\mathrm{km/h}$

Freight Trains with K-Block and Disc Breaks

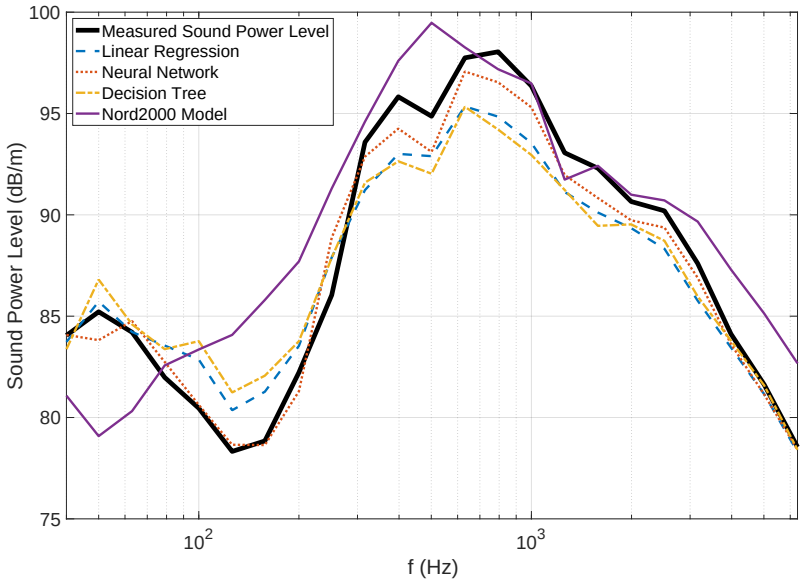

Figure D.36.: Freight Train in Dataset for Freight Trains with K-Block and Disc Breaks, $v_t = 58\,\mathrm{km/h}$

Freight Trains with Cast Iron Block Breaks

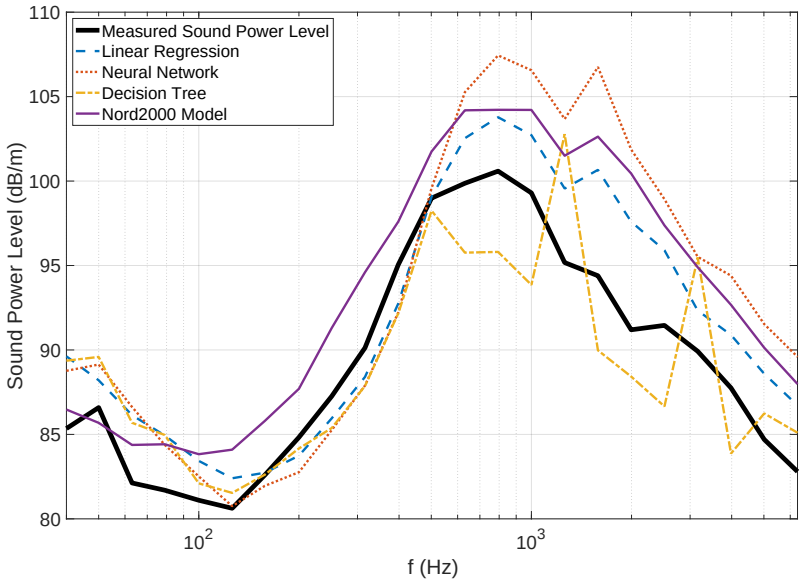

Figure D.37.: Freight Train in Dataset for Freight Trains with Cast Iron Block Breaks, $v_t = 93\,\mathrm{km/h}$

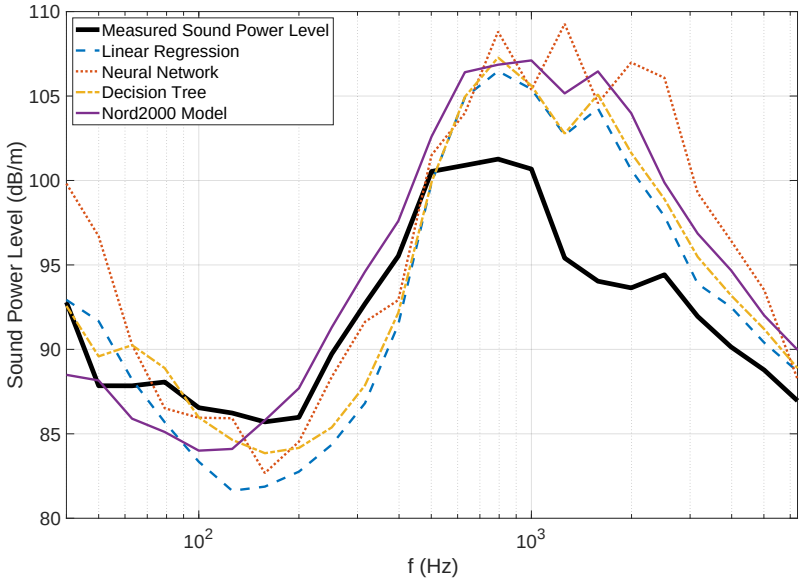

Figure D.38.: Freight Train in Dataset for Freight Trains with Cast Iron Block Breaks, $v_t = 111\,\mathrm{km/h}$

X2

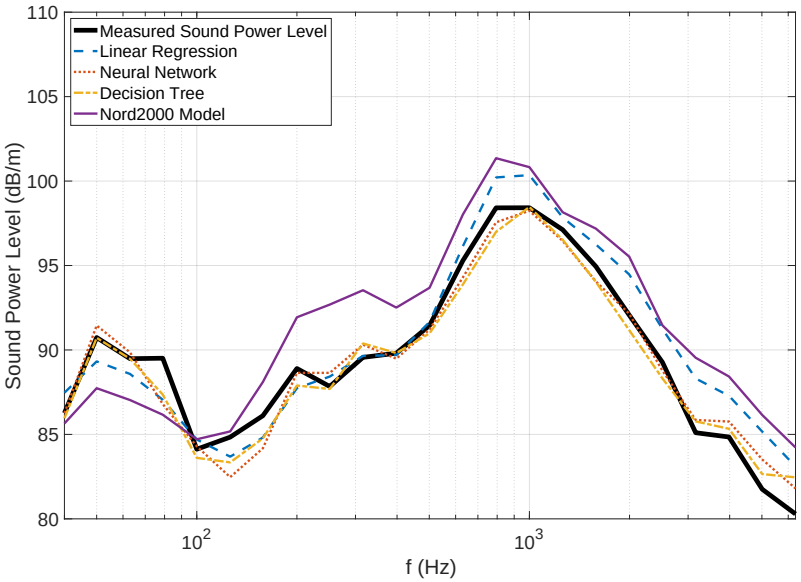

Figure D.39.: X2-Train in X2-Dataset, $v_t = 128\,\mathrm{km/h}$

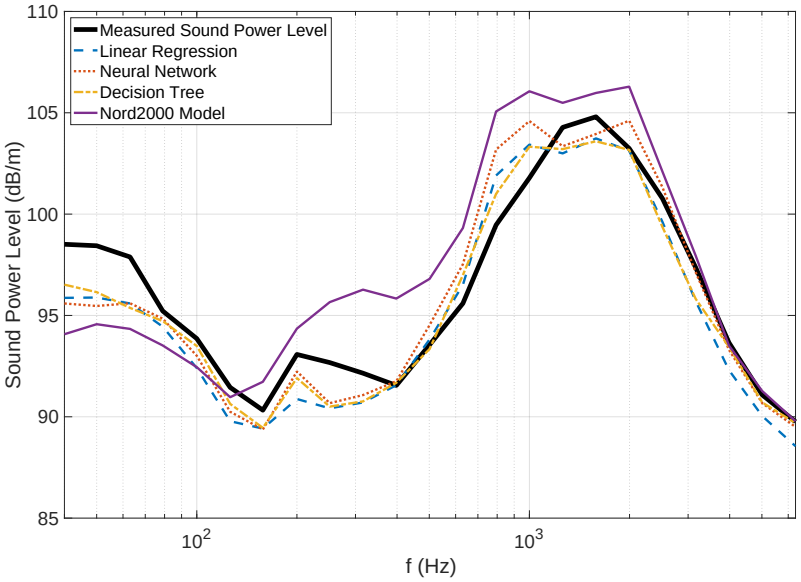

Figure D.40.: X2-Train in X2-Dataset, $v_t = 188\,\mathrm{km/h}$

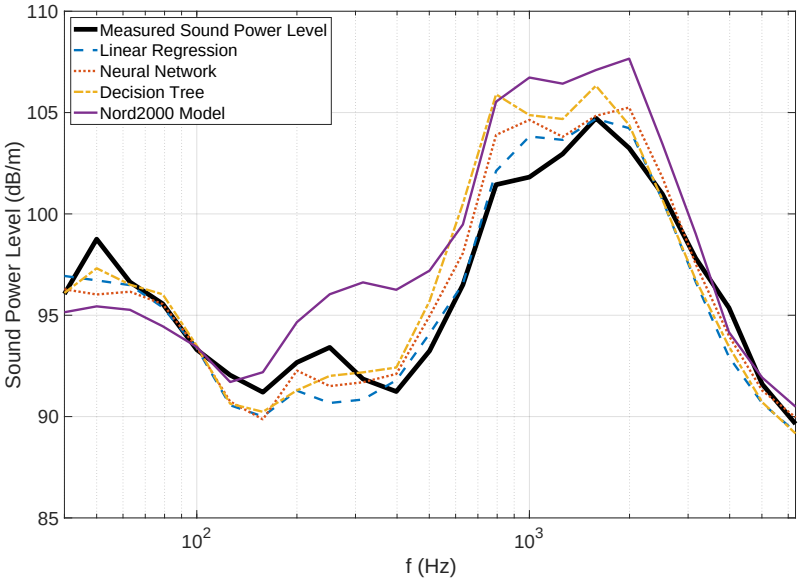

Figure D.41.: X2-Train in X2-Dataset, $v_\mathrm{t} = 198\,\mathrm{km/h}$

X11

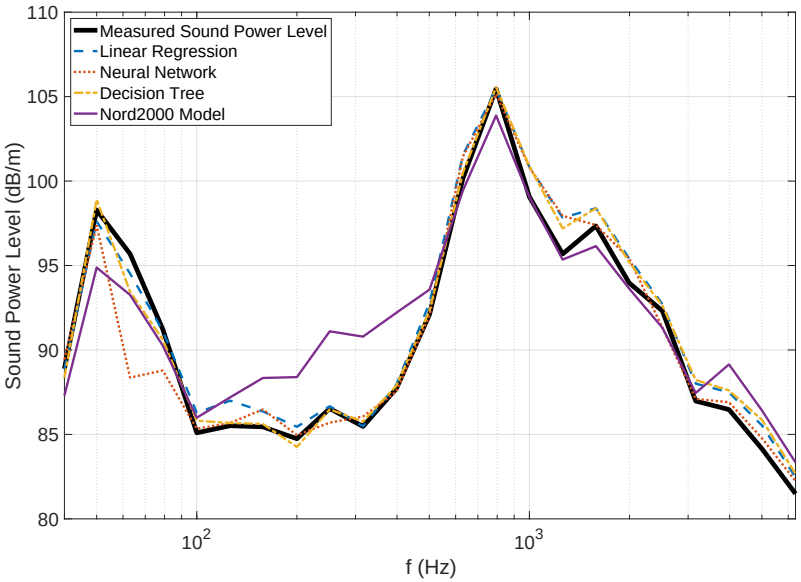

Figure D.42.: X11-Train in X11-Dataset, $v_t = 122\,\mathrm{km/h}$

X31

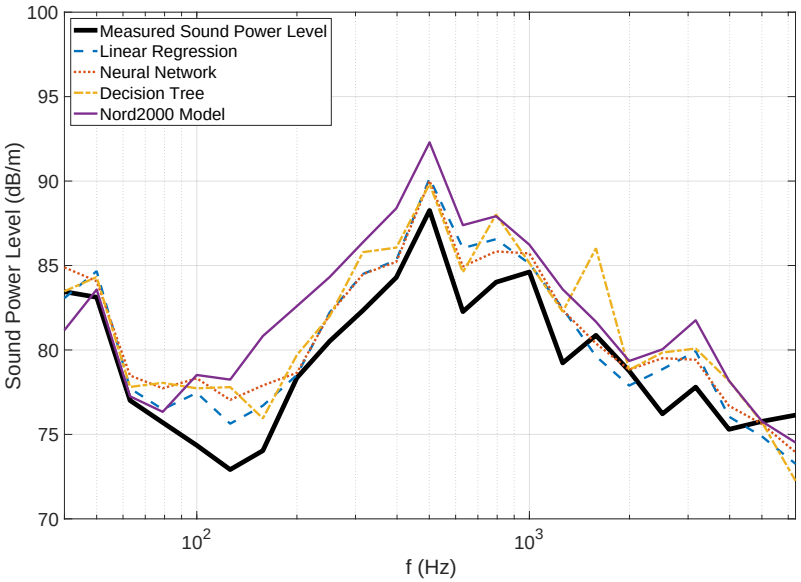

Figure D.43.: X31-Train in X31-Dataset, $v_t = 84\,\mathrm{km/h}$

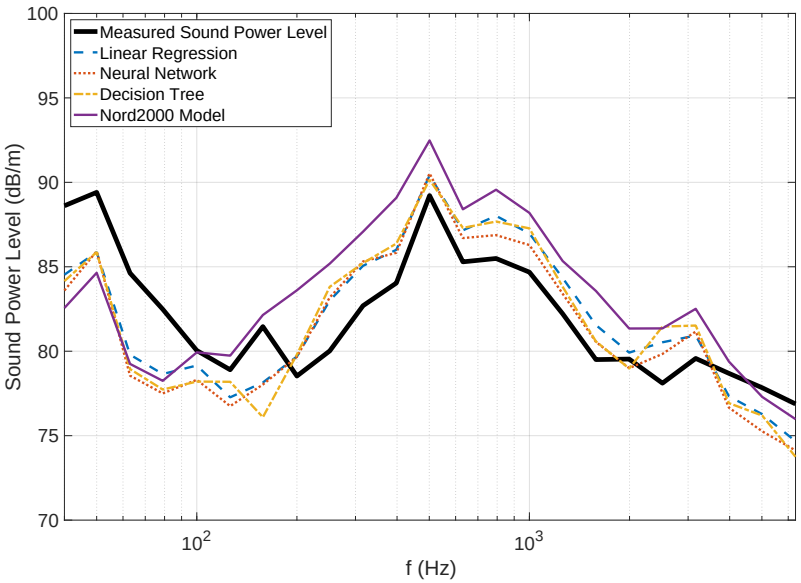

Figure D.44.: X31-Train in X31-Dataset, $v_t = 91\,\mathrm{km/h}$

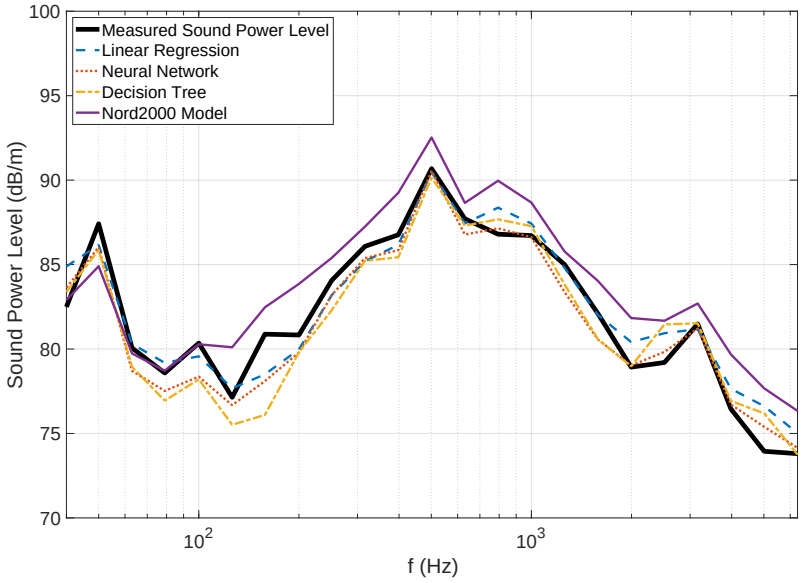

Figure D.45.: X31-Train in X31-Dataset, $v_\mathrm{t} = 93\,\mathrm{km/h}$

X40

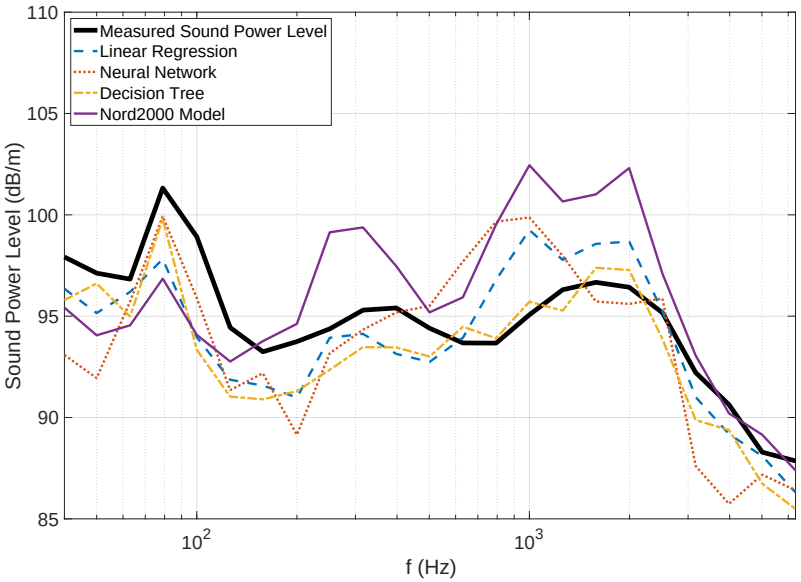

Figure D.46.: X40-Train in X40-Dataset, $v_t = 188\,\mathrm{km/h}$

X50

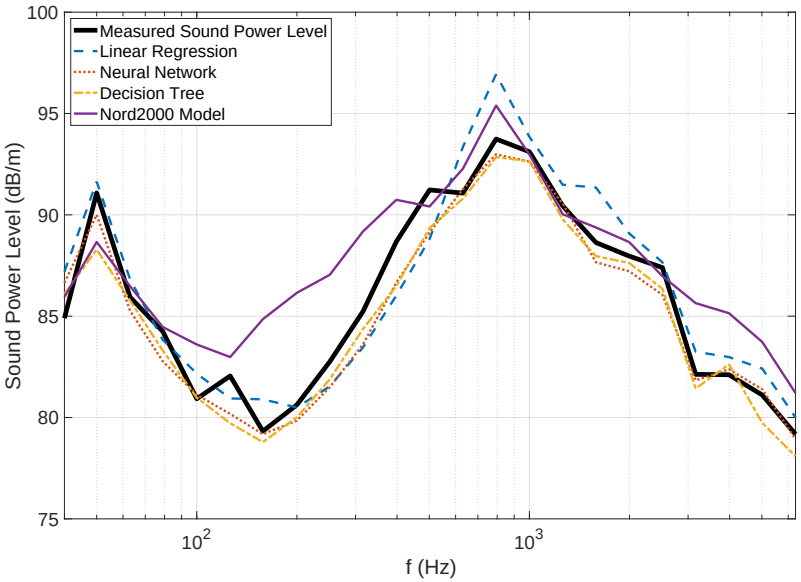

Figure D.47.: X50-Train in X50-Dataset, $v_t = 110\,\mathrm{km/h}$

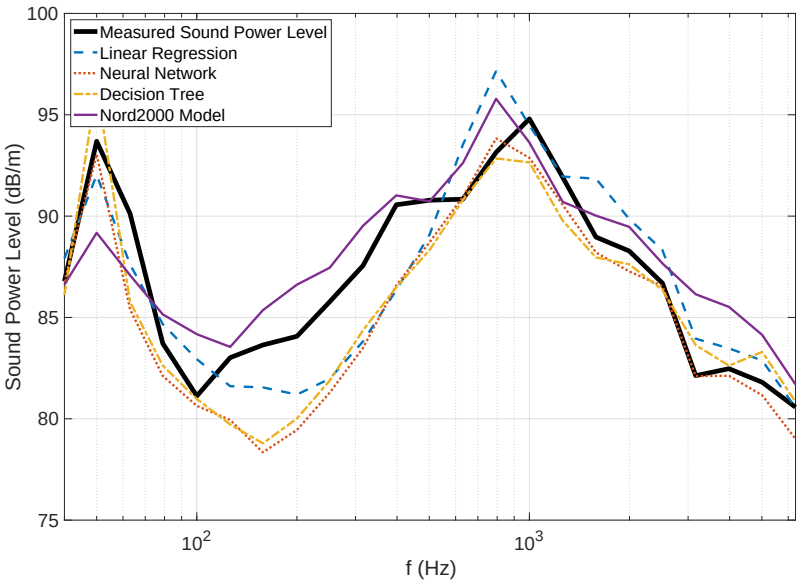

Figure D.48.: X50-Train in X50-Dataset, $v_t = 115\,\mathrm{km/h}$

X60

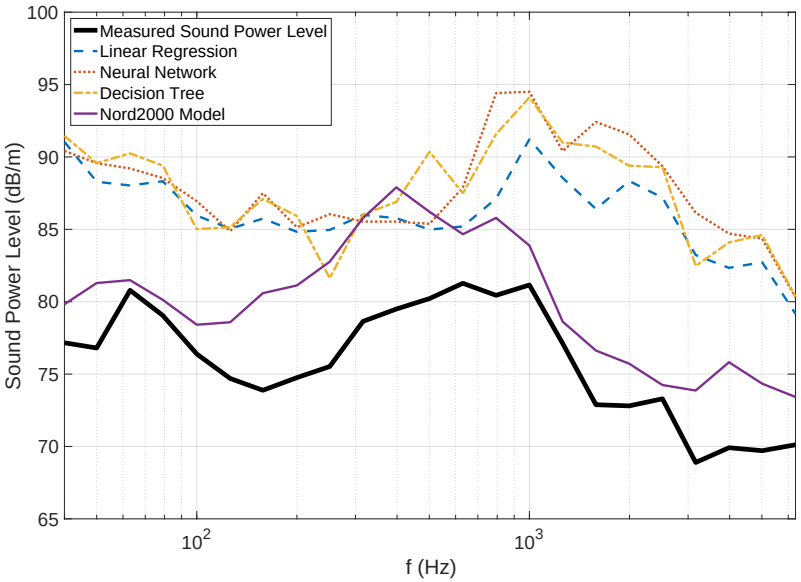

Figure D.49.: X60-Train in X60-Dataset, $v_\mathrm{t} = 74\,\mathrm{km/h}$

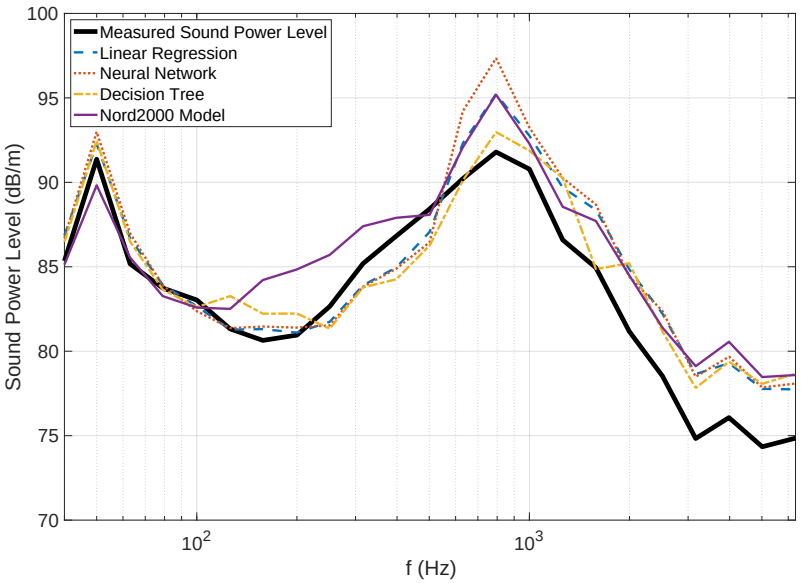

Figure D.50.: X60-Train in X60-Dataset, $v_\mathrm{t} = 114\,\mathrm{km/h}$

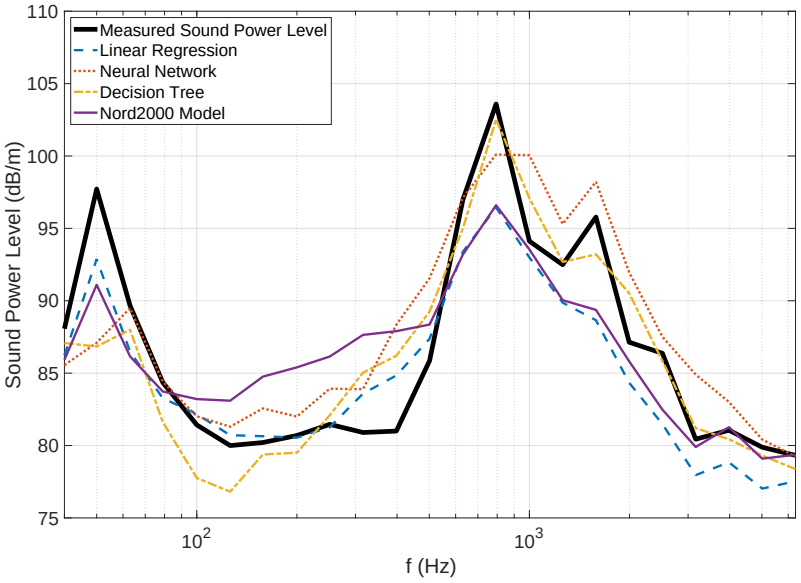

Figure D.51.: X60-Train in X60-Dataset, $v_\mathrm{t} = 122\,\mathrm{km/h}$

X74

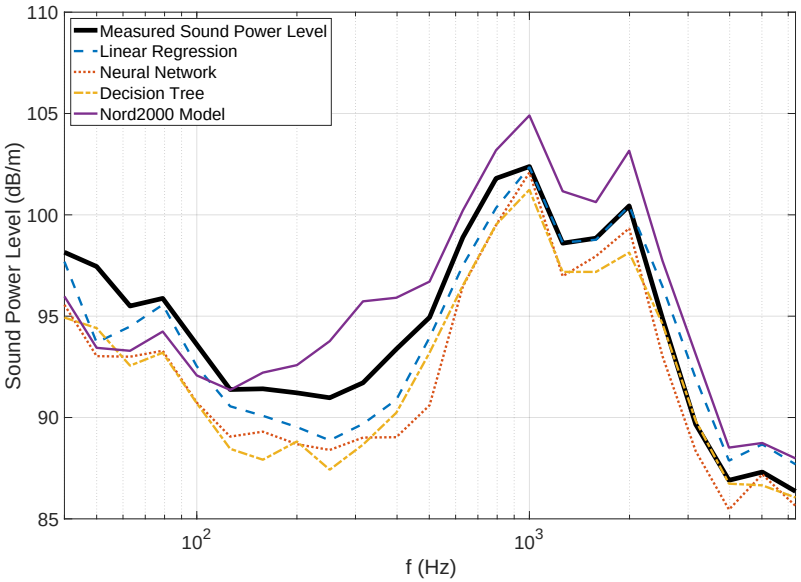

Figure D.52.: X74-Train in X74-Dataset, $v_t = 180\,\mathrm{km/h}$

Y31

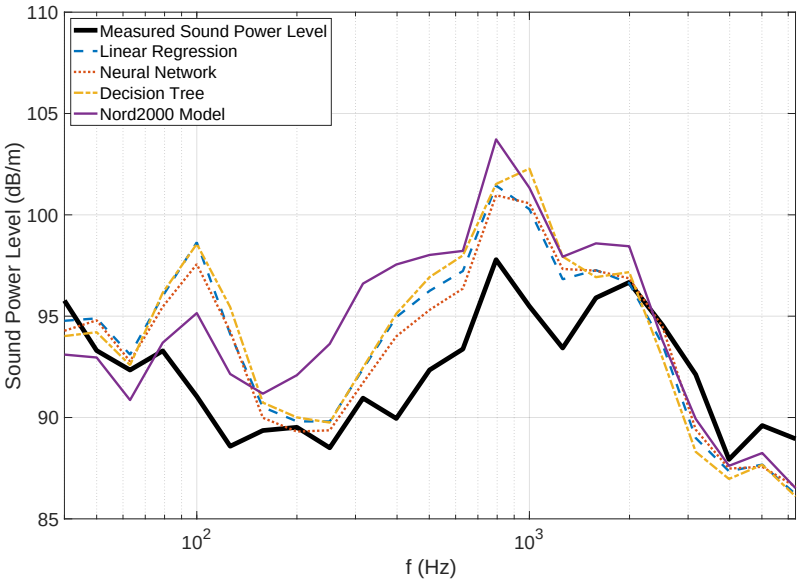

Figure D.53.: Y31-Train in Y31-Dataset, $v_t = 139\,\mathrm{km/h}$

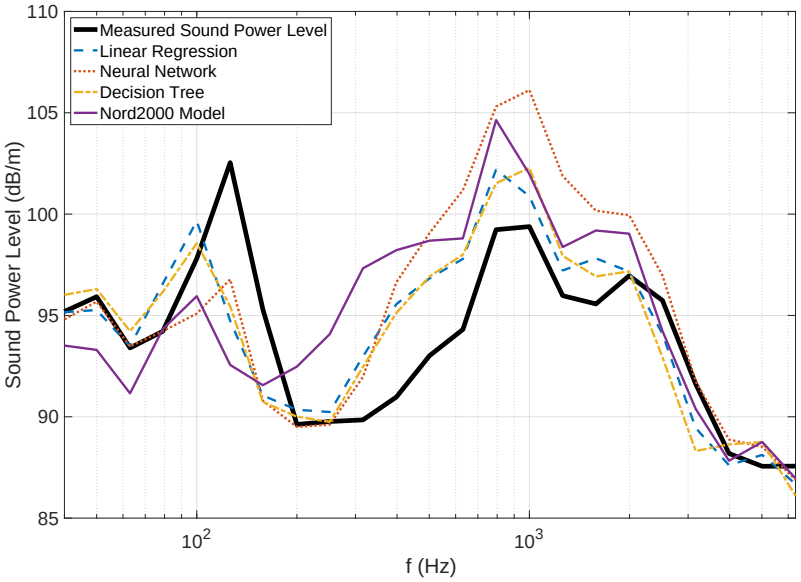

Figure D.54.: Y31-Train in Y31-Dataset, $v_t = 144\,\mathrm{km/h}$

E. Source Positions

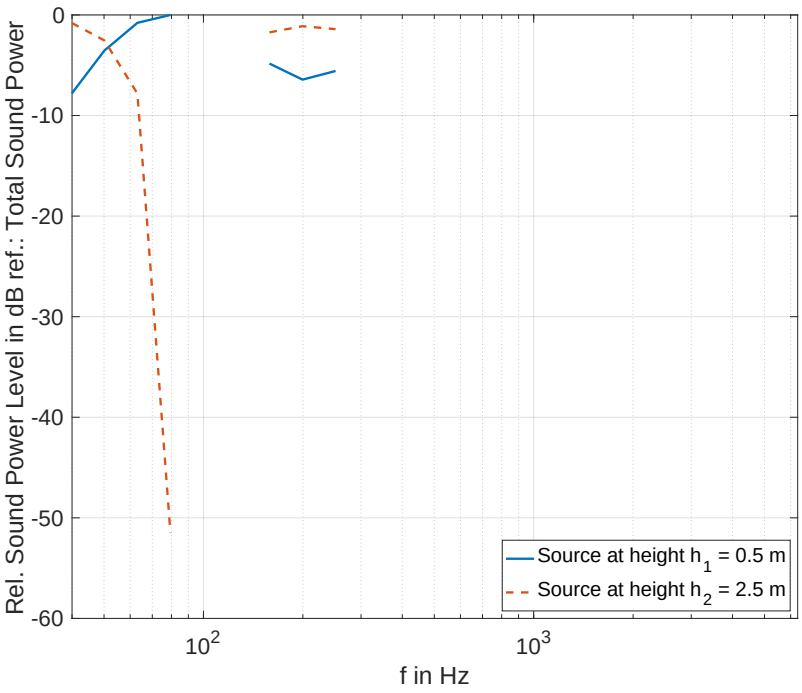

Figure E.1.: Relative Sound Power Level, ER1-trains

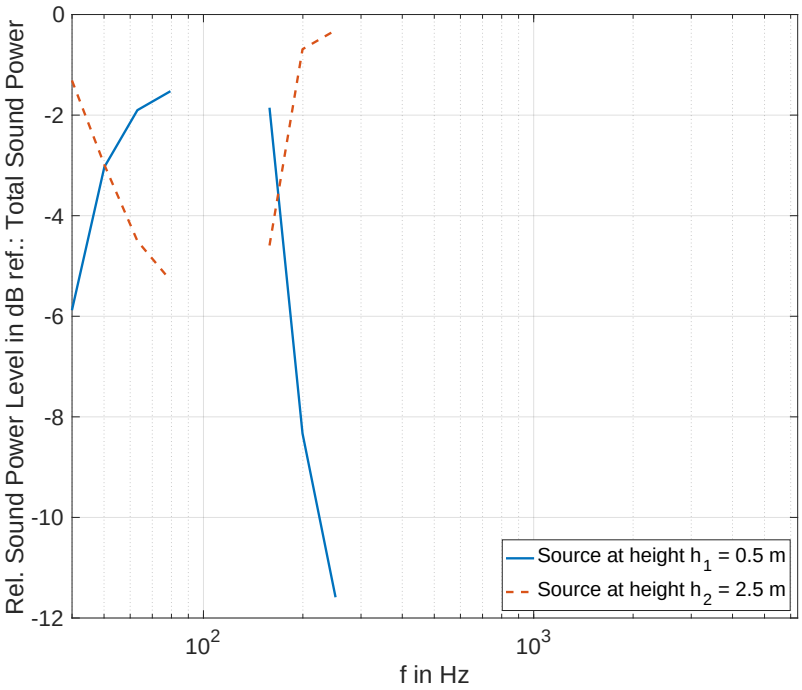

Figure E.2.: Relative Sound Power Level, FLIX-trains

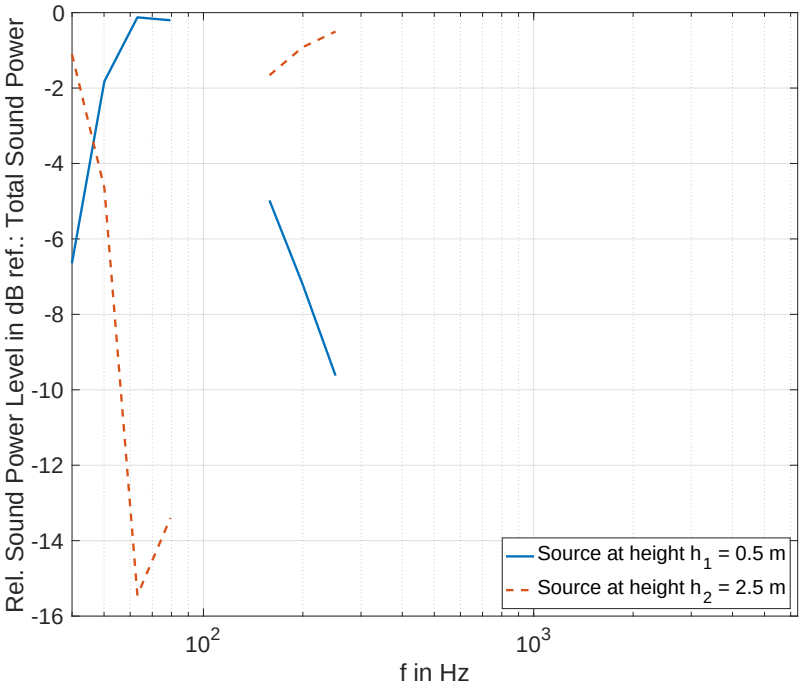

Figure E.3.: Relative Sound Power Level, GTD-trains

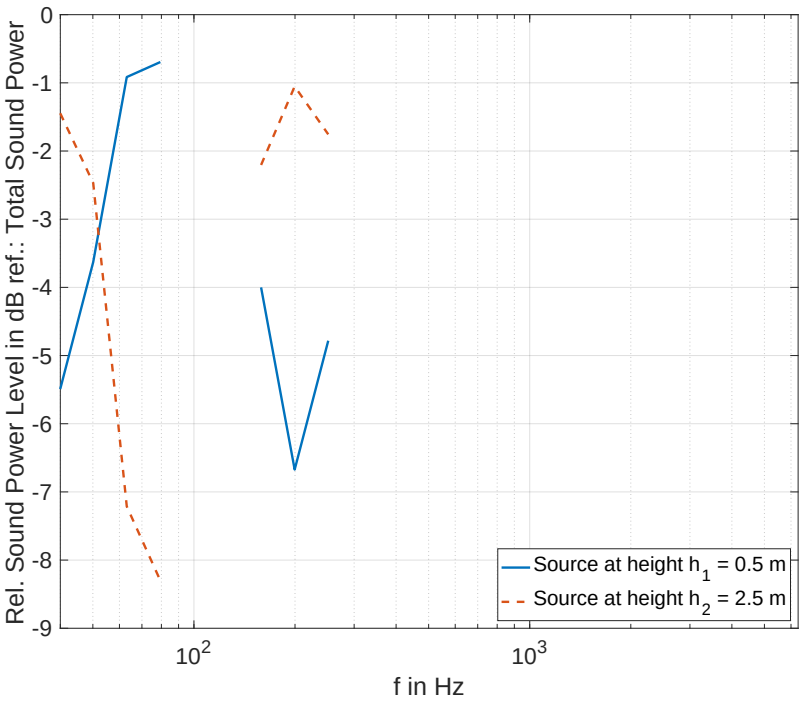

Figure E.4.: Relative Sound Power Level, GTE-trains

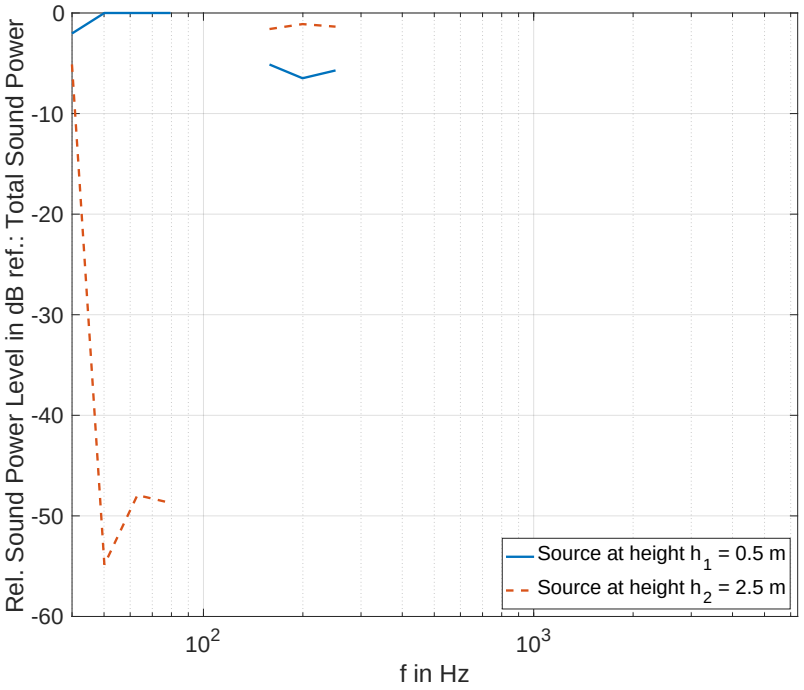

Figure E.5.: Relative Sound Power Level, GTK-trains

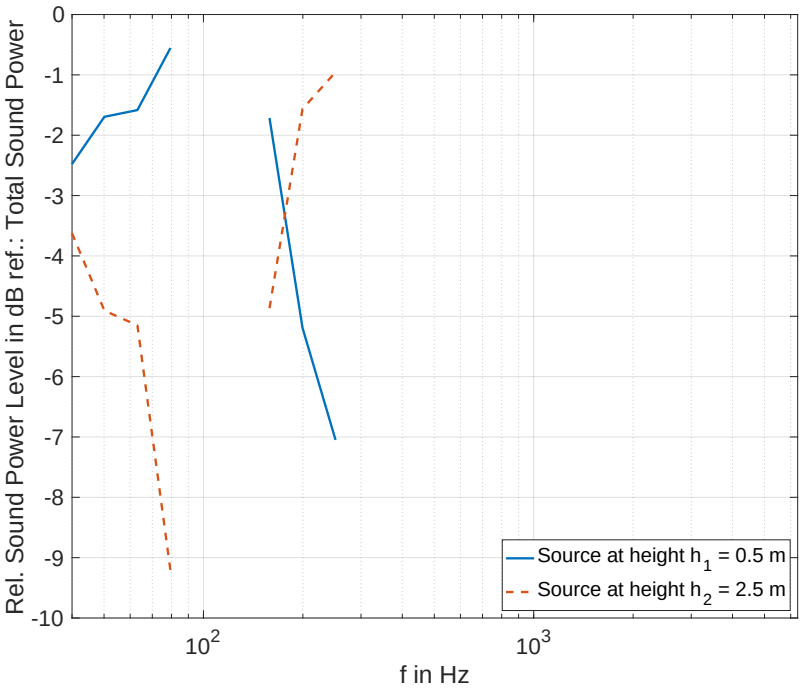

Figure E.6.: Relative Sound Power Level, PT-trains

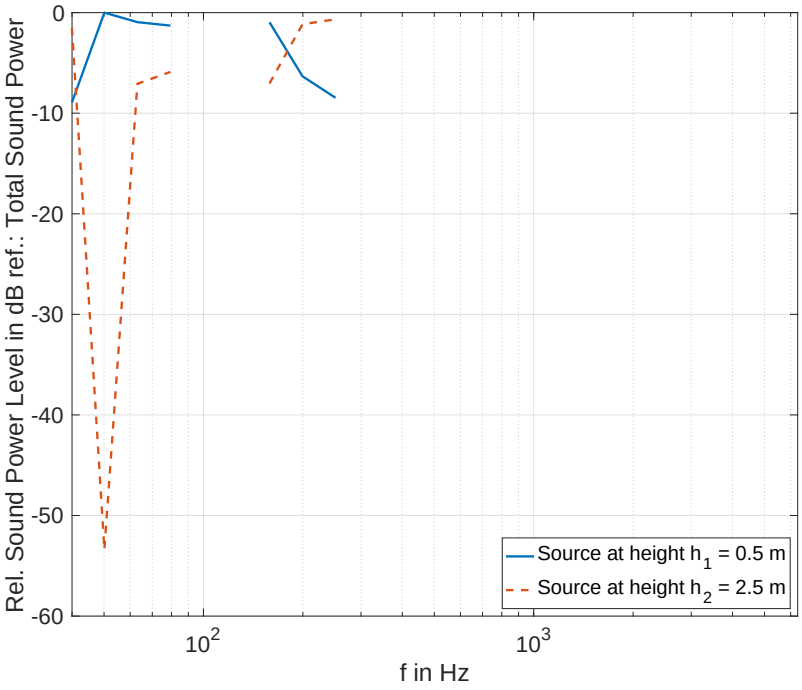

Figure E.7.: Relative Sound Power Level, X11-trains

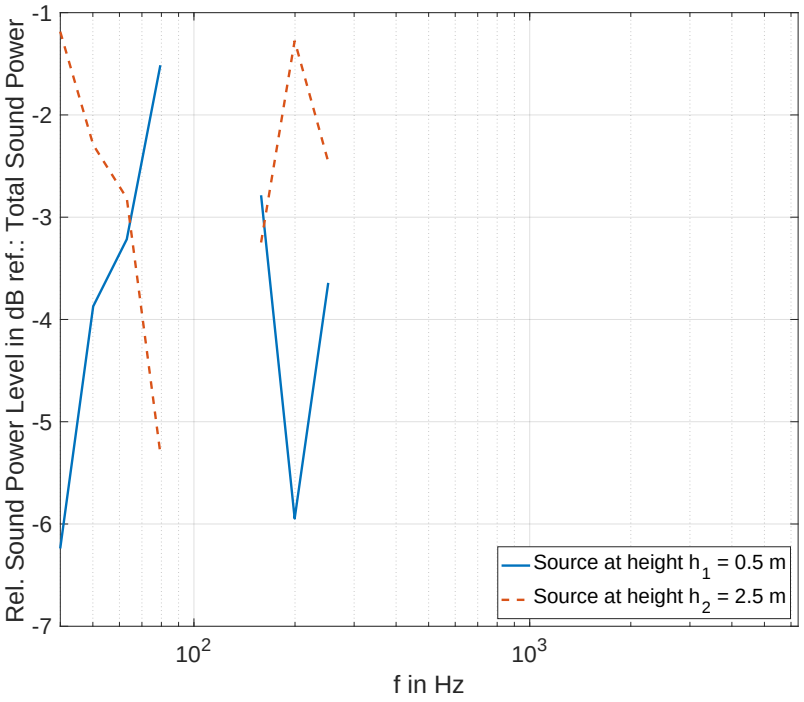

Figure E.8.: Relative Sound Power Level, X40-trains

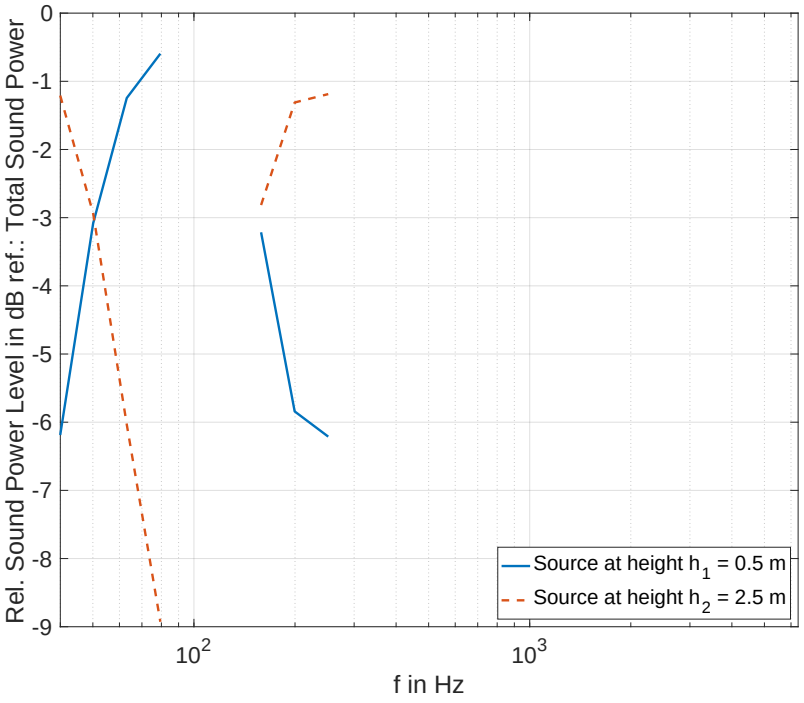

Figure E.9.: Relative Sound Power Level, X55-trains

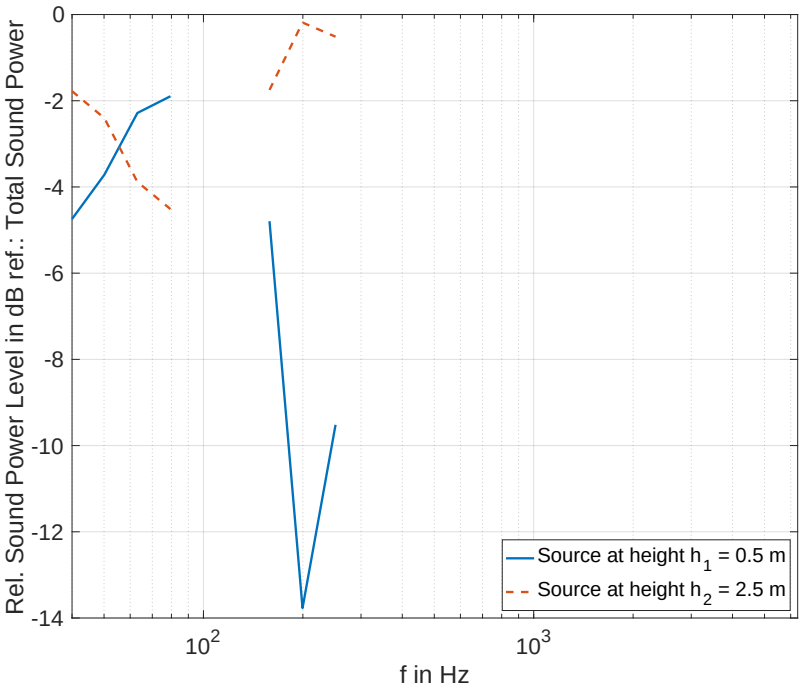

Figure E.10.: Relative Sound Power Level, X60-trains

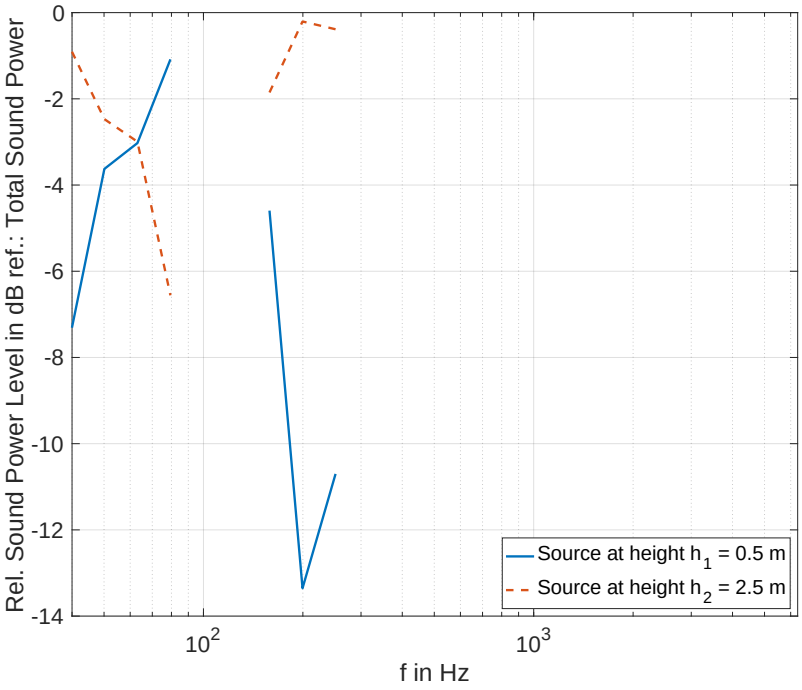

Figure E.11.: Relative Sound Power Level, X74-trains

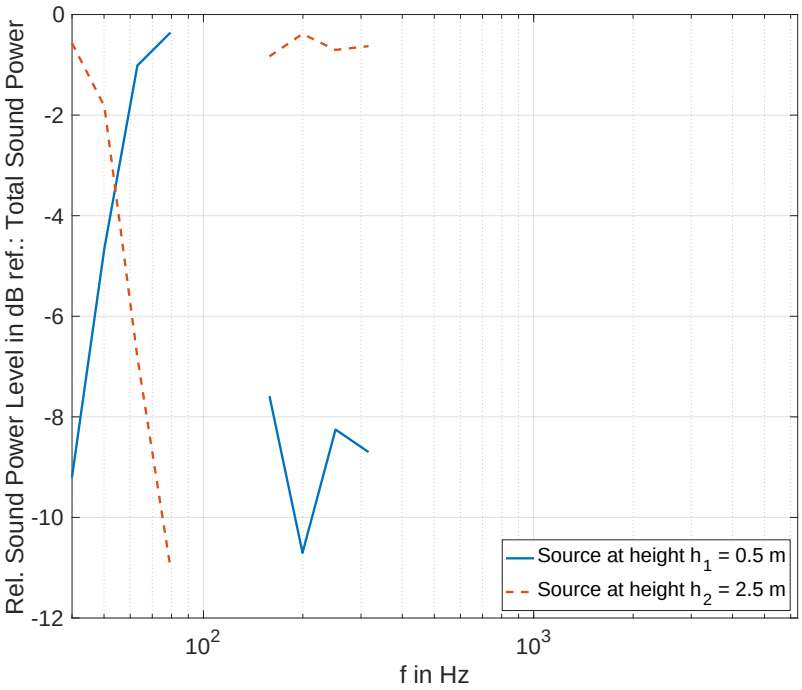

Figure E.12.: Relative Sound Power Level, Y31-trains